Response Analysis of an Industrial Power System with Arc Furnaces Utilising Artificial Intelligence

Abu Mohammad Osman Haruni
B.Sc. Eng (Electrical and Electronic)

Submitted in fulfilment of the requirements for the degree of
Masters of Engineering Science

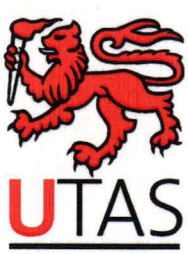

Centre for Renewable Energy and Power Systems

University of Tasmania

October 2008

Declaration of Originality

The work continued in this thesis has not been published previously at this or any other educational institutions. To the best of my knowledge, this thesis contains no material previously published or written by other person except where due reference is made.

Abu 21.10.08

Abu Mohammad Osman Haruni

Statement of Authority of Access

This thesis contains confidential information and is not to be disclosed or made available for loan or copy without the expressed permission of the University of Tasmania. Once released, the thesis may be made available for loan and limited copying in accordance with the Copyright Act 1968

Abu 21.10.08

Abu Mohammad Osman Haruni

Keywords

Electric arc furnace, load modelling, conventional modelling, black-box modelling, artificial intelligence, artificial neural network, fuzzy inference system, adaptive neuro-fuzzy inference system.

Abstract

The growing popularity of the electrical arc furnace in metallurgical industries causes significant impact on power grids, transient stability and quality of power supply. Being non-linear in nature, arc furnaces produce harmonics and inter-harmonics of arc voltage and current in electrical networks. Moreover, due to random load variation, the phenomenon of voltage fluctuation is found during arc furnace operation. Therefore, it is important to model the random behaviour of the arc furnace. The aims of this thesis are to investigate the applicability of the conventional and "black box" modelling techniques in modelling the response of an arc furnace. Conventional modelling approaches are used to obtain the instantaneous voltage and current wave forms of the arc furnace, while black box modelling approaches such as artificial neural networks (ANN) and adaptive neuro-fuzzy inference system (ANFIS), are used to capture the random and time varying pattern of arc furnace power consumption which is due to random changes of the bus voltage. The ANFIS model is also used for predicting the bus voltage of the arc furnace. To evaluate the performance of the proposed models, several case studies are presented and outputs of the proposed models are compared with the actual data recorded on a metallurgical plant.

Table of Content

List of Figures

List of Tables

Acknowledgements

Firstly, I would like to express my deepest and sincerest gratefulness to the Almighty, the most compassionate and merciful who guides me in the most appropriate way towards the completion of my research.

I would express my sincere gratitude to my supervisors Prof. Michael Negnevitsky, University of Tasmania, Dr. Md. Enamul Haque, Lecturer, University of Tasmania, and Associate Professor Kashem Mohammad Muttaqi, University of Wollongong for their invaluable support and constant guidance. Their valuable advice and insight kept me motivated in my research. I would also like to acknowledge the contribution made by Dr. Ashish P. Agalgaonkar, Research Fellow, University of Wollongong, during my research.

I would like to thank all the academic staff and post graduate students of school of engineering, University of Tasmania, for providing a healthy and helpful academic environment.

I would like to thank Mrs. Louise Oxley and Ms. Morag Porteous, English Language Centre, University of Tasmania, for their invaluable assistance during thesis writing.

I would like to express my deepest gratitude to all members of my family especially to my parents. I would also like to acknowledge the support that I have received from my relatives and friends.

Finally, I would like to thank the graduate research unit of the University of Tasmania for providing financial support.

Introduction

In last few decades, the use of the Electric Arc Furnace **(EAF)** to produce steel in the metallurgical industries has grown significantly since its first operation in the 1900s. Currently EAF is the second most important means of steel production next to the blast furnace/ basic oxygen furnace. In 2006, about 32% of steel was produced worldwide using EAF [1].

An EAF is a reactor used in the steel processing industries to charge the scraps, direct-reduced-iron (DIR) and other raw materials along with the lime and fluxes by means of both electrical and chemical energy. The heat is generated by the current passing through the electrode and by the radial energy evolved from the electrode [2]. The other form of energy is the chemical energy that is generated as a result of combustion and the oxidizing reaction during operation. The normal operation of the arc furnace can be divided into two stages, one is the meltdown stage and the other is the refining stage. In the meltdown stage, the raw materials are melted. In the refining stage, the melted materials are separated into slag and metals. The arc furnace ranges in size from small units of approximately one ton up to approximately about 400 ton. The arc furnace used in the research laboratory and by the dentists is only about few dozen grams in capacity [2].

The arc furnace can be categorised in two groups based on the type of the current they consume. The first is the alternating current (ac) arc furnace and the second is the direct current (dc) arc furnace. In the ac arc furnace, the three phase alternative current passes through the electrodes to the charge materials and from electrode to electrode. On the other hand, in case of the dc arc furnace, the direct current passes through the electrode to the charge materials. The electrode of the arc furnace is round in section and typically in segments with threaded couplings. They are automatically raised or lowered by a positioning system using either the electric winch hoist or hydraulic cylinders.

Due to random movements of the melting materials and random changes in the arc electrode length during operation, the power consumption of the arc furnace is random and time-varying, and hence the arc current is non-sinusoidal. Consequently, the voltage-current (v-i) relationship of the arc furnace is complex and highly non-linear. Fig. 1 shows how the real power varies with the variation

in bus voltage of the electric arc furnace. Each point of Fig. 1 represents the voltage magnitude and the power consumption of the arc furnace in different time. From Fig. 1, it is apparent that the relationship between the arc voltage and the arc power is random, which is difficult to model explicitly using mathematical equations. In addition to that, during melting period, scraps create a condition similar to a short circuit from the secondary side of the arc furnace transformer which causes a large current flow into the arc furnace. This causes large fluctuations in voltage. Also when the voltage drops due to a flicker, the EAF current rises for the operating power level to meet the production output. This has an adverse effect on the expected life of the arc electrode.

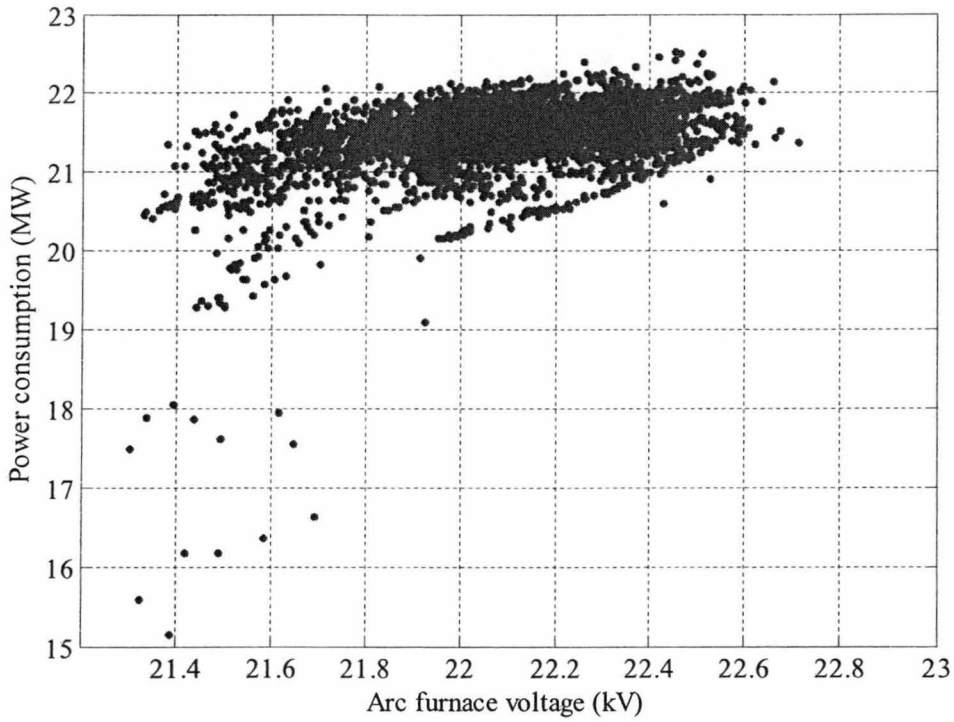

Figure 1. Arc furnace power vs arc furnace voltage.

Owing to inherent complexities and non-linearity, it is difficult to represent the arc furnace behavior using conventional methods. However, an accurate model of the arc furnace is essential from the view point of industry planners and operators. An accurate model is useful for pre-installation analysis as well as for post installation analysis such as short circuit analysis, transient over voltage analysis, or events such as loss of the generation unit or transmission line. In addition, it helps system operators to control the arc furnace. Furthermore, using an accurate model, plant planners or operators can identify

any inadequacies of the plant that would help them make decision for future expansion or modification of the existing plant. And finally, an accurate model helps system operators to optimize production.

Due to its inherent complexity and randomness, a mathematical representation of the arc furnace is a challenging task. However, a number of deterministic and stochastic approaches are proposed to model an arc furnace. These approaches are as follows:

- representing the arc furnace as a time domain control voltage source. This approach is based on the piece-wise linear approximation of the voltage-current (v-i) characteristics of the arc furnace,
- representing the relationship between arc voltage and arc electrode length,
- representing the arc furnace as a time varying resistance, and
- stochastic process.

However, in most cases, simplified assumptions are used and as a result, a model often fails to capture the significant features of the arc furnace. Considering the non-linear relationship between the arc voltage and the arc current and lack of knowledge associated with the process dynamic of an arc furnace, artificial intelligence techniques can be applied to extract nonlinear relationships between the input and the output pattern of arc furnaces. In recent years, AI techniques such as neural networks have been used for modelling a system where the mathematical models do not exist or are ill-defined. They have also been used successfully in systems that involve complex, multi-variable processes with time-varying parameters [3, 4].

The main objective of this research is to develop a reliable model of an arc furnace. In this thesis, "black-box" models using artificial neural networks (ANN) and fuzzy inference systems (FIS) are proposed to represent the arc furnace responses. The main advantages of the black-box modelling techniques are their capability of finding the complex, non-linear relationship between the input and output data, and hence predicting the system behaviours. The advantage of neural networks is their adaptive learning capability that enables them to improve their performance relatively quickly. On the other hand, fuzzy

logic is capable of handling the non-linear input/output relationship using a set of if-then rules. In this study, Multi layer perceptron (MLP) and adaptive neuro-fuzzy inference system (ANFIS) are used to predict the arc furnace responses. These models are tested and validated using recorded data from a metallurgical plant in northern Tasmania. The plant is currently operating four arc furnaces for the production of ferromanganese and silica manganese.

The thesis contains 4 chapters. Chapter 1 investigates electrical load modelling techniques, the challenges of load modelling and its application to model an arc furnace, and the relative advantages and usefulness of load modelling. Chapter 2 outlines component based approaches to modelling an arc furnace. A number of an arc furnace models is discussed in this chapter. In Chapter 3, a detailed study of the computation intelligent techniques and their application in modelling the arc furnace responses is presented. In Chapter 4, several case studies are provided to evaluate the application of the proposed arc furnace models. Finally a conclusion and future work recommendations are presented.

Articles in refereed conference

- A. M. O. Haruni, Kashem M. Muttaqi, M. Negnevitsky, "Analysis of Harmonics and Voltage Fluctuation using different Models of Arc Furnace", accepted for the presentation of Australasian Universities Power Engineering Conference (AUPEC'07), Perth, Australia, Dec. 09-12, 2007.
- A. M. O. Haruni, Kashem M. Muttaqi, M. Negnevitsky, "Artificial Intelligent Approach to Arc Furnace Response Prediction", accepted for the presentation of The Eighth International Conference on Intelligent Technologies (InTech 2007), Sydney, Australia, Dec. 12-14, 2007.

Chapter 1: Load Modelling Techniques

1.1 Introduction

The main objective of this chapter is to investigate the behaviour of an arc furnace as a 'load'. A load can be defined as a device or a set of devices that consumes power from the load bus [9]. In an industrial plant, the continuous variation in the magnitude and the frequency of the voltage in the load bus due to a small or large disturbance can have a significant impact on the power consumption (both active and reactive) of the load connected to the bus. A small disturbance is described as the continuous change of load in the load bus, and the operation of an on load tap changing (OLTC) transformer [5]. On the other hand, large disturbances are severe in nature which are caused by a short-circuit of the transmission line, or loss of a large generator, or transmission line of the system [5]. However, each load reacts differently according to its load characteristics because of the variation in bus voltage. Load characteristics can be defined as a set of parameters that characterises the behaviour of the load. A set of parameters such as power factor, variation of power with the change of voltage, and so on are examples of the load characteristic. Based on the load characteristics, loads can be classified in different categories [5, 6, 8, 9].

- Loads with 'fast dynamic' with electrical and mechanical characteristics such as induction motors play an important role in power systems as they consume approximately 60% to 70% of the total power supplied by the power generation unit. These loads require nearly constant torque at all speeds. As a result of voltage variation, the power consumption of motor loads varies momentarily but, they try to restore the operating power after a certain transient period to keep the constant torque.
- Discharge lighting loads exhibit significant discontinuities in under voltage conditions. Discharge lights such as mercury vapour, sodium vapour, and fluorescent lamps normally extinguish below a certain

voltage level and they restart again when the voltage recovers. They extinguish in the range of 0.7 pu to 0.8 pu of the operating voltage.

- Thermostatic control loads such as water heaters, ovens, electric heaters, and boilers behave similarly to a constant resistance load. Right after a voltage drop, the possible variation of input power of these devices has little effect on temperature. When the voltage drop occurs, the heat production decreases, and the 'on cycle' of the thermostat is prolonged in order to recover the desired temperature level. Therefore, during low voltage conditions, it takes more time to increase the temperature to a desired level. On the other hand, these loads are not affected by the voltage variation if they are on the 'off cycle'.
- Response of on load tap changers (OLTC) on distribution transformers, voltage regulators, and voltage controlled capacitors plays an important role in the load restoration process. Although these devices are not load components, they are seen from the transmission system as a part of the load component. After a disturbance, while they restore the voltage level of the sub-transmission and distribution system to the pre-disturbance value, they affect the status of the voltage sensitive loads. The control action of this restoration process begins about one minute after voltage variation in the load bus and voltage restoration process is achieved in 2 to 3 minutes.
- Some industrial loads such as electric arc furnaces, rolling mills exhibit a complex response due to the change in bus voltage.

However, in most cases including arc furnaces, a load bus is a composite bus which is the factorial composition of different load classes. A load class refers to the type of load such as industrial, residential, and commercial which is often a combination of different load components such as air conditioners, lighting loads, heating loads, motor loads, and so on [5, 9]. A typical composite load bus containing the different load classes and combination is shown in the Fig. 1.1.

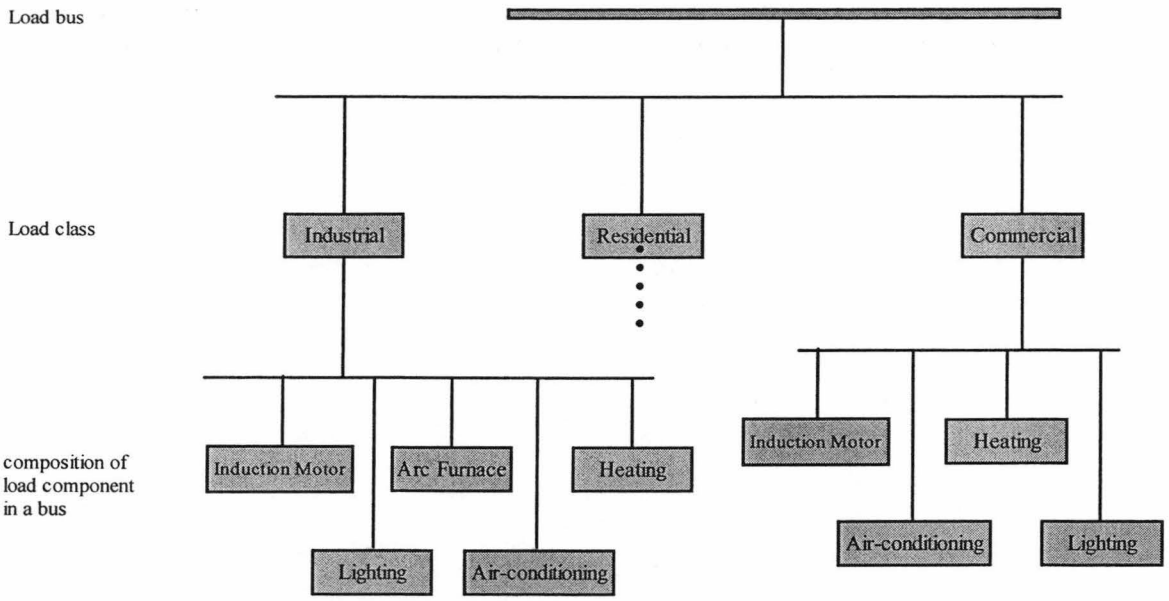

Figure 1.1. Composite load bus.

It is difficult to forecast the load behaviour for a number of reasons [9]:

- The large number of diverse loads connected to the same bus.
- Uncertainties regarding certain load characteristics. For example, in the case of industrial loads such as electric arc furnaces, steel rolling mills, and other loads involving different process industries, the load response is highly random and time-varying. As a result, these loads cannot be modelled accurately using physical modelling approaches.
- Ownership and location of load devices are not directly accessible to the electric utility.
- Lack of precise information about the load composition. For example, the aggregated loads seen from bulk power delivery transformers are the most uncertain power system components, due to the uncertainty of the participation of individual loads.
- Daily, weekly, and seasonal changes of load compositions on the same load bus. In the case of residential and commercial loads, during winter time, electric heating loads are used extensively, while during summer, air conditioning or electric cooling loads are often used. In the case of industrial

loads, during weekdays, the load bus could be a combination of different industrial loads such as arc furnaces, motors, and so on which consume a large amount of power form the utility. However, during weekends and at night time, the industrial load bus could be a combination of lighting and heating loads.

1.2 Load modelling

A load model can be defined as a mathematical representation of the relationship between the bus voltage (magnitude and frequency) and the power (active and reactive) consumption by the load or the current flowing into the load [9].

In general, a load can be modelled using two different approaches based on the load characteristics with respect to time. The first approach is based on a static load model and the second is on a dynamic load model. In the static model, the load response with the variation of voltage is considered as instantaneous. On the other hand, in the dynamic model, the load response is not instantaneous but is a function of time. Both static and dynamic load models can be implemented using two ways. One is the physical modelling approach and the other is the black box modelling approach. The physical model is based on the fundamental engineering knowledge about the physical phenomenon. The physical model is able to provide satisfactory results when it is simulated for a relatively simple system. However, in most practical cases, when the system is more complex, due to the difficulties in obtaining all the physical parameters that affect the system, it is often useful to use the empirical relationship between input and output characteristics of the system. When model is based on the empirical relationships, the model is called the measurement based model or empirical model or black-box model. Measurement based model is often applied to a complex system and it establishes the relationship between inputs and outputs based on measured data [6].

In this chapter, detailed studies of various static and dynamic load modelling approaches using either physical approach or measurement-based approach are presented.

1.3 Static Load Modelling

Static load can be described as the relationship of the real and the reactive power flow in a load bus as a function of load bus voltage at any instant of time. Resistive and lighting loads are examples of the static load. Static load models can be classified into different categories [5-9, 10, 11]:

- Constant impedance load model;
- Constant current load model;
- Constant power load model;
- Polynomial load model;
- Exponential load model.

1.3.1 Constant Impedance Model

Constant impedance model can be defined as a model where the load power is proportional to the square of the load voltage [9]. Mathematically, the constant impedance model can be defined by the following equations [9]:

$$P = P_O\left(\frac{V}{V_O}\right)^2 \tag{1.1}$$

$$Q = Q_O\left(\frac{V}{V_O}\right)^2 \tag{1.2}$$

1.3.2 Constant Current Model

Constant current model can be defined as a model where the load power is directly proportional to the load voltage [9]. Mathematically, the constant current model can be defined by the following equations [9]:

$$P = P_O\left(\frac{V}{V_O}\right) \tag{1.3}$$

$$Q = Q_O\left(\frac{V}{V_O}\right) \tag{1.4}$$

1.3.3 Constant Power Model

Constant power model can be defined as a model where the load power is not a function of load voltage [9]. In case of the constant power model, the load power remains constant regardless any variation occurs in bus voltage. Mathematically, the constant power model can be defined by the following equations [9]:

$$P = P_O \tag{1.5}$$

$$Q = Q_O \tag{1.6}$$

In Eqs (1.1) – (1.6), P_O and Q_O are the pre-disturbance real and reactive power consumption by load bus, respectively; P and Q are the post-disturbance power real and reactive consumption, respectively; V is the load bus voltage after disturbance; V_O is the pre-disturbance voltage of the load bus.

1.3.4 Polynomial Load Model

Polynomial load model can be defined as the load power is a polynomial function of bus voltage [9]. Polynomial load model can be expressed mathematically by the following equations [9]:

$$P = P_O\left(a_O\left(\frac{V}{V_O}\right)^2 + a_1\left(\frac{V}{V_O}\right) + a_2\right) \tag{1.7}$$

$$Q = Q_O\left(a_3\left(\frac{V}{V_O}\right)^2 + a_4\left(\frac{V}{V_O}\right) + a_5\right) \tag{1.8}$$

In Eqs (1.7) – (1.8), P_O and Q_O are the pre-disturbance real and reactive power consumption by load bus, respectively; P and Q are the post-disturbance power real and reactive consumption, respectively; V is the load bus voltage after disturbance; V_O is the pre-disturbance voltage of the load bus.

From Eqs (1.7) – (1.8), parameters a_O and a_3 determine the percentage of constant impedance load characteristics, a_1 and a_4 determine the percentage of constant current load characteristics and a_2 and a_5 determine the percentage of constant power load characteristics in the load bus.

Fig. 1.2 shows the graphical representation of the load response due to the variation of voltage magnitude for the constant impedance, constant current, constant power and polynomial models. In Fig. 1.2, the values of the parameters are as: $P_O = Q_O = 2.5$ (pu), $a_O = a_3 = 0.3$, $a_1 = a_4 = 0.4$, and $a_2 = a_5 = 0.3$.

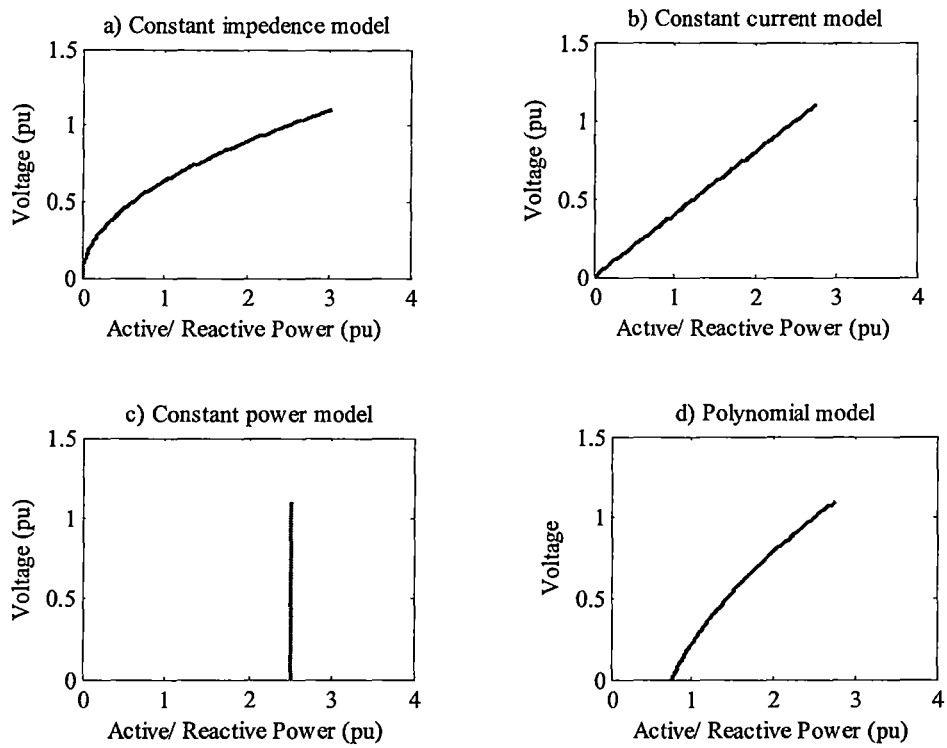

Figure 1.2. Graphical representation of characteristics of the constant impedance, constant current, constant power and polynomial load models.

1.3.5 Exponential Load Model

Exponential load model is defined as the active and reactive power of the load is an exponential function of the bus voltage [9]. The mathematical expression of the exponential load model is given below [9]:

$$P = P_O\left(\frac{V}{V_O}\right)^{np} \tag{1.9}$$

$$Q = Q_o\left(\frac{V}{V_o}\right)^{nq} \tag{1.10}$$

where, as above P_o and Q_o are the pre-disturbance real and reactive power consumption by load bus, respectively; P and Q are the post-disturbance power real and reactive consumption, respectively; V is the load bus voltage after disturbance and V_o is the pre-disturbance voltage of the load bus.

Parameters np and nq describe the real and reactive power dependency of bus voltage. The exponent value of np (or nq) is nearly equal to the value of the slope of the active power (or reactive) variation with respect to the change of voltage. Typical values of np normally range from 0.5 to 1.8 for different loads while typical values of nq normally range from 1.5 to 6. Common values of np and nq are given for different load in Table 1.1.

Table 1.1: Voltage dependency parameters (np and nq) for static load.

Load	np	nq
Air conditioner	0.50	2.50
Space heater	2.00	0.00
Fluorescent light	1.00	3.00
Pumps, fans and other motors	0.08	1.60
Small induction motor	0.05	0.50
Large induction motor	0.10	0.60

Fig. 1.3 and Fig. 1.4 show the graphical representation of load response of an air conditioner, space hearer, fluorescent light and induction motor.

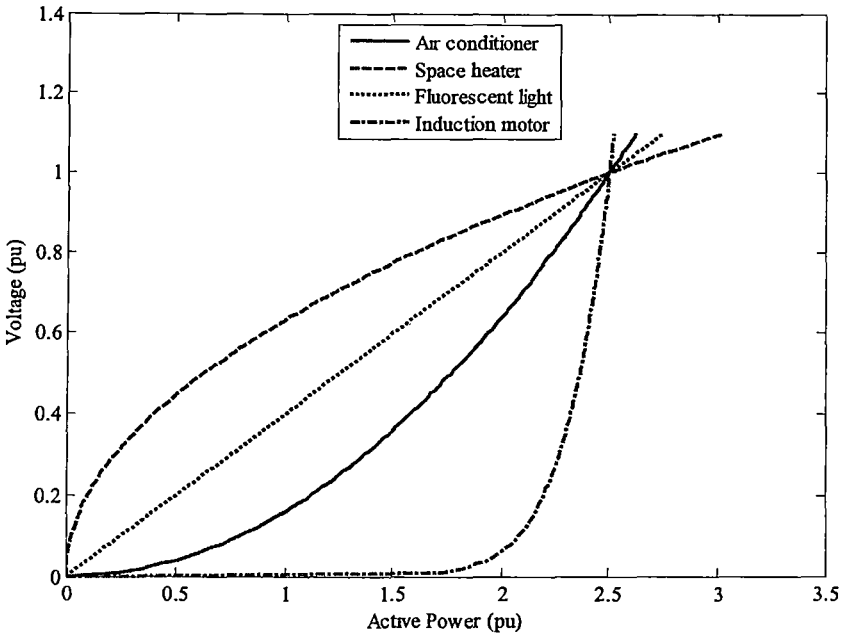

Figure 1.3. Active power response due to voltage variation of air conditioner, space hearer, fluorescent light and induction motor.

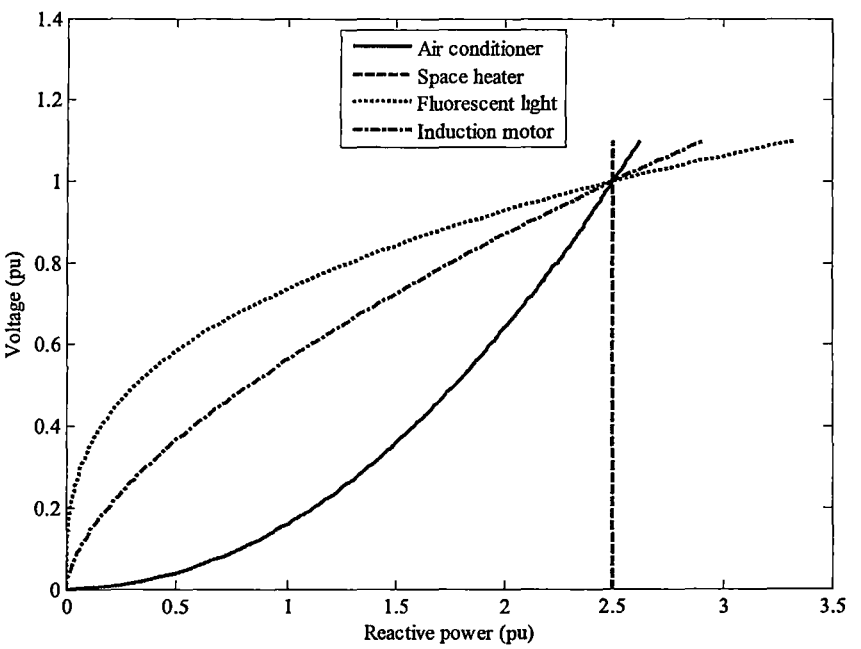

Figure 1.4. Active power response due to voltage variation of air conditioner, space hearer, fluorescent light and induction motor.

1.4 Dynamic Load Modelling

A dynamic model can be expressed as the relationship between active and reactive power of the load bus at any instant of time as function of voltage magnitude not only at that same instant of time but also at the past instant of time. Differential equations are used to represent the dynamic loads. Dynamic model can be classified in two categories [9, 12-16].

- Exponential load recovery model
- Adaptive load recovery model

1.4.1 Exponential Load Recovery Model

Exponential load recovery model are used to capture the dynamic characteristics of the load restoration with an exponential recovery process [6]. The mathematical expression for the exponential load recovery model is given in the following [6]:

$$T_p \frac{dP_r}{dt} + P_r = P_O\left(\frac{V}{V_O}\right)^{\alpha_s} - P_O\left(\frac{V}{V_O}\right)^{\alpha_t} \tag{1.11}$$

$$P_d = P_r + P_O\left(\frac{V}{V_O}\right)^{\alpha_t} \tag{1.12}$$

$$T_q \frac{dQ_r}{dt} + Q_r = Q_O\left(\frac{V}{V_O}\right)^{\beta_s} - Q_O\left(\frac{V}{V_O}\right)^{\beta_t} \tag{1.13}$$

$$Q_d = Q_r + Q_O\left(\frac{V}{V_O}\right)^{\beta_t} \tag{1.14}$$

1.4.2 Adaptive Load Recovery Model

In adaptive load model, the power demand is represented by a non-linear function of voltage multiplied by its recovering load stages. Mathematical representation of the adaptive load recovery model is as follows [16]:

$$T_p \frac{dP_r}{dt} = P_O\left(\frac{V}{V_O}\right)^{\alpha_s} - P_r\left(\frac{V}{V_O}\right)^{\alpha_t} \tag{1.15}$$

$$P_d = P_r\left(\frac{V}{V_O}\right)^{\alpha_t} \tag{1.16}$$

$$T_q \frac{dQ_r}{dt} = Q_O\left(\frac{V}{V_O}\right)^{\beta_s} - Q_r\left(\frac{V}{V_O}\right)^{\beta_t} \tag{1.17}$$

$$Q_d = Q_r\left(\frac{V}{V_O}\right)^{\beta_t} \tag{1.18}$$

where, T_p and T_q are the exponential load recovery time constants for active power and reactive power, respectively; P_r and Q_r are the active power and reactive power recovery, respectively; P_d and Q_d are the active and reactive power demand, respectively; P_O and Q_O are the active power and reactive power consumption by the load at the pre-fault voltage, respectively; V is the supply voltage; V_O is the pre-fault supply voltage; α_s is the steady-state active power-voltage dependency; β_s is the steady-state reactive power-voltage dependency; α_t is the transient active power–voltage dependency and β_t is the transient reactive power-voltage dependency.

The block diagram representing the exponential load recovery model and the adaptive load recovery model is shown in Fig. 1.5 and Fig. 1.6.

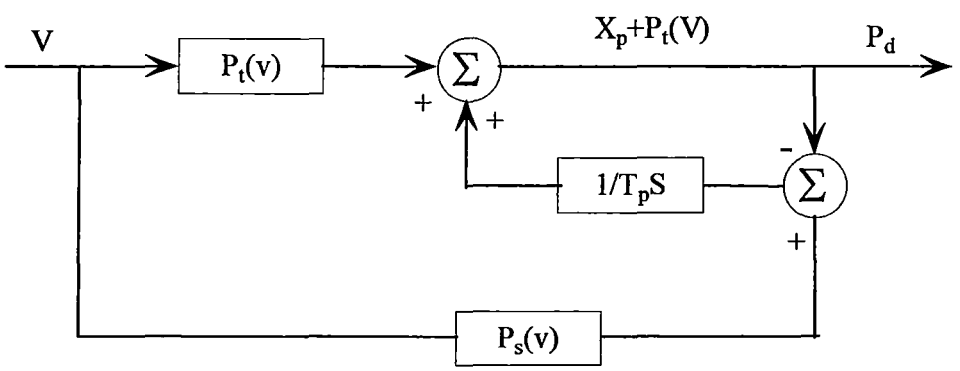

Figure 1.5. Block diagram of the exponential recovery model.

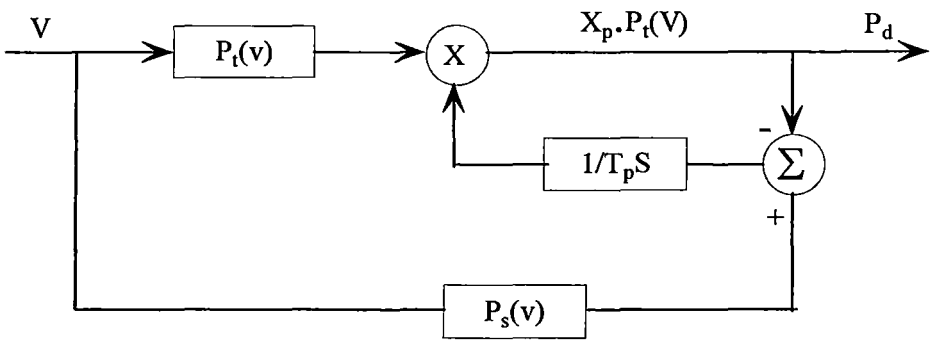

Figure 1.6. Block diagram of the adaptive recovery model.

In the dynamic load model, the load behaviour is characterised by a time constant, a transient, and a steady state power-voltage dependency. The time constant (T_p or T_q) represents the time that is required to reach the output power of about 63% of its final value. The steady-state active/ reactive load voltage dependency (α_s or β_s) represents how much of the active or reactive power is restored after recovery. A value of 0 (zero) represents the full power recovery while values other than zero mean partial recovery. The negative value of the power-voltage dependency represents an overshoot of the load after recovery. Similarly, the transient active/ reactive load–voltage dependency (α_t or β_t) represents how the load behaves during transient conditions. The value of transient power-voltage dependency equals to 0 represents the load behaviour during the transient conditions similar to a constant power load, while the values of 1 and 2 represent the load behaviour similar to constant current and constant impedance load, respectively. The graphical representation of the dynamic power restoration process due to voltage variation is shown in Fig. 1.7.

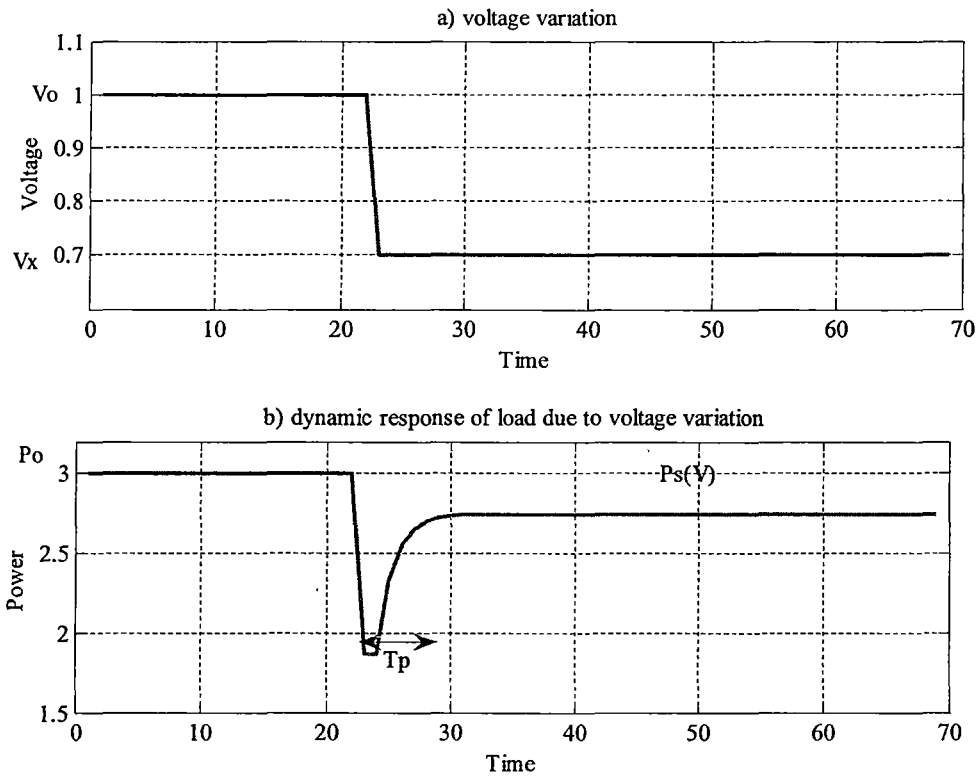

Figure 1.7. a) voltage drop and b) Dynamic response of the load due to voltage variation.

1.4.3 Linearization and parameter optimization of the dynamic model

Dynamic models consist of a set of non-linear equations, Eqs (1.11) – (1.18), where the real and reactive power have a non-linear dependency on voltage variations of the load bus. The non-linear equations are useful in simulating load power due to large variations in bus voltage. However, in practical cases, while small disturbances may occur frequently, the possibility of a large voltage variation is relatively low. Thus, in order to simplify an estimation of the model parameters for small disturbance analysis using conventional mathematical tools, linearization process is often used [6, 7, 17, 18].

Linearisation of Eqs (1.11) and (1.12) is obtained on operating voltage V_p. Small deviation of the operating voltage is denoted by Δ. Eq. (1.11) becomes as follows:

$$T_p \frac{d\Delta P_r}{dt} + \Delta P_r = \alpha_s P_O \left(\frac{V_p}{V_O}\right)^{\alpha_s - 1} \left(\frac{\Delta V}{V_O}\right) - \alpha_t P_O \left(\frac{V_p}{V_O}\right)^{\alpha_t - 1} \left(\frac{\Delta V}{V_O}\right) \tag{1.19}$$

Eq. (1.12) can be rewritten as:

$$\Delta P_d = \Delta P_r + \alpha_t P_O \left(\frac{V_p}{V_O}\right)^{\alpha_t - 1} \left(\frac{\Delta V}{V_O}\right) \tag{1.20}$$

Let us consider

$$A_s = \alpha_s \left(\frac{V_p}{V_O}\right)^{\alpha_s - 1}, \tag{1.21}$$

$$A_t = \alpha_t \left(\frac{V_p}{V_O}\right)^{\alpha_t - 1}, \text{ and} \tag{1.22}$$

$$v = \left(\frac{\Delta V}{V_O}\right). \tag{1.23}$$

The space state representation of Eqs (1.19) and (1.20) are given by:

$$T_p \frac{d\Delta P_r}{dt} + \Delta P_r = A_s P_o v - A_t P_o v \tag{1.24}$$

$$\Delta P_d = \Delta P_r + A_t P_o v \tag{1.26}$$

Applying Laplace transformation in Eq. (1.19);

$$sT_p \Delta P_r + \Delta P_r = A_s P_o v - A_t P_o v$$

$$\Rightarrow (sT_p + 1)\Delta P_r = (A_s - A_t)v$$

$$\Rightarrow \Delta P_r = P_o v \frac{(A_s - A_t)}{(sT_p + 1)} \tag{1.27}$$

By substituting the value of ΔP_r from Eq. (1.27) to Eq. (1.26),

$$\Delta P_d = P_o \left(v \frac{(A_s - A_t)}{(sT_p + 1)} + A_t v \right) \tag{1.28}$$

$$\Rightarrow \frac{\Delta P_d}{P_o} = v \frac{(A_s - A_t)}{(sT_p + 1)} + A_t v$$

$$\Rightarrow \frac{\Delta P_d}{P_o} = \frac{v(A_s - A_t) + A_t v(sT_p + 1)}{(sT_p + 1)}$$

$$\Rightarrow \frac{\Delta P_d}{P_o} = v\left(\frac{A_s + sA_tT_p}{(sT_p + 1)}\right) \tag{1.29}$$

Eq. (1.28) represents the deviation of load when the voltage change occurs. The equation is characterized by three parameters A_s, A_t, and T_p. A_s represents the steady-state dependency of power-voltage, A_t represents the transient dependency of power-voltage, and T_p is the time constant. Applying the final value theorem, replacing $s = 0$ in the Laplace domain, the steady state time domain solution can be fond. As a result, the steady-state parameter A_s can be determined from Eq. (1.29):

$$A_s = \frac{\frac{\Delta P_d}{P_0}}{\frac{\Delta V}{V_0}} \tag{1.30}$$

where ΔP_d is the difference between the pre-disturbance load power P_O and the final steady-state load power P. Also, ΔV is the difference between the initial pre-disturbance voltage V_0 and the voltage after the step change V_x.

Applying the initial value theorem, replacing $s = \infty$, the transient parameter A_t can be determined from Eq. (1.29):

$$A_t = \frac{\frac{\Delta P_d}{P_0}}{\frac{\Delta V}{V_0}} \tag{1.31}$$

In this case, ΔP_d is the difference between the pre-disturbance power P_0 and the transient power which occurs immediately after the step-change in voltage magnitude.

The value of α_s can be obtained by substituting the value of A_s from Eq. (1.30) to Eq. (1.21) while the value of α_t can be obtained the value of A_t from Eq. (1.31) to Eq. (1.22).

The parameter vector $(\theta = \alpha_s, \alpha_t, T_p)$ of the exponential recovery model is different for each load and even it can vary for the composite load based on the time

and season. The parameters of the exponential load recovery model are generally obtained using a measurement based approach. The identification of the parameter values of static models is straightforward, compared to identifying the parameters in dynamic load models using normal operation data. The algorithm of capturing an optimum value of the parameters uses N samples of the input signal as voltage $V(t_k)$ and the output signal as power $P(t_k)$. The objective here is to optimise the parameter vector $(\theta = \alpha_s, \alpha_t, T_p)$ in such a way that the difference between the input signal and output signal is minimised [13, 17, 19]. The measured data corresponds to the load power subject to variations of the bus voltage. The objective function is to be minimised using a quadratic least square criterion is:

$$F(\theta) = \sum_{k=1}^{N} (P_{simulated}(t_k, \theta) - P_{measured}(t_k, \theta))^2 \qquad (1.32)$$

Replacing $P_{simulated}(t_k, \theta)$ by the $(P_o + \Delta P_d)$, where P_o is the pre-disturbance power and ΔP_d is the measured variation of power due to disturbance.

where, $\Delta P_d = P_o . \dfrac{A_s + sA_t T_p}{1 + sT_p}$;

$\Delta P_d = P_o - P_{simulated}(t_k, \theta)$;

$\Delta V = (V_O - V(t_k, \theta))$;

1.5 Application of load models

Models discussed in this chapter are suitable for different types of loads based on their characteristics. Static models are suitable for loads such as air conditioner, water heater, deep fryer, dishwasher, cloths washer and dryer, refrigeration, television, incandescent, florescent lights, and so on because of their instantaneous response to voltage variation. Loads like induction motor, OLTC (on load tap changer) exhibit dynamic response due to a voltage variation and hence they are modelled using dynamic load models. Some industrial loads, on the other hand, such as electric arc furnace, rolling mills exhibit complex relationships between the input voltage and the output power. Those loads follow highly random and time

varying relationships with the voltage and power consumption. Fig. 1.8 shows the time series data of the arc voltage and power (real and reactive):

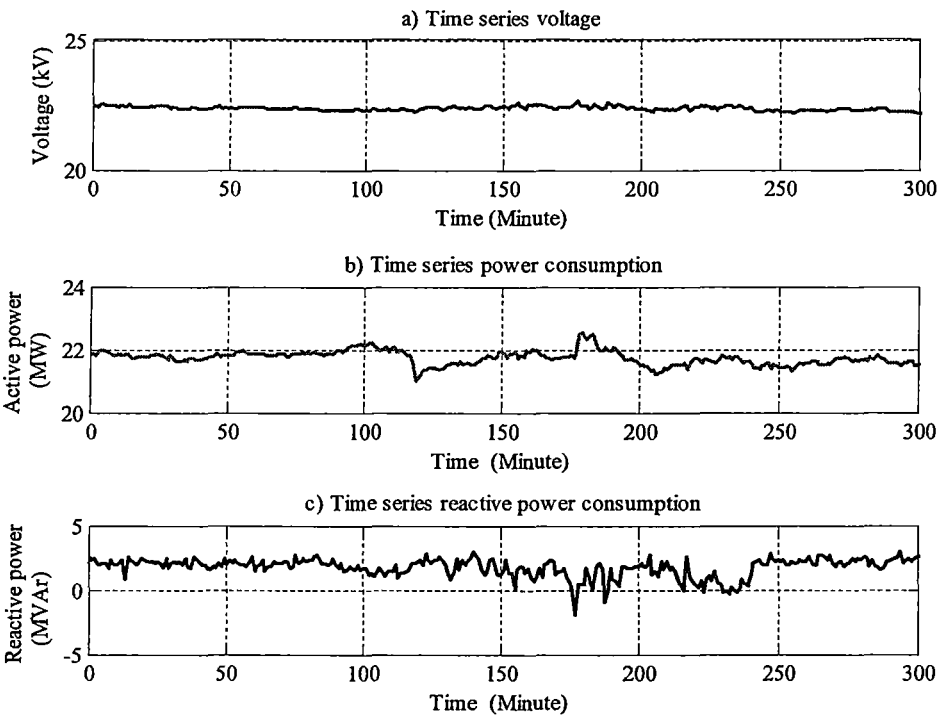

Figure 1.8. Time series arc voltage and power (real and reactive) of arc furnace

It is apparent from Fig. 1.8, that although the bus voltage of the arc furnace remains almost constant, both the active and reactive power consumption vary randomly.

In order to establish a relationship between the arc voltage and the power consumption (both real and reactive), the exponential model (discussed in Section 1.2.5) is applied. In order to do so, the first task is to determine the load voltage dependency parameters (np and nq). Measurement based approach is adopted to determine the value of the load voltage dependency parameters. Mathematically, load voltage dependency parameter can be obtained in the following.

From Eq. (1.9) in Section 1.2.5:

$$P = P_o\left(\frac{V}{V_o}\right)^{np} \qquad \Rightarrow \ln(P) = \ln\left(P_o\left(\frac{V}{V_o}\right)^{np}\right)$$

$$\Rightarrow \ln(P) = \ln(P_o) + \ln\left(\left(\frac{V}{V_o}\right)^{np}\right) \qquad \Rightarrow \ln(P) - \ln(P_o) = np \ln\left(\frac{V}{V_o}\right)$$

$$\Rightarrow \ln\left(\frac{P}{P_o}\right) = np \ln\left(\frac{V}{V_o}\right) \qquad \Rightarrow np = \frac{\ln\left(\frac{P}{P_o}\right)}{\ln\left(\frac{V}{V_o}\right)} \tag{1.33}$$

Reactive power voltage dependency constant (nq) can also be obtained by following the similar procedure from Eq. (1.10).

$$nq = \frac{\ln\left(\frac{Q}{Q_o}\right)}{\ln\left(\frac{V}{V_o}\right)} \tag{1.34}$$

By substituting the values of the arc voltage, real and reactive power, the parameters are calculated and plotted in Fig. 1.9.

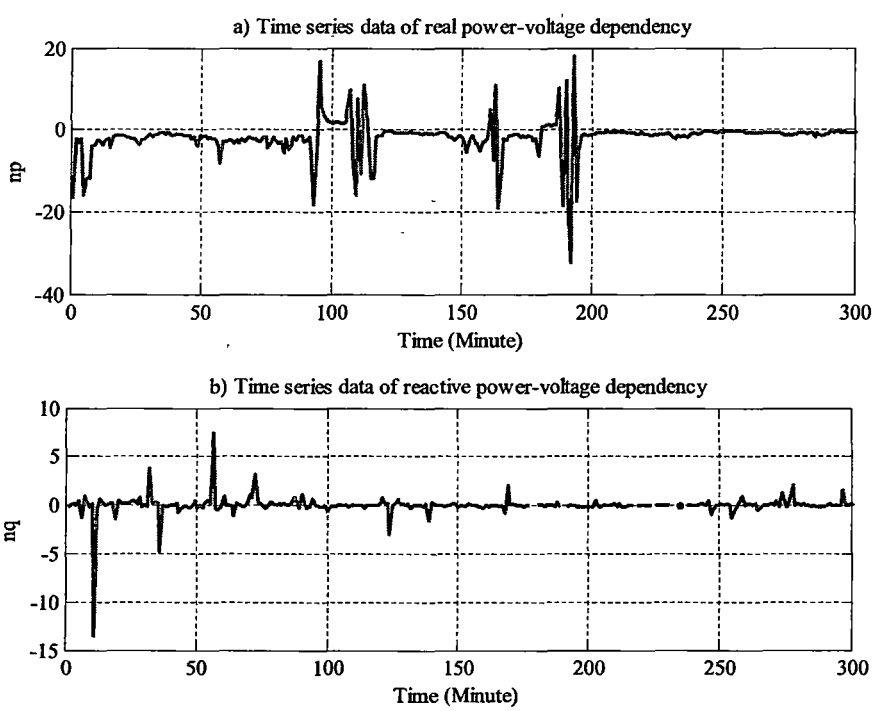

Figure 1.9. Graphical representation of the load voltage dependency for the arc furnace: a) active power-voltage dependency, b) reactive power voltage dependency.

From Fig. 1.9, it is apparent that the static value of load-voltage parameter is not constant over time for loads the electric arc furnace; rather it is highly random and time variant. As a result it is obvious that the exponential static model alone is not useful for modelling of an arc furnace. Later in this thesis, artificial intelligence techniques will be applied in conjunction with this model to extract the nonlinear time variant pattern of arc furnace load pattern.

Let us now investigate the behaviour of the arc furnace. To model arc furnace, linearization form of the exponential load recovery model is used. The first step is to obtain the value of the parameter vector $(\theta = \alpha_s, \alpha_t, T_p)$ using the measurement based approach. The graphical representation of the voltage disturbance of the arc furnace load bus and the response of the arc furnace load due to this disturbance is shown in Fig. 1.10.

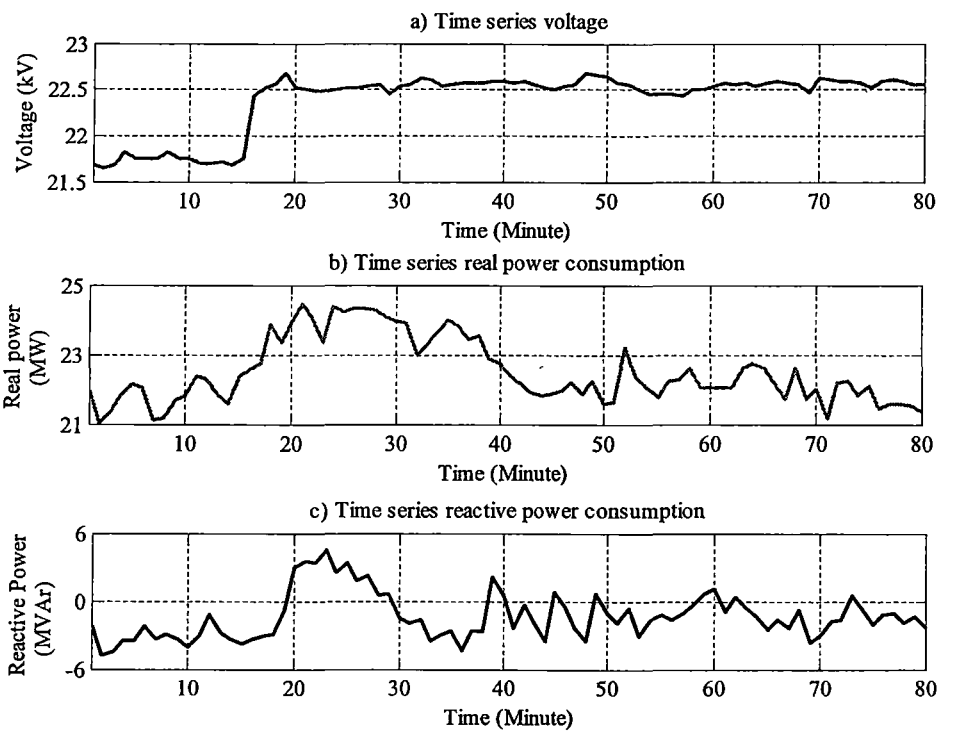

Figure 1.10. Time series arc voltage and power (real and reactive) of arc furnace to investigate dynamic response

From Fig. 1.10, it can be seen that a sharp voltage variation occurs at time of 16 minutes where the voltage raises from 21.7 k volts to 22.45 k volts. In response to

the voltage variation, the real and the reactive power also change sharply. The steady-state and transient exponential parameters (α_s and α_t) of the exponential recovery model for real power can be determined by using Eqs (1.21), (1.30), (1.22), and (1.31). For example, the steady-state exponential parameter requires the value of pre-disturbance voltage (V_O), the difference between pre-disturbance voltage and post disturbance voltage (ΔV), pre-disturbance average power (P_O), and the difference between the pre-disturbance and the steady state post disturbance power (ΔP). The value of pre-disturbance voltage (V_O) is obtained by averaging of the bus voltage from time of 1 minute to approximately time of 16 minute. The post disturbance voltage is the average value of the load voltage from time of 17 minute to time of 80 minute. Similarly, pre-disturbance power (P_O) is obtained by averaging of the consumed real power from time of 1 minute to approximately time of 16 minutes. The steady-state post disturbance power is determined by averaging the data from time of 55 minutes to time of 80 minutes. The steady stage quantity (A_s) is obtained by substituting the values ΔP, P_O, ΔV, and V_O in Eq. (1.21). Using similar approach, transient quantity (A_t) is also obtained. Steady state exponential parameter (α_s) is evaluated by equating Eqs (1.21) and (1.30) and transient exponential parameter (α_t) is evaluated by equating Eqs (1.22) and (1.31). The representation of the arc furnace load response is shown in Fig. 1.10.

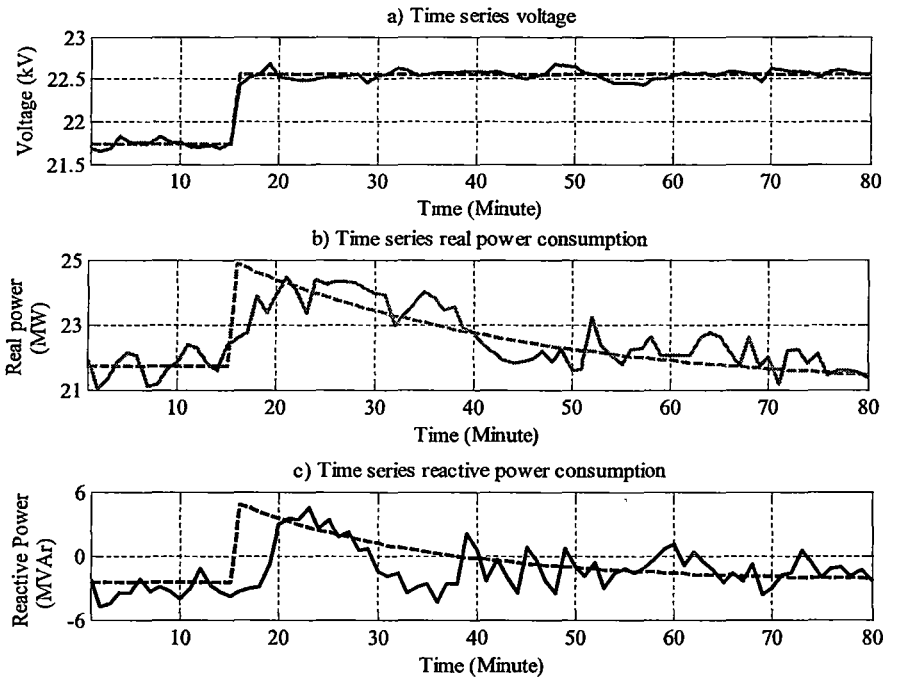

Figure 1.11. Modelling of arc furnace load responses due to a voltage variation using dynamic load modelling technique, a) real power response, b) reactive power response.

In Fig. 1.11, the solid line represents the real data and the dotted line represents the simulated value. It is apparent that, the arc furnace response is dynamic after a voltage variation and the linear exponential dynamic recovery model is capable to extract the dynamic nature of arc furnace response. However, this model is unable to characterise the chaotic and the time varying pattern of the arc furnace response.

1.6 Conclusion

This chapter discussed different definitions and classifications of load. A brief overview of composite load bus and the challenges of the evaluation of load component in the composite bus were presented. Details of different load modelling techniques were also provided. A study of the arc furnace behaviour and its modelling was presented. It was demonstrated that an exponential load model (static model) and a dynamic exponential recovery model (dynamic model) failed to

capture the arc furnace behaviour because of the random and time varying nature of the relationship between the arc voltage and power.

Chapter 2: Conventional modelling approach of arc furnace

2.1 Introduction

The main focus of this chapter is to investigate the use of conventional approaches to modelling an arc furnace. In conventional approaches, arc furnaces can be modelled on the basis of their physical properties using mathematical formulas. Conventional modelling approaches are useful in simulating the arc furnace voltage and current responses in a continuous time domain, and hence can be used for harmonics analysis of the arc voltage and current. However, in practical cases, the arc current and the arc voltage are not static; rather they are highly time-varying and random. In order to predict the dynamic characteristics of the arc furnace, a random noise can be added to conventional models. These dynamic models of the arc furnace are useful for flicker analysis.

A number of conventional methods have been developed and used in this research as outlined as below:

- Model 1 is based on a piece-wise linear approximation of the relationship between the arc voltage and the arc current in different operating regions [20, 21].
- Model 2 is based on a piece-wise linear approximation of the relationship between the arc voltage and the arc current in different operating regions, which is derived from the arc model proposed by Cassie [22].
- Model 3 is based on a piece-wise non-linear approximation of the relationship between the arc voltage and the arc current in different operating regions [23, 24].
- Model 4 establishes the relationship between the arc voltage and the arc current based on the relationship between the arc voltage and the arc electrode length [25].

- Model 5 establishes the relationship between the arc voltage and the arc current based on the non-linear characteristics of current controlled time-varying arc resistance [26].
- Model 6 establishes the relationship between the arc voltage and the arc current based on Mayr's arc model [27].
- Model 7 establishes the relationship between the arc voltage and the arc current based on the time switch model of an arc furnace [28].

Detailed studies of these models are outlined in the following sections.

2.2 Model 1

Model 1 is based on the piece-wise linear approximation of the relationship between the arc voltage (v) and the arc current (i) in different operating regions [20, 21]. The mathematical representation of the arc voltage is as follows:

$$v = \begin{cases} iR_1; & 0 \le i \le i_{ig} \\ iR_2 + V_{ig}(1 - \dfrac{R_2}{R_1}); & i_{ig} < i \le i_{ex} \end{cases} \tag{2.1}$$

From Eq. (2.1), the arc voltage (v) is a multi-valued function of the arc current (i) and each cycle of the arc voltage can be separated into two stages. The first stage is the pre-ignition stage, which represents the first part of Eq. (2.1) and the second stage is the ignition stage which represents the second part of Eq. (2.1). R_1 in Eq. (2.1) represents the arc resistance in the pre-ignition stage. Arc ignites during the ignition stage when the arc current reaches the arc ignition current (i_{ig}). During this stage, a negative resistance (R_2) is developed in conjunction with the resistance in the pre-ignition stage (R_1). The arc extinguishes and returns back to its pre-ignition stage when the arc current is below some specific current known as the arc extinction current (i_{ex}). The mathematical representation of the arc ignition current (i_{ig}) and the arc extinction current (i_{ex}) is shown as follows:

$$i_{ig} = \frac{V_{ig}}{R_1} \tag{2.2}$$

$$i_{ex} = \frac{V_{ex}}{R_2} - V_{ig}\left(\frac{1}{R_2} - \frac{1}{R_1}\right) \tag{2.3}$$

where, V_{ig} and V_{ex} represents the arc ignition voltage and the arc extinction voltage respectfully.

The graphical representation of the $(v-i)$ characteristics of the arc furnace is shown in Fig. 2.1.

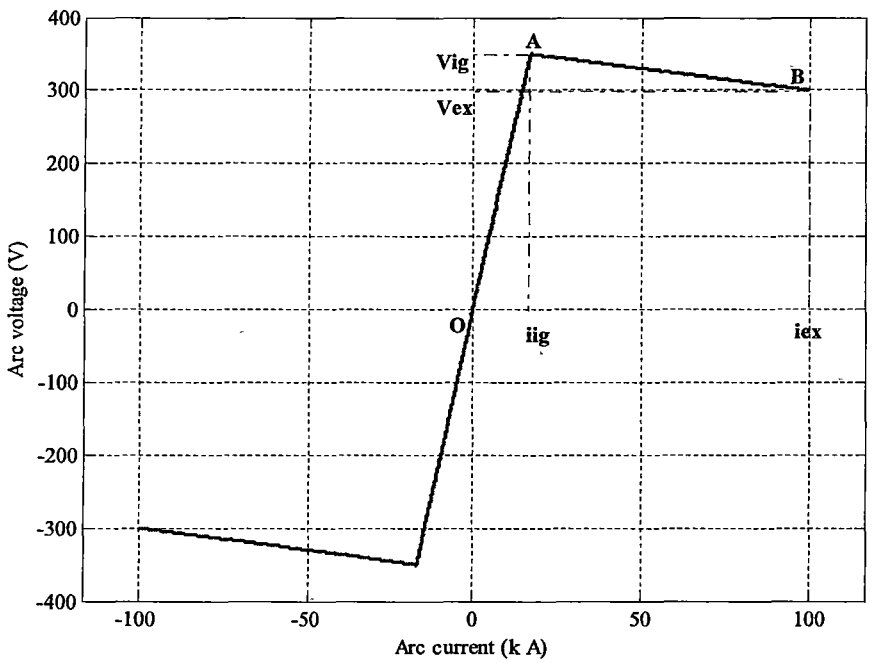

Figure 2.1. The $v-i$ characteristic of Model 1.

In Fig. 2.1, the segment OA represents the pre-ignition stage and the slope of the line OA represents the arc resistance (R_1) of this stage. The segment AB represents the ignition stage and the slope of this segment represents the arc resistance (R_2). Normally the value of the R_1 is assumed to be several times higher than the value of R_2.

However, in practical cases, because of the random nature of the arc furnace, all $(v-i)$ cycles of the arc furnace are different from each other and the parameters describing the furnace behaviour change randomly. Dynamic behaviour of the arc

furnace can be represented by incorporating stochastic changes of the arc resistance, R_1 in Eq. (2.1). In the case of the white noise variation, the dynamic arc resistance is shown as follows:

$$R_1(t) = R_1(1 + BLW) \tag{2.4}$$

where, BLW is the white noise.

Following assumptions are undertaken to investigate the dynamic properties of Model 1:

- Measures must be taken to ensure that the arc resistance remains constant for at least half of a cycle of the fundamental frequency.
- Variation of the arc resistance from each half cycle ensures the non-symmetry of the $(v-i)$ characteristics of Model 1, which matches the characteristics of the real arc furnace. Fig 2.2 shows the time series white noise.

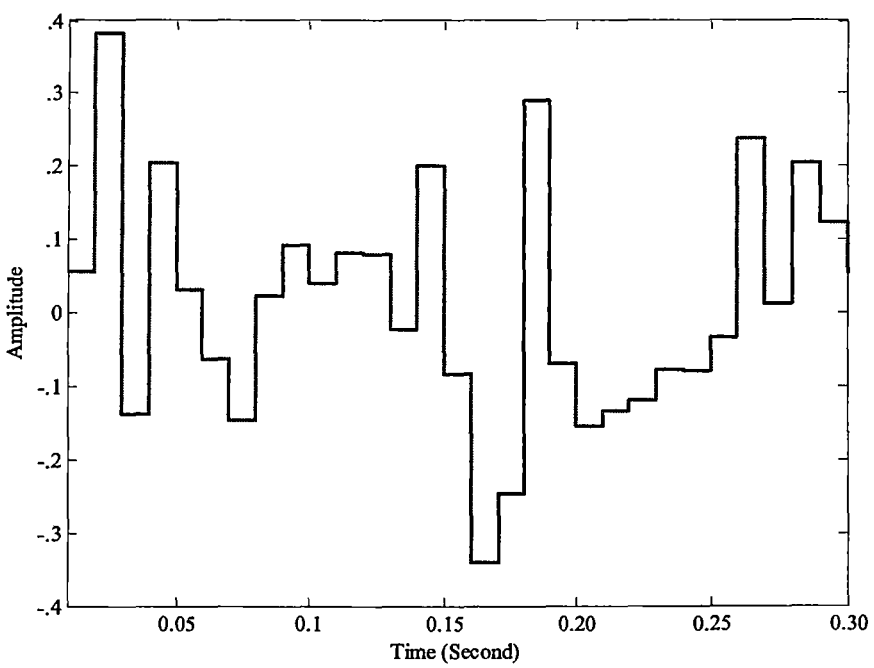

Figure 2.2. Variation of arc resistance using a white noise.

The dynamic $v-i$ characteristic of the arc furnace is shown in Fig. 2.3.

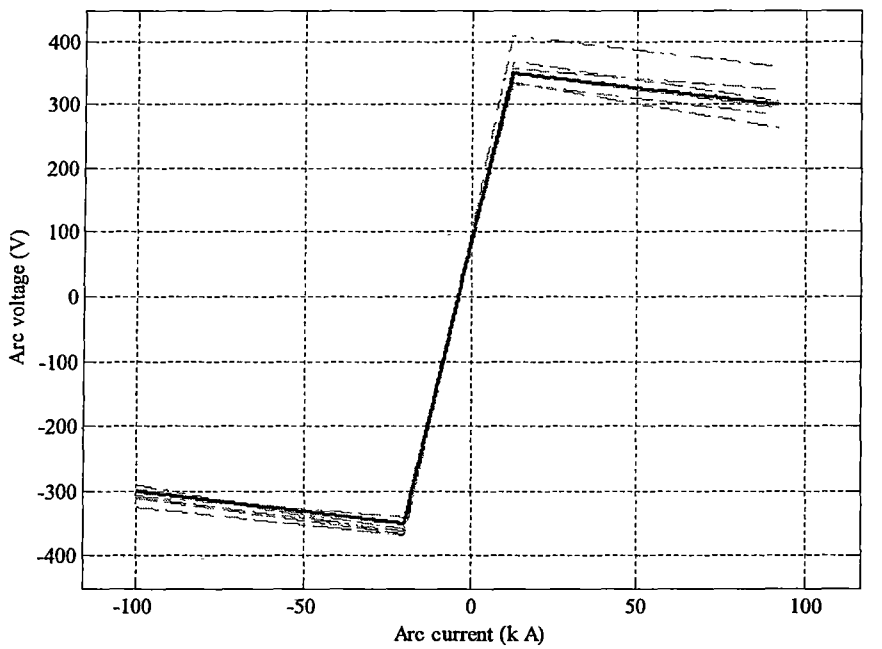

Figure 2.3. Dynamic $(v-i)$ characteristic of Model 1.

In Fig. 2.3, the solid bold line represents the $(v-i)$ characteristics of Model 1 without the white noise; and the dotted line represents the $(v-i)$ characteristics of Model 1 subject to the white noise of the arc resistance (R_1). It is evident from Fig. 2.3 that for each cycle of the $(v-i)$ characteristic, the arc ignition voltage varies with the variation of the arc resistance (R_1). An increase of the arc resistance (R_1) due to the noise results a proportional increment of the arc ignition voltage (V_{ig}) and the arc extinction voltage (V_{ex}). However, the ignition current (i_{ig}) and the arc extinction current (i_{ex}) are assumed to be constant for all cycles.

2.3 Model 2

Model 2 is based on the simplified linear approximation of the $v-i$ characteristics of the high current electric arc model proposed by Cassie [22]. The mathematical representation of the arc voltage is as follows:

$$v=\begin{cases} iR_1; & \left(i\le i_1 \quad \& \quad \dfrac{di}{dt}>0\right) \quad or \quad \left(i\le i_4 \quad \& \quad \dfrac{di}{dt}<0\right) \\ R_2(i-i_1)+V_1; & i_1<i\le i_2 \quad \& \quad \dfrac{di}{dt}>0 \\ R_3(i-i_2)+V_2; & i_3<i\le i_2 \quad \& \quad \dfrac{di}{dt}<0 \\ R_4(i-i_3)+V_3; & i_4<i\le i_3 \quad \& \quad \dfrac{di}{dt}<0 \end{cases} \tag{2.5}$$

In Model 2, similar to Model 1, each cycle of the arc voltage is divided into two stages. The first one is the pre-ignition stage, which represents the first part of Eq. (2.5). The second is the ignition stage which represents the 2nd, 3rd, and the 4th parts of Eq. (2.5). A graphical representation of the $v-i$ characteristic of Model 2 is shown in Fig. 2.4.

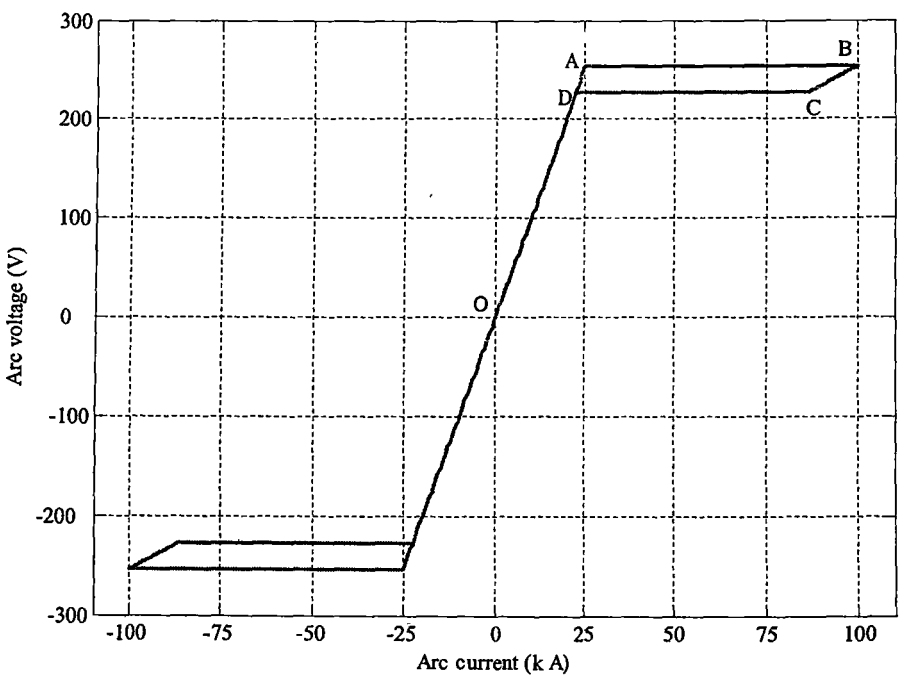

Figure 2.4. The $v-i$ characteristics of Model 2.

In Fig. 2.4, different segments (segment OA, AB, BC, CD, DO) are characterised by the arc resistances R_1, R_2, R_3, and R_4, respectively. R_1 (the slope of line OA and DO) represents the arc resistance during pre-ignition stage

when the arc goes from its extinction to the ignition stage or vice-versa. The value of R_1 is relatively high and is defined by the voltage necessary to establish the arc. R_2, R_3, and R_4 represent respected resistances when the arc is established. R_2 (the slop of the line AB) corresponds to the voltage variation during the ignition period when the arc current is increasing. R_3 (the slop of the line BC) corresponds to the arc voltage drop estimated by the degree of imbalance between phases. R_4 (the slop of the line CD) corresponds to the voltage variation during the ignition period when the arc current is decreasing.

Expressions for currents, i_1, i_2, i_3, and i_4 can be represented as follows:

$$\begin{cases} i_1 = \dfrac{V_1}{R_1} \\ i_2 = f(V_1, R_2) \\ i_3 = f(V_2, R_3) \\ i_4 = \dfrac{V_3}{R_4} \end{cases} \tag{2.6}$$

For modelling dynamic characteristics of Model 2, stochastic changes are incorporated in the arc resistance in different operating regions. The arc resistances $(R_1, R_2, R_3, and\ R_4)$ after incorporating the band limit white noise are represented in Eq. (2.7).

$$\begin{cases} R_1(t) = R_1(1 + BLW) \\ R_2(t) = R_2(1 + BLW) \\ R_3(t) = R_3(1 + BLW) \\ R_4(t) = R_4(1 + BLW) \end{cases} \tag{2.7}$$

where, BLW is the white noise.

The dynamic $v - i$ characteristic of Model 2 is shown in Fig. 2.5.

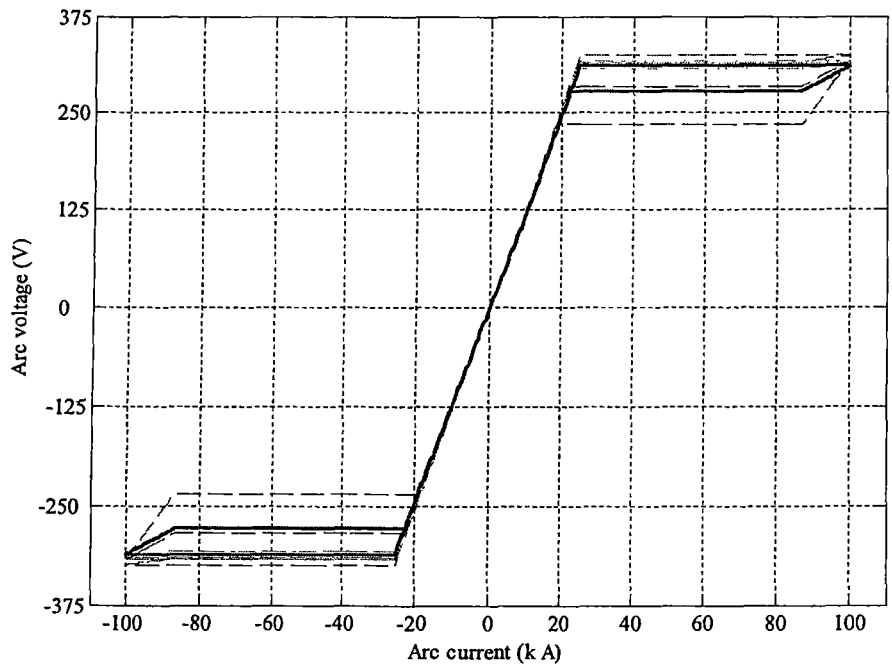

Figure 2.5. Dynamic $(v-i)$ characteristics of Model 2.

It is evident from Fig. 2.5 that the arc voltage in each part in Eq. (2.5) changes due to the changes of the arc resistance. In Fig. 2.5, the solid bold line represents the $v-i$ characteristics of Model 2 without the white noise, and the dotted line represents the $v-i$ characteristics of Model 2 subject to the white noise of the arc resistance. It can be noted that an increase of the arc resistance causes the proportional increase of the arc voltage in each part of Eq. (2.5). However, it is assumed that, due to the changes of the arc resistance, the arc current remains constant.

2.4 Model 3

Model 3 is based on the non-linear approximation of the voltage-current $(v-i)$ relationship of the arc furnace [23, 24]. In Model 3, the melting process of the arc furnace is divided into three stages. In the first stage, the arc voltage increases from the extinction voltage $(-v_{ex})$ to the arc ignition voltage (v_{ig}). During this stage, the arc furnace acts as a resistance and the arc current changes its polarity. Arc

ignites in the second stage, when the arc voltage reaches the ignition voltage (v_{ig}), which is assumed to be the beginning of the arc melting process. At the beginning of this stage, a sudden exponential voltage drop occurs in the arc electrode until the arc current increases to its peak value. The third part of Eq. (2.9) represents the same stage, when the arc voltage drops smoothly as the arc current decreases from its peak value. This stage continues until the arc voltage drops below the arc extinction voltage. The fourth part of Eq. (2.9) represents third stage, when the arc extinguishes and the system returns back to its first stage.

$$v=\begin{cases} iR_1, & 0\le i\le i_1 \quad \& \quad \dfrac{di}{dt}>0 \\ V_1+(V_{ig}-V_1)\exp\left(\dfrac{(i-i_1)}{i_T}\right), & i_1<i\le i_2 \& \dfrac{di}{dt}>0 \\ R_3(i-i_2)+V_2, & i_2<i\le i_3 \& \dfrac{di}{dt}<0 \\ iR_1, & 0\le i\le i_4 \quad \& \quad \dfrac{di}{dt}<0 \end{cases} \tag{2.9}$$

The graphical representation of the $v-i$ characteristics of Model 3 is shown in Fig. 2.6.

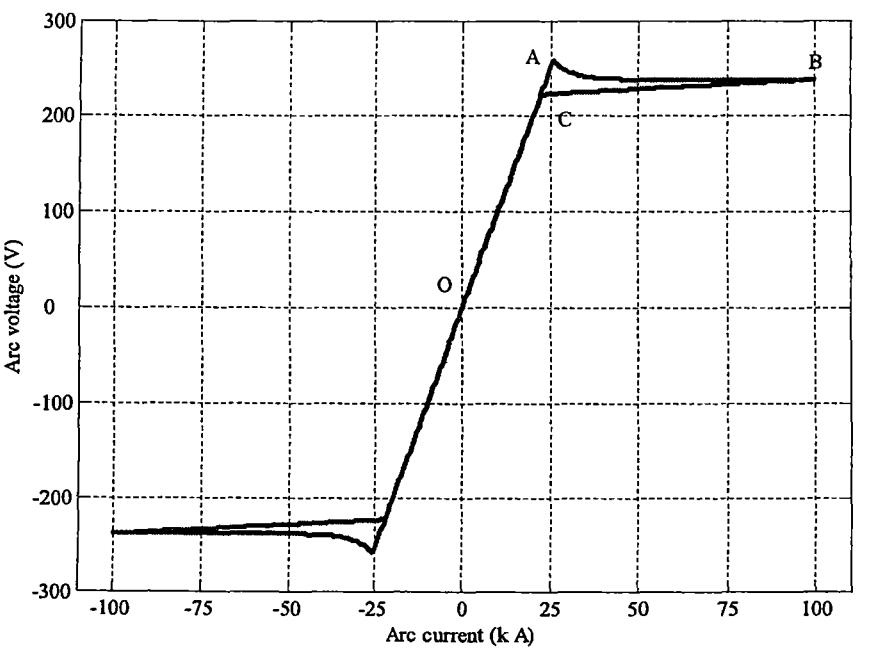

Figure 2.6. The $(v-i)$ characteristic of Model 3.

In Fig. 2.6, the slops of segments OA and OC represent the value of the resistance, R_1. The segments AB and BC represent the ignition process of the arc furnace.

In order to incorporate the dynamic properties, stochastic changes are added to the arc resistance (R_1 *and* R_3) as well as the time constant (i_T) in Eq. 2.8. The dynamic $v-i$ characteristic of Model 3 is shown is Fig. 2.7. Here the solid bold line represents the $v-i$ characteristics of Model 3 without the band limit white noise; and the dotted line represents the $v-i$ characteristics of Model 3 subject to the band limit white noise. The arc voltage changes due to random variations of the arc resistance. Similar to the previous models, the arc voltage increases due to the random increment of the arc resistances (R_1, *and* R_3). The transient condition decays fast if the time constant decreases due to the random change of the time constant (i_T).

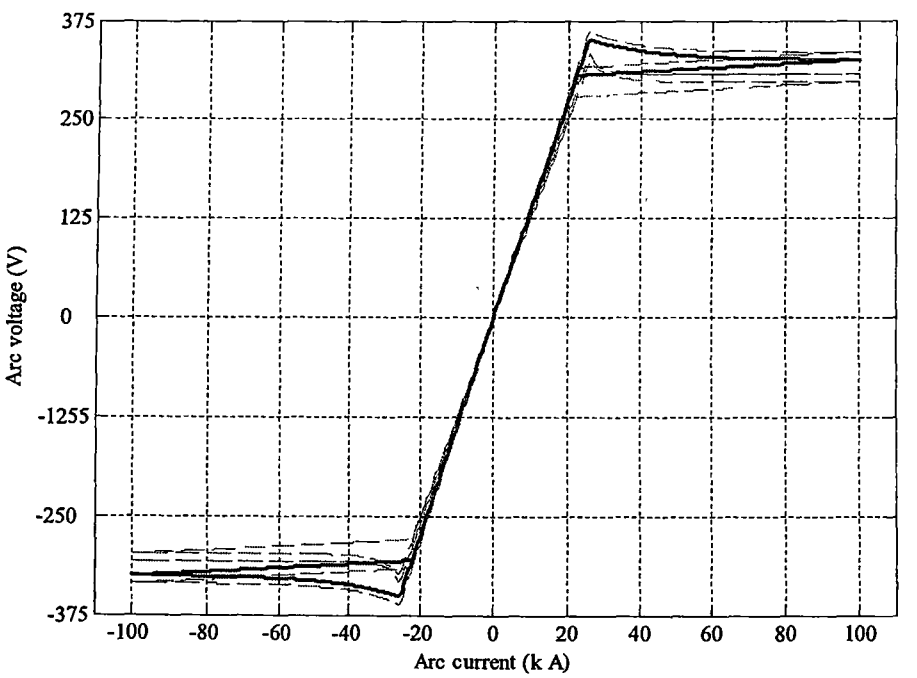

Figure 2.7. Dynamic ($v-i$) characteristic of Model 3.

2.5 Model 4

In this model, the arc voltage is considered as a function of the arc electrode length [25]:

$$v = sign(i)\left(V_D + \frac{C}{D+|i|}\right) \tag{2.9}$$

where, v and i are the arc voltage and arc current, respectively. V_D is the threshold value of the arc voltage when the arc current increases. V_D depends on arc length which is given by the following equation [25]:

$$V_D = A + Bl \tag{2.10}$$

where, l is the length of electrode, A is the constant representing the sum of the voltage drop in anode and cathode, and B is the constant representing the voltage drop per unit length.

The $v-i$ characteristic of the arc furnace is shown in Fig. 2.8.

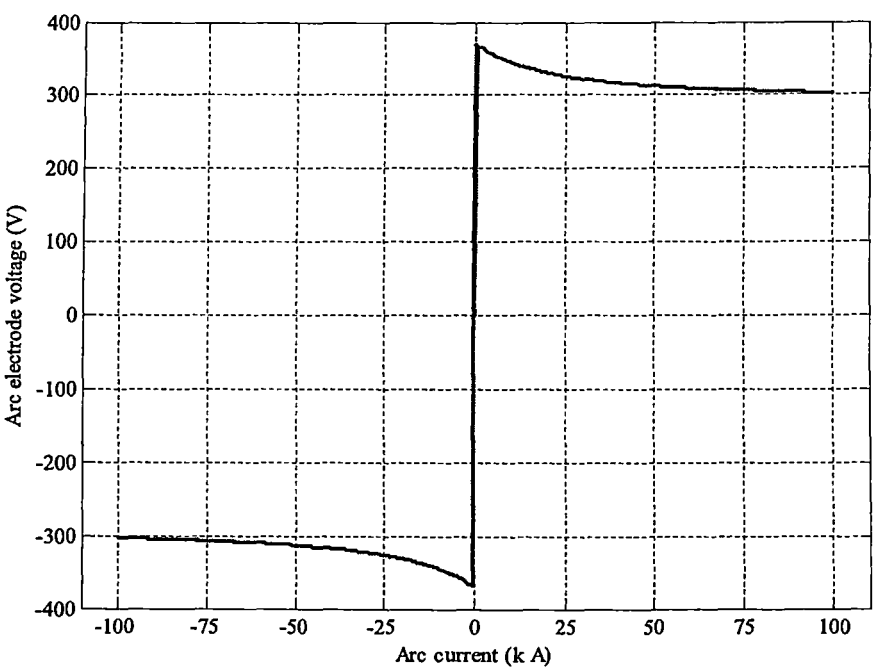

Figure 2.8. The $(v-i)$ characteristics of Model 4.

It can be seen that, the arc voltage establishes rapidly as the arc current passes its zero crossing value. As the arc establishes, the voltage drops rapidly during the transient period but becomes almost constant in the steady-state period.

In reality, however, the arc electrode length is not constant; rather it is a random function of time because of random operation dynamics of the arc furnace. By applying the stochastic changes of the arc length, the random pattern of the $v-i$ characteristic of Model 4 can be obtained as shown in Fig. 2.9. A mathematical representation of the dynamic arc electrode length is given as follows:

$$l(t)=l(1+BLW) \tag{2.11}$$

where, BLW is the white noise.

In Fig. 2.9, solid bold line represents the $v-i$ characteristics of Model 4 without the white noise, and the dotted line represents the $v-i$ characteristics of Model 4 subject to the white noise. From Fig. 2.9, the arc voltage changes as a result of the random changes of the arc electrode length. As the arc electrode length increases, the arc voltage also increases.

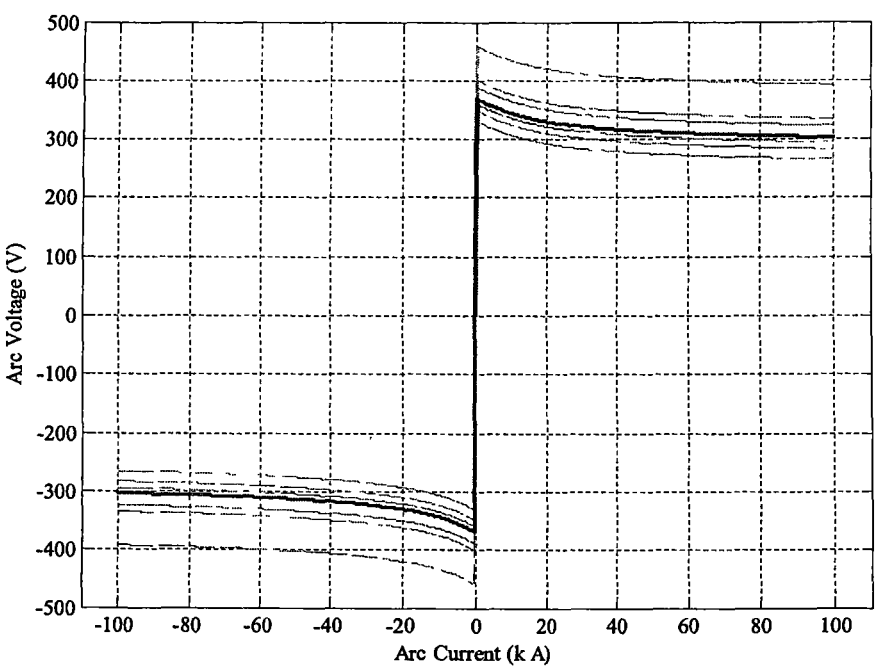

Figure 2.9. Dynamic $(v-i)$ characteristics of Model 4.

2.6 Model 5

In Model 5, the arc furnace is assumed to be a current controlled variable resistance. In this model, each cycle of arc voltage is divided into three stages based on the following assumptions [26]:

- The first stage is known as the pre-ignition stage. During this stage, the arc voltage increases from zero, the current passes its zero crossing point, and the arc starts igniting. This stage terminates as the arc voltage reaches a specific value called the arc ignition voltage (V_{ig}). During this stage, the arc circuit can be described as an open circuit with a leakage resistance (R_g). This resistance is assumed to be the resistance of foamy slag.
- The second stage is known as the ignition stage. This stage starts just after the pre-ignition stage when the arc voltage reaches the arc ignition voltage (V_{ig}). During this stage the arc voltage drops exponentially during a small transient period. After the transient period, the arc voltage becomes constant (proportional to the arc electrode length). In this stage, an exponential function and the time constant (τ_1) are used to express the transient period.
- The third stage is known as the arc extinction stage. During this stage, the arc starts extinguishing and the arc voltage (v) drops smoothly. At the end of this stage, the arc voltage drops rapidly. To characterize the exponential property of the arc resistance in this stage, an exponential function is used with the time constant (τ_2).

The non-linear resistance is governed by the following equation [26]:

$$R_A = \begin{cases} R_{ig}; & 0 \le |I| < I_{ig} \text{ and } \dfrac{d(|I(t)|)}{dt} > 0 \\ \dfrac{\left(V_D - (V_{ig} - V_D)e^{(|I| - I_{IG})/\tau_1}\right)}{|I|}; & |I| \ge I_{IG} \text{ and } \dfrac{d(|I(t)|)}{dt} > 0 \\ \left(V_T - (V_{ig} - V_T)e^{(|I|)/\tau_2}\right) \Big/ (|I| + I_{ig}); & \dfrac{d(|I(t)|)}{dt} < 0 \end{cases} \quad (2.12)$$

where, V_{ig}, V_T, and I_{ig} are found from the following equations [26] :

$$V_{ig} \approx 1.15 V_D \tag{2.13}$$

$$I_{ig} = \frac{V_{ig}}{R_G} \tag{2.14}$$

$$V_T = \frac{(I_{max} + I_{ig}) V_D}{I_{max}} \tag{2.15}$$

The constant voltage (V_D) which is proportional to the arc length is expressed as follows:

$$V_D = A + BL \tag{2.16}$$

Where, L represents the length of electrode, A is the constant that represents the sum of anode and cathode voltage drop, and B is the constant that represents the voltage drop per unit length.

The expression for the arc voltage is given as:

$$V(t) = R_A(t) I_A(t) \tag{2.17}$$

The graphical representation of the arc resistance-current characteristic is shown in Fig. 2.10.

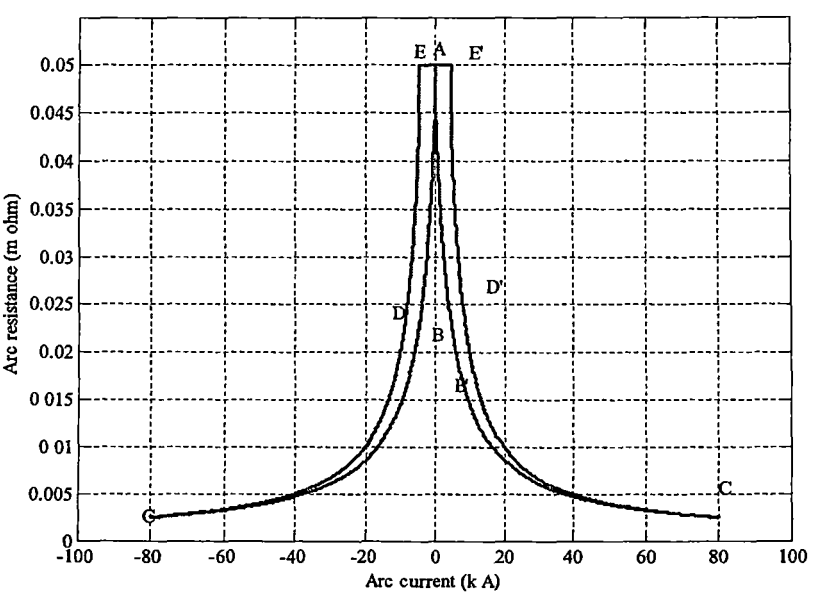

Figure 2.10. The arc current vs arc resistance.

In Fig. 2.5, lines EA and EA' represent the pre-ignition stage, where the arc resistance is assumed to be constant. Lines ABC and A'B'C' represent ignition stage of the arc resistance-current characteristic. During the ignition stage, the arc resistance decreases exponentially until it reaches the value corresponds to the arc extinction stage. Lines CDE and C'D'E represent the extinction period where the arc resistance increases exponentially until it reaches some constant value. The dynamic property of the arc resistance-current characteristic can be achieved by adding some stochastic variations to the arc resistance. The dynamic arc resistance-current characteristics are shown in Fig 2.11. In Fig. 2.11, solid bold line represents the arc resistance-current characteristic of the Model 5 without the white noise, and while the dotted line represents the resistance-current characteristics of Model 5 subject to the white noise.

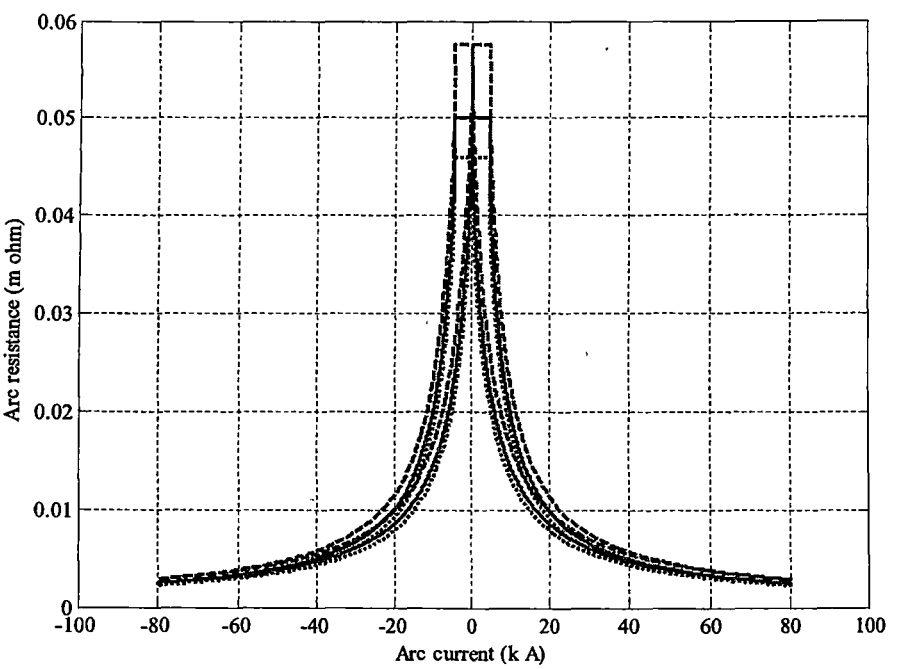

Figure 2.11. Dynamic arc current – resistance characteristics.

The voltage current $(v-i)$ characteristic of Model 5 is derived from Eq. 2.17 based on the arc resistance-current relationship. Fig. 2.12 shows the $v-i$ characteristics of Model 5. Lines AB and AB' represent the pre-ignition stage, line

BC and B'C' represent the ignition stage, and lines CA and C'A represent the arc extinction stage. The $v-i$ characteristic of Model 5 reveals that during the pre-ignition stage, the arc voltage increases linearly with respect to the arc current. Once the arc current reaches the arc ignition current, the arc voltage reduces rapidly and settles at a constant value which is proportional to the arc electrode length. During the extinction stage, the arc voltage reduces exponentially.

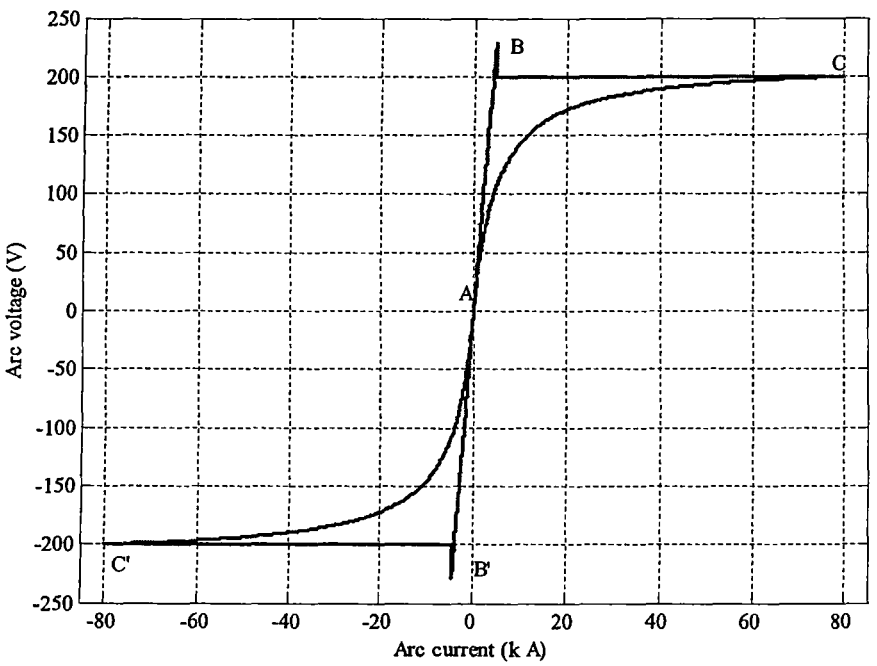

Figure 2.12. The $v-i$ characteristics of Model 5.

The dynamic voltage-current $(v-i)$ characteristics shown in Fig. 2.13 are obtained based on the dynamic relationship between the arc resistance and the arc current.

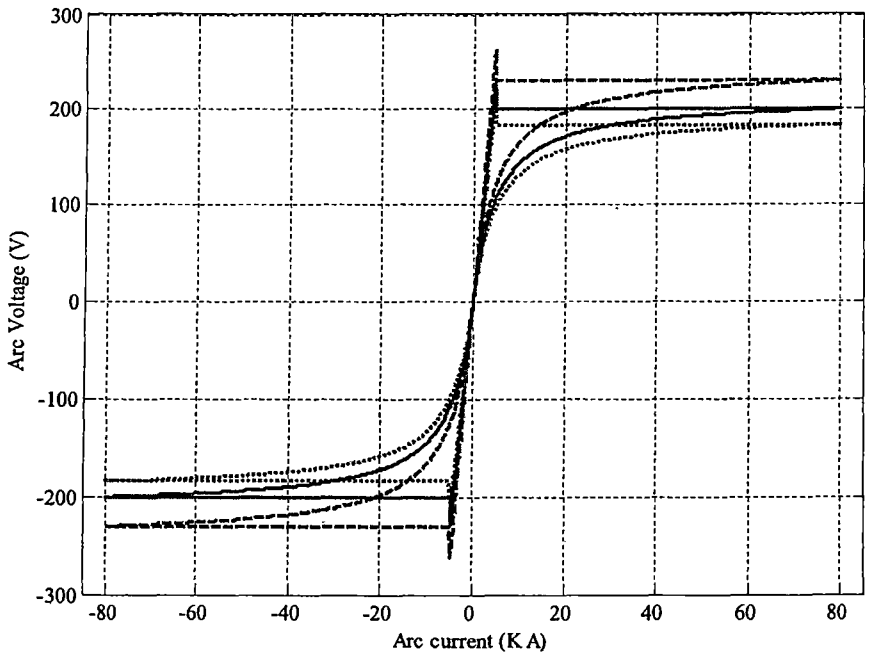

Figure 2.13. Dynamic $v-i$ characteristics of Model 5.

In Fig. 2.13, the solid bold line represents the $v-i$ characteristics of the Model 5 without the white noise, and the dotted line represents the $v-i$ characteristics of Model 5 subject to the white noise.

2.7 Model 6

A simplified form of the arc current and voltage can be derived from Mayr's arc model [27]:

$$i_a = \sqrt{2} I \sin \omega t \tag{2.18}$$

$$v_a = \frac{2V_0 \sin \omega t}{1 - \dfrac{\sin(2\omega t + \psi_a)}{\sqrt{1+(\tau_a)^2}}} \tag{2.19}$$

where i_a and v_a are the arc current and the arc voltage, respectively;

and $V_0 = \dfrac{P_{ro}}{\sqrt{2}I}$, $\tan\psi_a = \dfrac{1}{2\omega\tau_a}$

where, τ_a is the arc time constant and P_{ro} is the arc column power at the moment of interruption.

The $v-i$ characteristic of Model 6 is shown in Fig. 2.14.

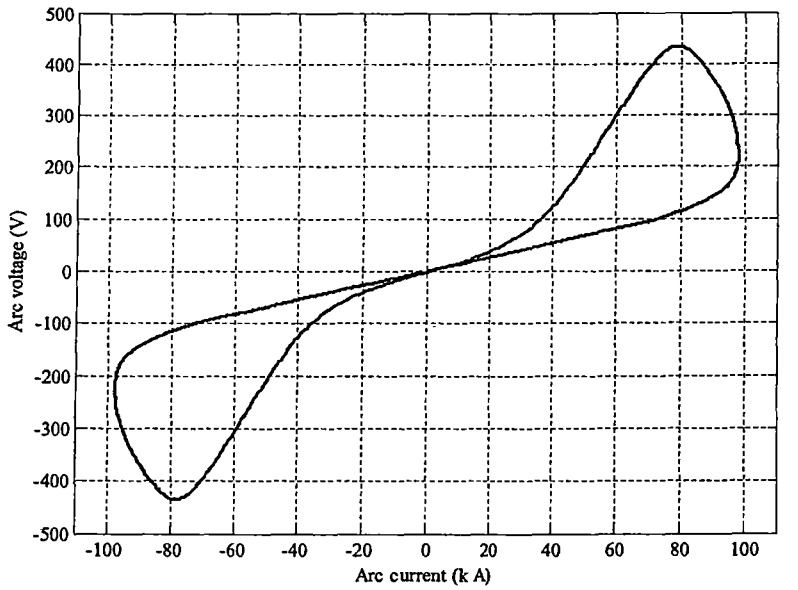

Figure 2.14. The $v-i$ characteristic of Model 6.

Dynamic characteristics of Model 6 are obtained by adding stochastic changes to the time constant (τ_a) in Eq. 2.19. The dynamic $v-i$ characteristics of Model 6 are shown in Fig. 2.15.

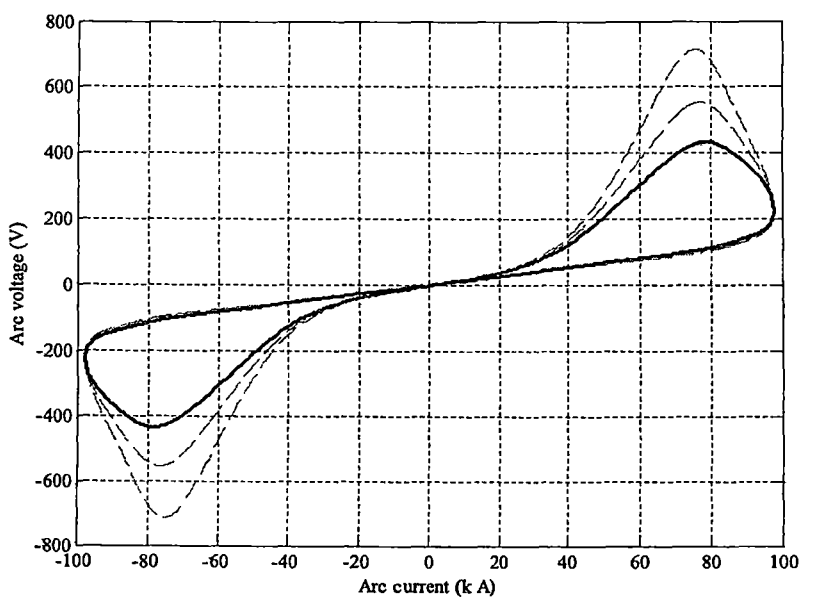

Figure 2.15. Dynamic $v-i$ characteristics of Model 6

In Fig. 2.15, the solid bold line represents the $v-i$ characteristics of the Model 6 without the white noise, and the dotted line represents the $v-i$ characteristics of Model 6 subject to the white noise. It can be noted that, as the time constant (τ_a) increases due to the random changes, the arc voltage also increases.

2.8 Model 7

In Model 7, the arc is simulated based on the consideration of stationary voltage-current characteristics and the ohmic property of the arc. Within a half cycle of current, the arc voltage in Model 7 is considered as a constant time function, which depends on the polarity of the arc current. Magnitude of the arc current and other stochastic changes that affect the arc voltage are neglected in this model. A mathematical representation of the arc voltage is given as follows:

$$v = V_D \; x \; sign(i) \tag{2.20}$$

where, $sign(i) = +1$, if i is positive and $sign(i) = -1$, if i is negative

The graphical representation of the $v-i$ characteristic of Model 7 is shown in Fig. 2.16

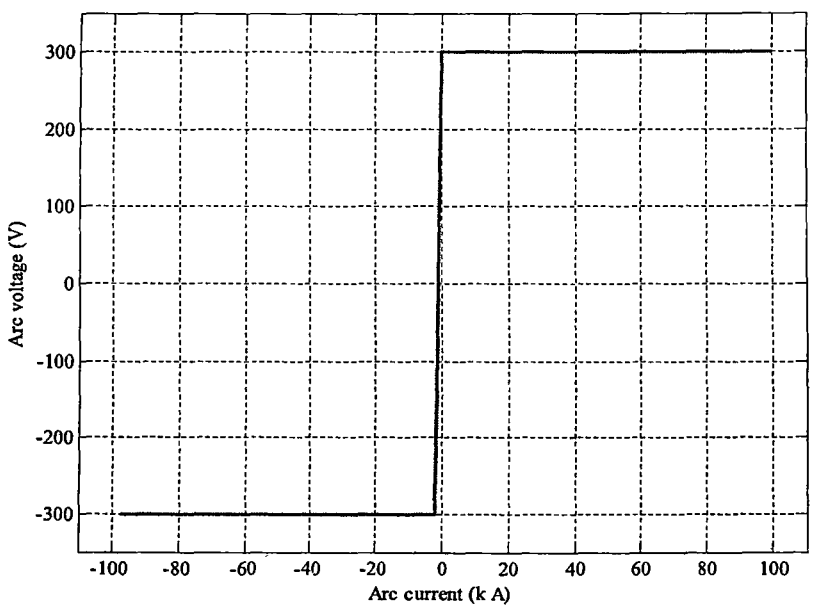

Figure 2.16. The $(v-i)$ Characteristic of Model 7.

The equivalent time switch circuit of Model 7 is shown in Fig. 2.17.

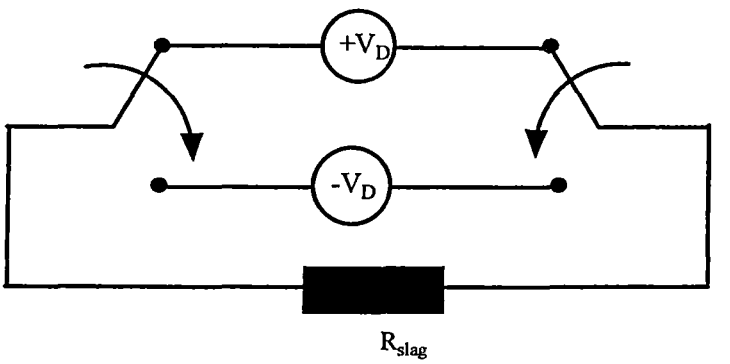

Figure 2.17. The equivalent time switch circuit of Model 7.

In Fig. 2.17, at time t_1, the arc extinguishes, the current changes its polarity and the arc voltage is developed due to the foamy sag in the arc furnace. When the voltage across the foamy slag increases and reaches the value of the arc ignition voltage (V_D) at time t_2, the arc establishes and keeps a constant voltage. The time interval between t_1 and t_2 is very small, and the arc current is assumed to be zero during this time. The ignition voltage of this model depends on the arc length. The accuracy of this model depends on the approximation of the arc voltage and the estimation of the switch times t_1 and t_2.

The dynamic $v-i$ characteristics of Model 7 are obtained by incorporating the white noise in the arc voltage. The dynamic arc voltage is represented as follows:

$$v(t) = V_D \; x \; sign(i) + BWL$$

The dynamic $v-i$ characteristics of Model 7 are shown in Fig. 2.18.

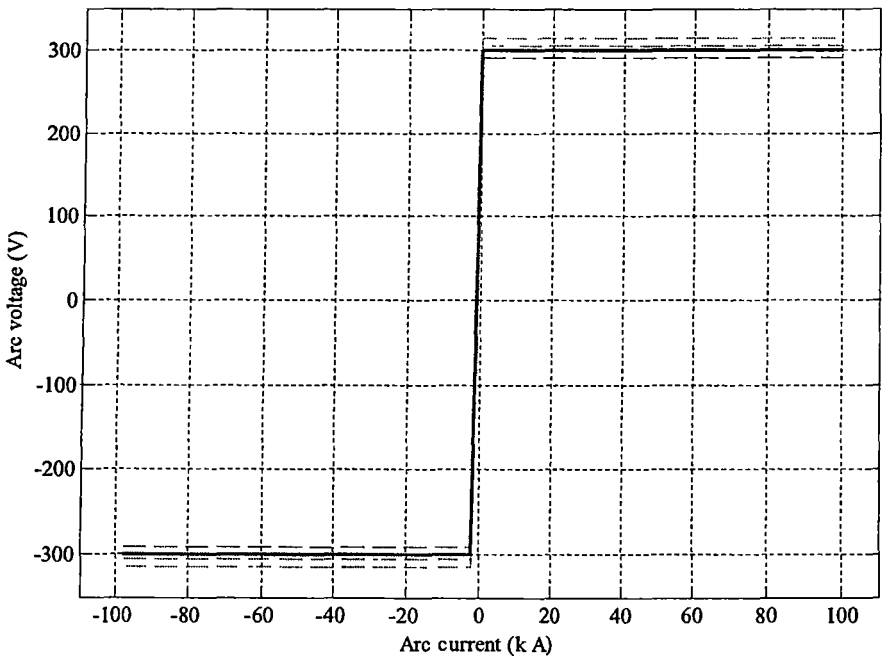

Figure 2.18. Dynamic $v-i$ characteristics of Model 7.

2.9 Conclusion

In this chapter, several conventional approaches to modelling the arc furnace were discussed and compared. The static and the dynamic $v-i$ characteristics were demonstrated and examined. The next step is to simulate the arc voltage and the arc current responses on a prototype industrial plant by implementing these models.

Chapter 3: Computational Intelligence Techniques for Arc Furnace Response Modelling

3.1 Introduction

The main focus of this chapter is to model arc furnace responses using computational intelligence techniques. These techniques mainly involve the application of artificial intelligence in order to extract relationships between the input and the output patterns of a complex, non-linear and time-varying systems. As the relationship between the arc voltage and the arc power is complex and highly time varying, computational intelligence techniques are used to establish a non-linear relationship between them [30]. Also, artificial intelligence techniques are often used successfully to predict non-linear system behaviour based on historical data [30]. In our research, we also implement a model using computational intelligence which is capable of predicting the short term behaviour of the arc voltage and power response.

Artificial intelligence (or AI) can be defined as the study and design of an intelligent agent that observes its environment and takes actions in order to maximize its chances of success [31]. In artificial intelligence, an intelligent agent is used to describe intelligent actors which examine and act upon their environment based on abstract capabilities such as perception, action and goal directed behaviour [31]. A system can be defined as intelligent if it interacts with its environment in a manner that would normally be regarded as intelligent if that interaction were carried out by a human being [4]. It can be implemented using conventional software techniques. An intelligent agent can be wholly autonomous, carrying out its own agenda, and acting as an agent like an intelligent human [31].

The term artificial intelligence is also used to describe a special property of machines or programs called 'intelligence'. Intelligence is a property of the human mind that covers human like abilities, such as the capacities to reason, to plan, to solve problems, to think abstractly, to comprehend ideas, to use language, and to learn.

Artificial intelligence techniques can be divided into two main branches which are known as Conventional AI and Computational Intelligence. Conventional AI is the branch of artificial intelligence that is used explicitly to represent human knowledge in the form of facts and rules [30]. Good examples of conventional AI are computer programs such as expert systems or knowledge based systems. These systems are able to utilize knowledge of a particular domain in such a way as to imitate a human expert on that subject matter [4]. However, expert systems are narrow in their domain of knowledge and when they are presented with a different task which they are not designed for; the expert systems may not be able to provide a satisfactory solution. Moreover, the main drawback of these systems is their inability to learn from their experiences. In contrast, computational intelligence has the ability to learn from its past experiences. Computational Intelligence involves iterative development or learning such as parameter tuning. Common computational intelligence systems include artificial neural networks, fuzzy inference systems, evolutionary computation and hybrid systems which are the combination of at least two of the systems mentioned above.

Let us now consider the most important techniques and tools of computational intelligence, which is known as the artificial neural network.

3.2 Artificial Neural Network (ANN)

The Artificial Neural Network (ANN) works in a way similar to a biological nervous system, such as the brain, and process information in a similar manner. Similar to a human brain, an ANN consists of an interconnected group of simple processors called artificial neurons that are used as a computational model for processing information [4]. The neurons of an ANN are connected by weighted links that pass signals from one neuron to another based on the strength of these connections. Each neuron receives a number of input signals through its connections and produces an output signal. The architecture of an ANN consists of different layers that includes an inputs layer, middle layers or hidden layers (multi-layer neural networks), and an output layer. A number of the input signal is applied to the input layer which is transmitted to the neurons in the middle layer of the network via

weighted links as shown in Fig. 3.1. Weights are the basic means of the long term memory which express the strength of connection between two neurons. Each neuron in the hidden layer produces an output signal based on its input signal and transmits that signal through its outgoing connection. The output signal sometimes split into a number of outgoing branches that broadcast the same signal to an incoming connection of a number of other neurons in the network.

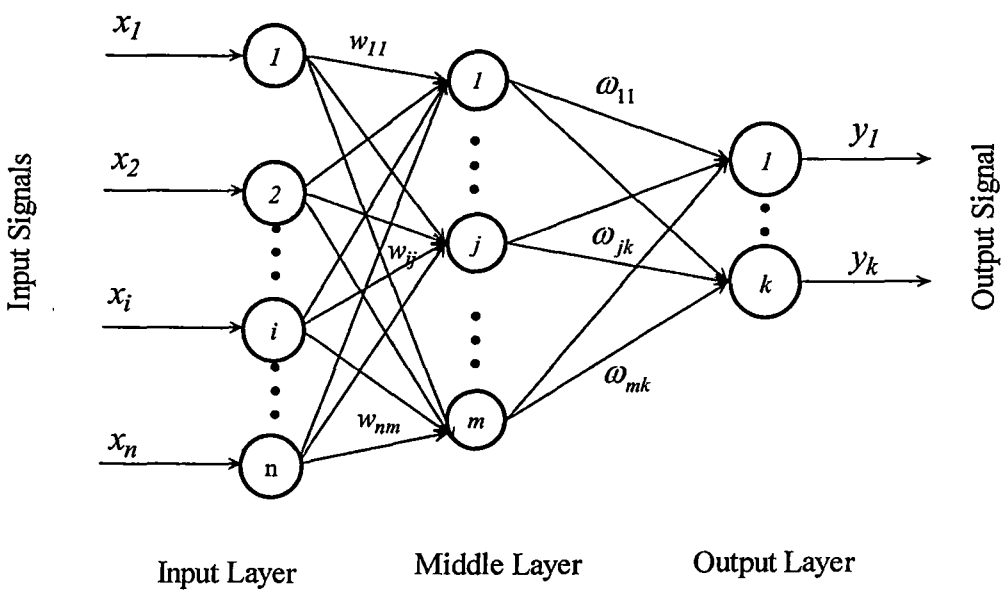

Figure 3.1. Architecture of a typical artificial feed-forward neural network.

A typical feed-forward artificial neural network shown in Fig. 3.1, where, x_1, x_2, ... x_i, ... x_n, represent a set of the input signals and y_1, and y_2, represent a set of the output signals. Each layer in Fig. 3.1 consists of a number of interconnected neurons. A weight between two neurons represents the strength of the connection. w_{ij} represents the weight between the ith neuron in the input layer and the jth neuron in the middle layer. ω_{jk} represents the weight between the jth neuron in the middle layer and the kth neuron in the output layer.

ANNs can be considered as an adaptive system that change their parameters based on the information that flows through the network. In more practical applications these networks are non-linear statistical data modelling tools and can be utilized to model complex relationships between inputs and outputs or for pattern

recognition. ANNs can be classified into two types, one is the feed forward network and the other is the feedback network [4]. Feed-forward networks allow signals to travel in one direction only i.e. from input to output. Here the output of any layer cannot affect that same layer. This type of network is mainly used for pattern recognition. On the other hand, feedback networks can have signals travelling in both directions. This type of network is dynamic as its state is continuously changing until reaching an equilibrium point. The network remains in the state of equilibrium until the input changes and a new equilibrium is needed.

The activation function in neural network plays an important role as it is responsible for the pattern of the output signal produced by the neuron. There are several activated functions that are often used in ANNs [4].

A. Step function

Step function can be defined as a function where the output is positive 1 if the input is higher than a threshold value and zero for other input values. The mathematical relationship between the input and output of the step function is shown as follows [33]:

$$Y = \begin{cases} +1 & if \quad X > \theta \\ 0 & if \quad X <= \theta \end{cases} \tag{3.1}$$

where X , Y, and θ are the input, the output, and the threshold value of the system. The graphical relationship between the input and the output of a neuron is shown in Fig. 3.2.

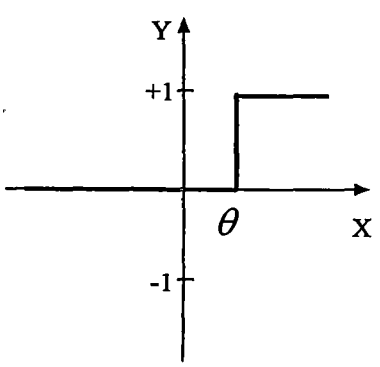

Figure 3.2. Step function.

B. Sign function

The output of sign function is positive 1 if the input is higher than a threshold value and negative 1 for other input values. The mathematical relationship between the input and output of the step function is given as [33]:

$$Y = \begin{cases} +1 & if \quad X > \theta \\ -1 & if \quad X <= \theta \end{cases} \tag{3.2}$$

where X , Y, and θ are the input, the output, and the threshold value of the system. The graphical representation of the sign activated function is shown in Fig. 3.3.

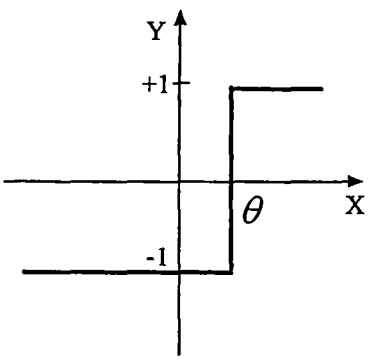

Figure 3.3. Sign function.

C. Sigmoid function:

The sigmoid function is used to produce sigmoid curve (s-shape) which can be defined using Eq. (3.3). The main feature of the sigmoid function is its ability to transfer any input ranged between minus infinite to plus infinite to a suitable output ranged between zero and one.

$$Y = \frac{1}{1+e^{-x}} \tag{3.3}$$

where X , and Y are the input, and the output of the system. The graphical representation of the sigmoid function is shown in Fig. 3.4.

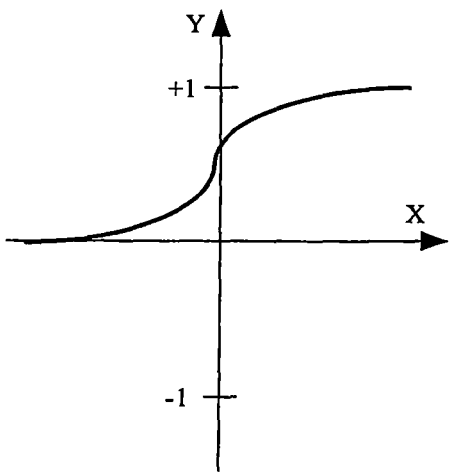

Figure 3.4. Sigmoid function.

D. Linear function

In the linear function, the relationship between the input and the output is represented by a linear function. Mathematical expression between the input and the output is given as follows:

$$Y = mX + c \tag{3.4}$$

where X , and Y are the input, and the output of the system, m and c are parameters that define the slope and intersection with Y axis. The graphical representation of the linear function is shown in Fig. 3.5.

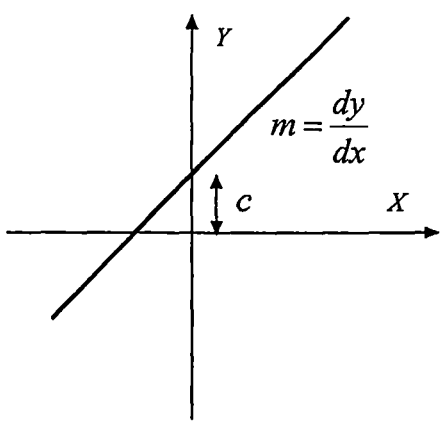

Figure 3.5. Linear function.

The performance of an ANN largely depends on the proper training of the network. In order to train a neural network, the weights must be adjusted in such a way that the error between the desired output and the actual output is reduced. Let us

consider a simple network that consists of a single neuron with adjustable weight and a hard limiter as shown in Fig. 3.6. To train this particular network, the perceptron training algorithm [4] is used which is discussed below:

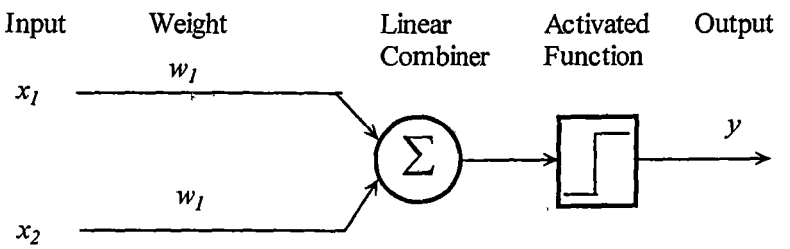

Figure 3.6. Single Layer two input perceptron.

In Fig. 3.6, the weighted sum of the inputs is applied to the hard limiter which produces an output of (+1) for a positive input and 0 for a negative input. The expression of the weighted input and the activation function is shown in Eq. (3.5) and Eq. (3.6).

$$X = x_1 w_1 + x_2 w_2 \tag{3.5}$$

$$Y = \begin{cases} +1, & \text{for } X > \theta \\ 0, & \text{for } X \leq \theta \end{cases} \tag{3.6}$$

The perceptron training algorithm begins by initializing the network. Here the initial weights, $w_1(j)$ and $w_2(j)$, and the threshold value, θ, are usually set to random values, which range typically -0.5 to +0.5. The perceptron is activated when the input signals, $x_1(j)$ and $x_2(j)$, and the desired output, $Y_d(j)$, are applied. The actual output, Y(j), is then calculated at iteration j and compared to the desired output.

The network adapts by making small changes in the weights by an amount which is proportional to the difference between the desired output and the actual output of the perceptron. The error at iteration j is given in Eq. (3.7). If the error at iteration j is positive, the perceptron output Y(j) needs to be decreased. However, if the error at iteration j is negative, we need to increase the perceptron output Y(j).

$$e(j) = Y(j) - Yd(j) \tag{3.7}$$

where $e(j)$ is the error at iteration j (j is a positive integer 1,2,3...).

The next stage in the perceptron training algorithm is updating the weights. The weights at iteration $(j+1)$ are updated as shown in Eq. (3.8) below.

$$w_i(j+1) = w_i(j) + \Delta w_i(j) \tag{3.8}$$

where i is the weight number;

$\Delta w_i(j)$ is the weight correction at iteration j.

The weight corrections are determined by the Delta Rule [4], as shown in Eq. (3.9).

$$\Delta w_i(j) = \alpha \times x_i(j) \times e(j) \tag{3.9}$$

where α is the learning rate.

This process is repeated until the error between the desired output and the actual output becomes sufficiently small and the solution converges. Let us consider an arc furnace model using the perceptron model. The input of the model is the voltage and the current of the arc furnace and the output is the real power as shown in Fig. 3.7.

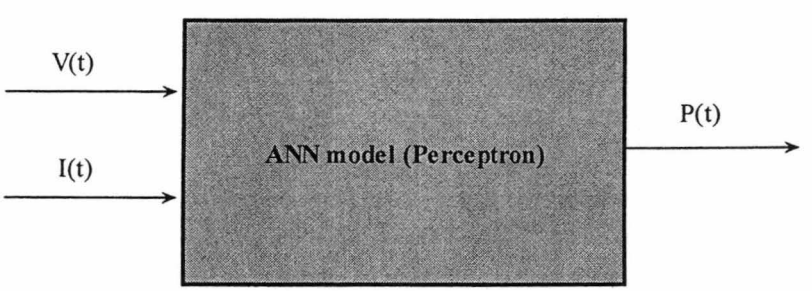

Figure 3.7. Perceptron model.

In this model, we use 600 data sets; among them, 300 data sets are used to train the model and 300 data for testing the model. The time series data patters of the arc voltage, arc current and the arc furnace power consumption are shown in Fig. 3.8.

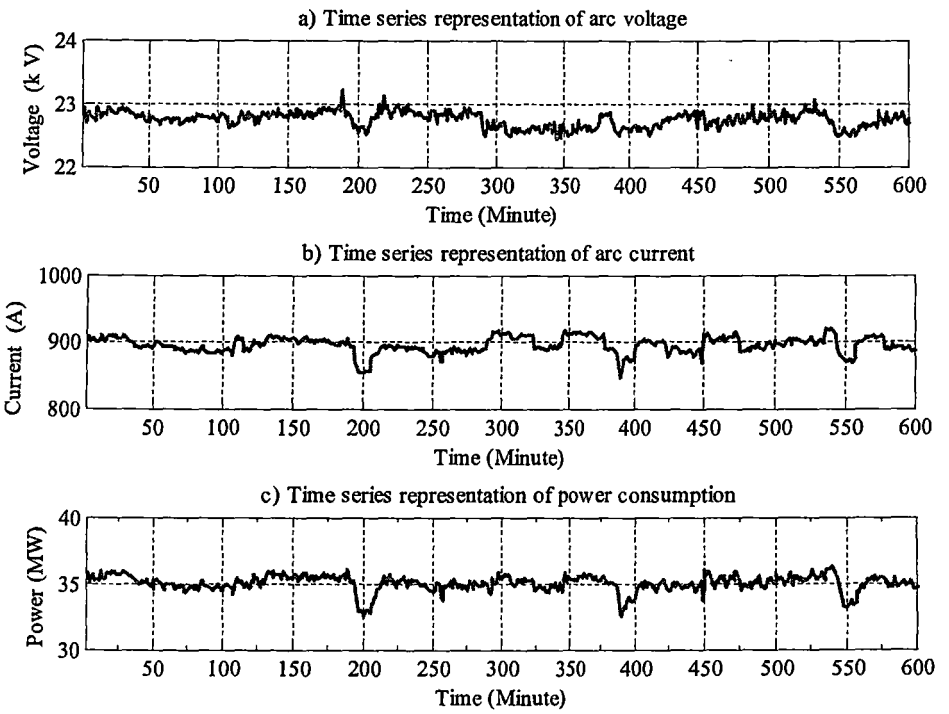

Figure 3.8. Time series representation of a) voltage, b) current, and c) power consumption of the arc furnace.

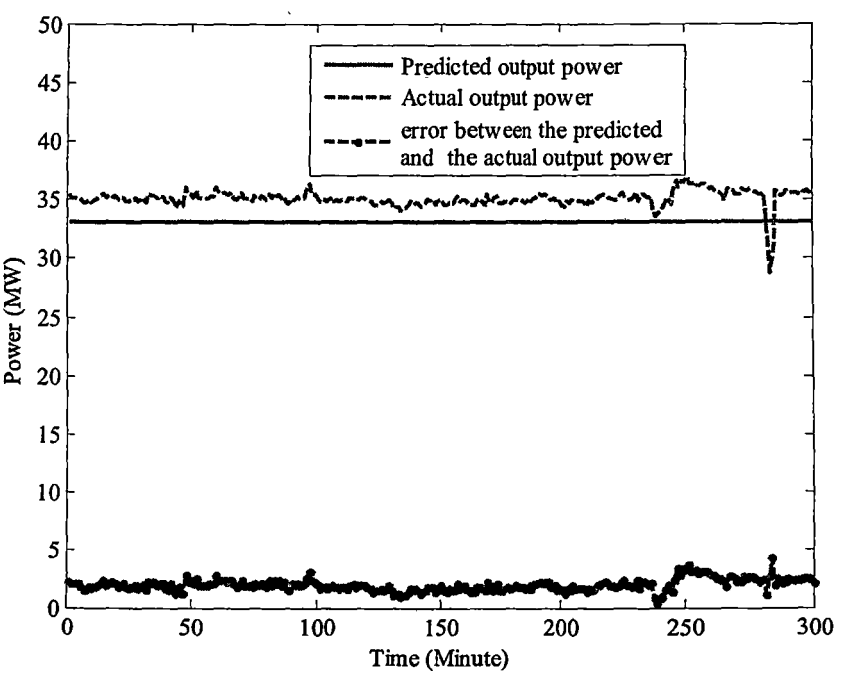

Figure 3.9. Perceptron Output.

After training the perceptron using first 300 data set, the output of the perceptron network is obtained for next 300 data which is shown in Fig. 3.9. In Fig. 3.9, the solid bold line represents the output of the perceptron network, the dotted line represents the actual data collected from the metallurgical plant and the dotted bold line at the bottom of the graph represents the error between the perceptron output and the real data. It is evident that a simple perceptron network cannot represent time-varying nature of the arc power. The fact is that this model can only learn linearly separable functions shown in Eq. (3.3). This learning algorithm can be represented by drawing a simple line between two types of data. In a perceptron model, for a net weighted input higher than a threshold value, the output of the model is 1; and for the other values of the net weighted input, the output is zero which does not represents the arc power characteristics. As the perceptron model cannot produce acceptable results, a multi-layer perceptron (MLP) is used in order to improve the neural network performance.

3.2.1 Multi-Layer Perceptron

A Multi-Layer Perceptron (MLP) is a neural network that has one input and one output layer and at least one hidden layer in the middle. The input layer consists of a number of neurons to receive input signals. Neurons in the input layer rarely have computational ability; they mainly distribute input signals to the appropriate neurons in the hidden layer. The hidden layers consist of a number of computation neurons. The weights associates with the neurons in the hidden layer represent the features of the input patterns. The output layer consists of a number of the computational neurons that receive the stimulus pattern from the hidden layer and establish the output pattern. Back propagation algorithm is the most widely used method to determine the dynamics of the multi-layered feedback perceptron networks. An example of multi-layer perceptron is shown in Fig. 3.10.

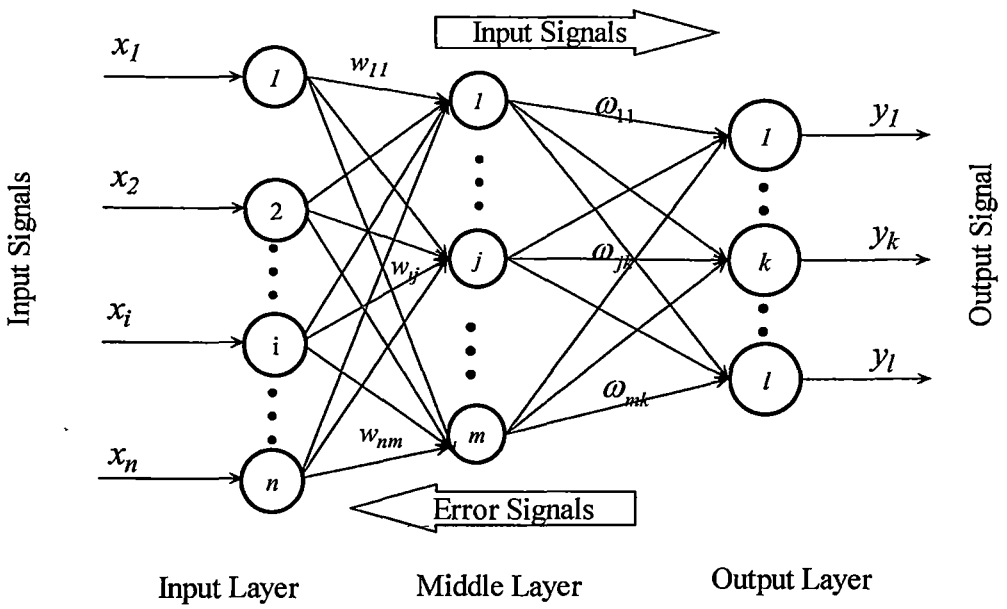

Figure 3.10. Multi-Layer Perceptron.

Let us consider a set of inputs, $x_1, x_2, \ldots x_i, \ldots x_n$, applied to the MLP and a set of outputs, y_1, and y_2, as shown in Fig. 3.10. In this example, we consider a simple input layer consisting of n input neurons, a simple hidden layer with m computational neurons and a simple output layer with 1 output neurons. w_{ij} represents the weight between the ith neuron in the input layer and jth neuron in the hidden layer, and ω_{jk} represents the weight between the jth neuron in the middle layer and the kth neuron in the output layer. The first step is to determine the net weighted input vector which is given in the Eq. 3.10.

$$X = \sum_{i=1}^{n} x_i w_i - \theta \tag{3.10}$$

where X is the weighted sum of the input signals;

x is the input signal;

w is the weight value of the connecting link;

n is the number of inputs;

θ is the threshold value.

The output is compared with the desired output and error is generated which is the difference between the MLP output and the desired output. The expression for error signal is given in Eq. (3.12).

$$e(k) = Y(k) - Yd(k) \tag{3.12}$$

where $e(k)$ is the error at iteration k (k is a positive integer 1,2,3...).

The error is propagated backward to the hidden layer; the weight of the neurons located in the hidden layer are updated in a manner similar to the perceptron model:

$$w_{ij}(k+1) = w_{ij}(k) + \Delta w_{ij}(k) \tag{3.13}$$

where $\Delta w_{ij}(k)$ is the weight correction at iteration k.

The weight correction depends on the output of the network and the error gradient at neuron l in the output layer at iteration k. The error gradient is given in Eq. (3.14).

$$\delta(k) = \frac{\delta(y_l(k))}{\delta(x_l(k))} . e_l(k) \tag{3.14}$$

For sigmoid activated function, the error gradient function can be expressed as follows:

$$\begin{aligned} \delta(k) &= \frac{\delta\left\{\dfrac{1}{1+e^{[-X_l(k)]}}\right\}}{\delta(x_l(k))} . e_k(k) \\ &= \frac{e^{[-X_l(k)]}}{\left\{1+e^{[-X_l(k)]}\right\}^2} . e_k(k) \end{aligned} \tag{3.15}$$

where $y_l(k) = \dfrac{1}{1+e^{[-X_l(k)]}}$

The weight correction factor is shown in the following equation.

$$w_{jk}(p) = \alpha y_j(p) \delta_k(p) \tag{3.16}$$

Weights are adjusted according to Eq. (3.13). This is achieved by propagating the error backwards through the network from the output layer to the input layer. Let us consider an arc furnace model using the MLP model. The input of

the model is the voltage and the current of the arc furnace and the output is the real power as shown in Fig. 3.12.

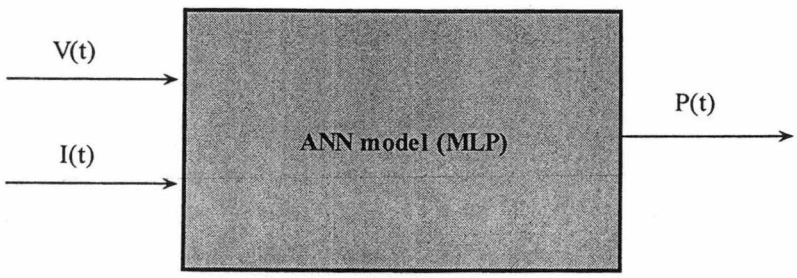

Figure 3.11. MPL model.

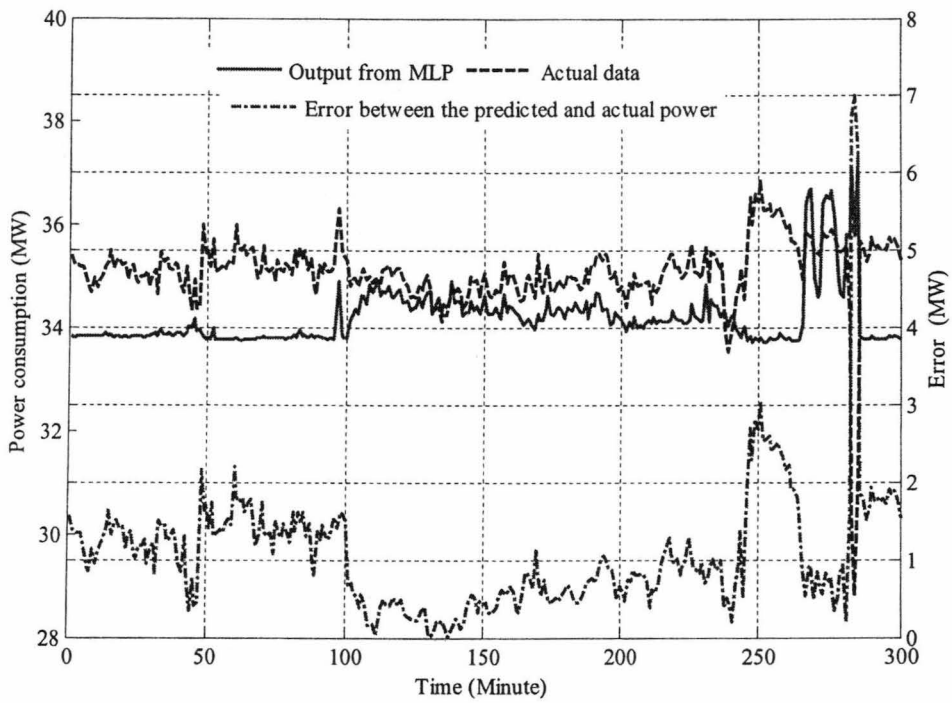

Figure 3.12. MPL Output

From Fig. 3.12, MLP model is able to capture the random pattern of the arc power based on the arc voltage and the arc current. In this figure, the bold line represents the predicted power, the thin line represents the actual power consumption from the arc furnace, and the dotted bold line represents the difference between the actual power and the predicted power. The accuracy level of the prediction is the key factor to evaluate the performance of the model. In MLP model, 5 neruons are used in the hidden layer which gives us satisfactory result as the MSE

(mean square error) is about 0.53 MW. However, the performance of the model can be further improved if fuzzy logic can be used in conjunction with neural network. Detailed study of the fuzzy inference system and Neuro-Fuzzy modelling techniques are discussed in the following sections.

3.3 Fuzzy Inference Systems

Fuzzy logic is derived from the fuzzy set theory that deals with the reasoning. Fuzzy logic is an extension of Boolean logic (true or false logic) that deals with the concept of partial truth and degrees of membership [4]. Unlike two-valued Boolean logic, Fuzzy logic uses a wide range of the of logic values between 0 (Completely false) and 1 (Completely true) and hence the fuzzy logic is multi-valued. Fuzzy logic is used to describe fuzziness or vagueness of a particular object based on the concept that all things admit to a degrees of membership function to that object. Fuzzy logic uses a defined list of if-then statements known as fuzzy rules [4]. These fuzzy rules are useful as they refer to variables and the adjectives that describe those variables. A typical example is shown below:

Rule 1

IF the voltage is high

THEN power loss in transmission system is low.

Rule 2

IF the voltage is low

THEN power loss in transmission system is high.

In these rule, the universe of discourse of the linguistic variable 'current' has a wide range between zero to several hundred ampere which includes fuzzy sets such as low, medium and high. The universe of discourse of the linguistic variable 'power consumption' can be low, medium and high which may varies from zero to several thousand watt, depends of the system of interest.

A fuzzy inference system can be defined as the mapping from the given input to an output using fuzzy set theory. Commonly used fuzzy inference systems are Mamdani-style inference system and Sugeno-style inference system. A detailed

study of Mamdani and Sugeno-type fuzzy inference system is outlined in the following sub-section.

3.3.1 Mamdani-style Inference Systems

Mamdani-style fuzzy inference system works in four stages. Detailed description of these stages is demonstrated below using a simple example. Let us consider a simple two input one output problem containing 3 rules:

Rule 1,	Rule 1,
IF voltage is high	IF V is A3
OR current is low	OR I is B1
THEN losses are low	THEN P is C1
Rule 2	Rule 2,
IF voltage is low	IF V is A1
AND current is high	AND I is B2
THEN losses are high	THEN P is C3
Rule 3	Rule 3
If voltage is low	If V is A1
OR current is low	OR I is B1
THEN losses are medium	THEN P is C2

Let us denote the linguistic variables – voltage, current and loss of a transmission line as V, I and P. A1, A2, and A3 (low, medium and high) are the linguistic values of universe of discourse V (voltage), B1, and B2 (low, and high) are the linguistic values of universe of discourse I (current), and C1, C2, and C3 (low, medium and high) are the linguistic values of universe of discourse P (loss).

The first step of the Mamdani-style fuzzy inference is the fuzzification of the input (Voltage and Current) and determines the membership function of each

element. For example, the membership functions of the inputs of the fuzzy system are shown as follows:

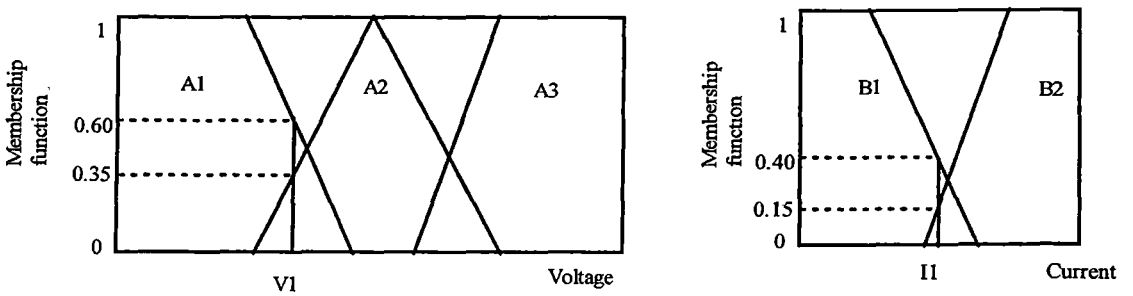

Figure 3.13. Membership function of the voltage and the current.

Fig. 3.13 represents the membership functions of the linguistic variables (Voltage and Current). The value of the membership function of the voltage (V1) which correspond to A1 (low) and A2 (medium) to the degree of 0.60 and 0.35 respectively. Similar approach is undertaken to find out the value of the membership function of the current which is 0.40 for B1 (when current is low) and 0.15 for B2 (when current is high)

The second step is the rule evaluation step. In this step, the fuzzified outputs are applied to the antecedents of the fuzzy rules and using fuzzy operators (such as AND, or OR), the antecedents are evaluated. A single number represents the output of this process. For example, in case of the rule 1, for the voltage (V1), and for the current (I1), the fuzzy expert system operates the union rule and evaluate rule 1 as shown in the following.

$$\mu_{A\cap B}(z)=\max[\mu_A(x),\mu_B(x)]=\max[0,0.40]=0.40$$

The graphical expression of the evaluation process of rule 1 is shown in Fig. 3.14.

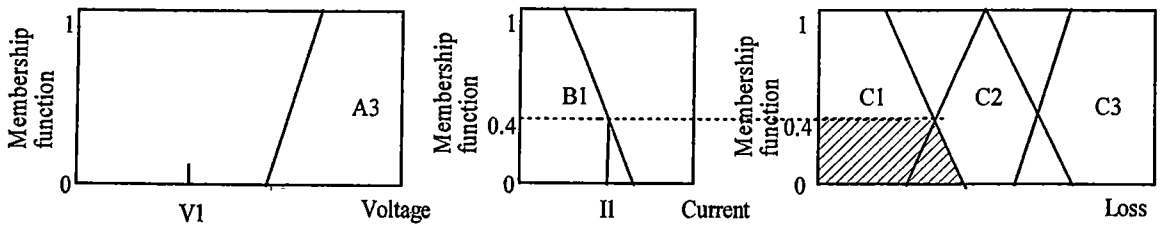

Figure 3.14. Rule 1 evaluation.

Similarly, for rule 2, fuzzy expert system can evaluate the value which is shown in the following:

$$\mu_{A\cap B}(z) = \min[\mu_A(x), \mu_B(x)] = \min[0.60, 0.15] = 0.15$$

The graphical expression of the rule 2 evaluation process is shown in Fig. 3.15.

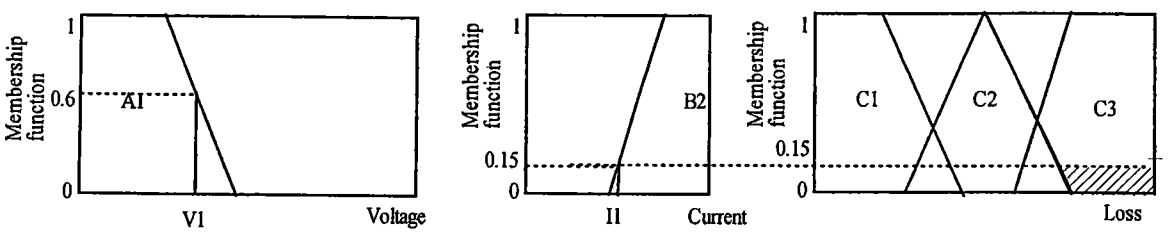

Figure 3.15. Rule 2 evaluation.

For the case of rule 3, $\mu_{A\cap B}(z) = \max[\mu_A(x), \mu_B(x)] = \max[0.60, 0.40] = 0.60$

The graphical expression of the rule evaluation process is shown in Fig. 3.16

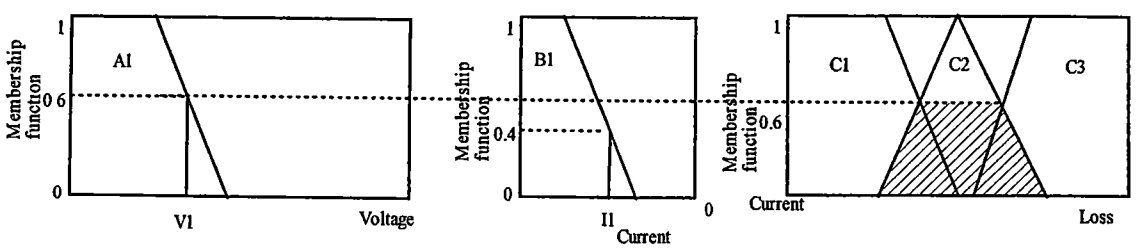

Figure 3.16. Rule 3 evaluation.

The third stage known as the aggregation of the rule output which combines all output number obtained from the rule evaluation stage. Fig. 3.17 shows the aggregation process.

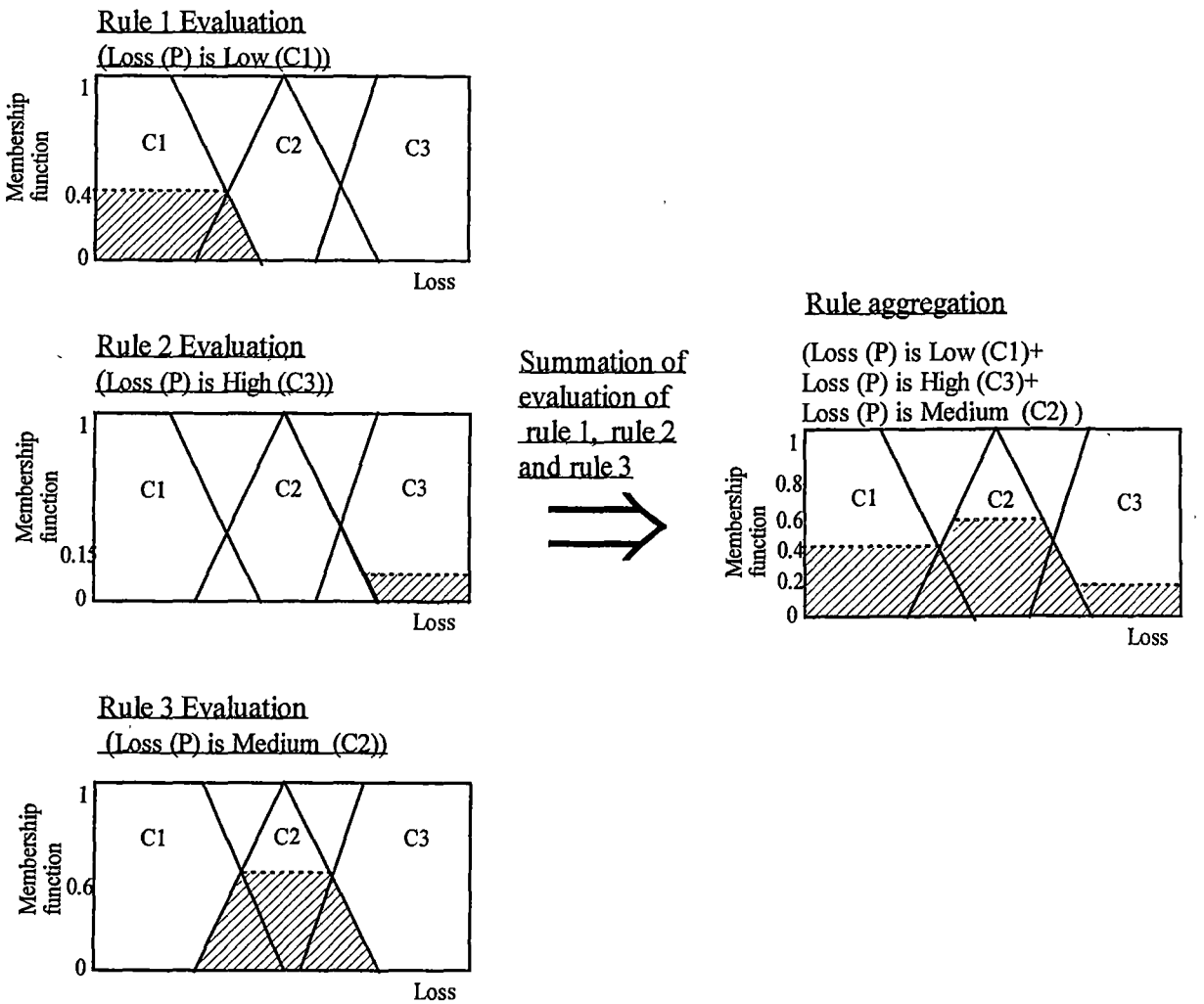

Figure 3.17. Rule aggregation process.

The fourth stage is known as defuzzificaton process. The most popular method for defuzzification process is the centroid technique which is used to find a point that represents the centre of the gravity. Mathematical expression of the centre of gravity (COG) is shown as follows:

$$COG = \frac{\int_a^b \mu_A(x) x dx}{\int_a^b \mu_A(x) dx}. \qquad (3.17)$$

However, in practical case, the simplified formula is used which is derived from Eq. (3.17) and shown as follows:

$$COG = \frac{\sum_{x=a}^{b} \mu_A(x)x}{\sum_{x=a}^{b} \mu_A(x)} \tag{3.18}$$

The COG of the example fuzzy inference system is calculated using the Eq. (3.18) which is as follows:

$$COG = \frac{(0+10+20+30).4+(40+50+60).6+(70+80+90+100).15}{(.4+.4+.4+.6+.6+.6+.15+.15+.15+.15)}$$

$$= \frac{165}{3.6} = 48.83$$

The result obtained from the defuzzification process demonstrates that, for a given crips input of voltage and current, the loss of transimission line is 48.83%. The graphical representation is shown as follows;

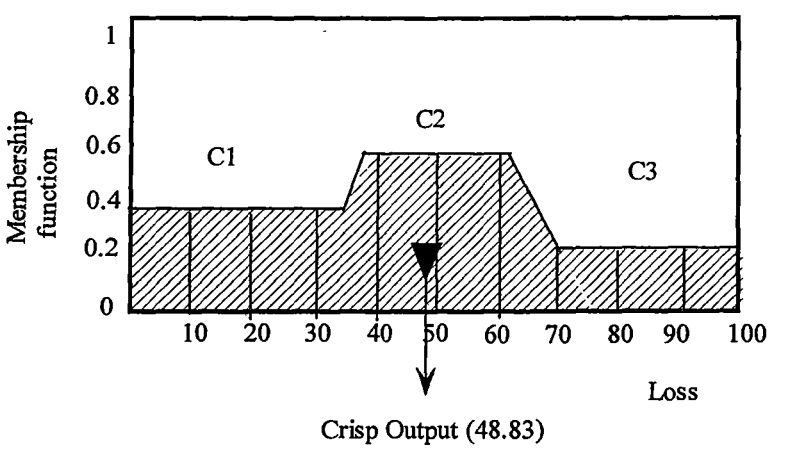

Figure 3.18. Defuzzification process.

3.3.2 Sugeno-style Inference Systems

The basic structure of the Sugeno-style inference system is similar to the Mumdani type inference system expect the evaluation of the membership function of the rule consequent part. In Sugeo-style, the membership function of the rule consequence is a function of the input parameters. The format of the Sugeno-type fuzzy rule is shown as below:

IF x is A

AND y is B

THEN z is f (x, y)

where x, y, and z are the linguistic variables; A and B are the fuzzy sets on universe of discourses of X and Y respectively, and f(x, y) is a mathematical function. The Sugeno-style inference system is demonstrated by using the above example presented in section 3.2.1. In this case, let us consider the zero order Sugeno-style fuzzy inference system, where the output of the rule consequence is a constant which is shown as follows:

IF x is A

AND y is B

THEN z is k,

where k is a constant.

Let us consider the same example that is used to demonstrate the Mamdani-style fuzzy inference system. Like the Mamdani style fuzzy system, Sugeno style employes four steps. In the firs step which is fuzzification process, works in a way similar to Mamdani-style inference system, which is shown in Fig. 3.13.

The second step is the rule evaluation stage. In rule evaluation stage, a single number is generated as a consequent of the evaluation of each rule. Unlike Mamdani-style fuzzy inference system, Sugeno-type fuzzy inference system uses a mathematical function instead of fuzzy set. The rule evaluation process is shown as follows:

For rule 1:

$$\mu_{A\cap B}(z) = \max[\mu_A(x), \mu_B(x)] = \max[0, 0.40] = 0.40$$

The graphical expression of the evaluation of rule 1 is shown in Fig. 3.19.

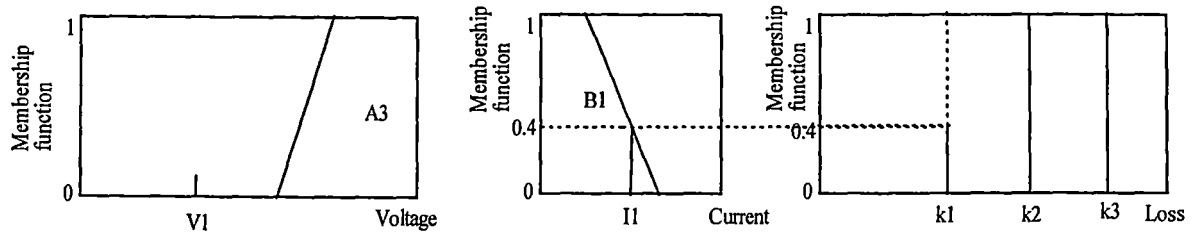

Figure 3.19. Rule 1 evaluation.

For rule 2:

$$\mu_{A\cap B}(z) = \min[\mu_A(x), \mu_B(x)] = \min[0.60, 0.15] = 0.15$$

The graphical expression of the rule evaluation process is shown in Fig. 3.20

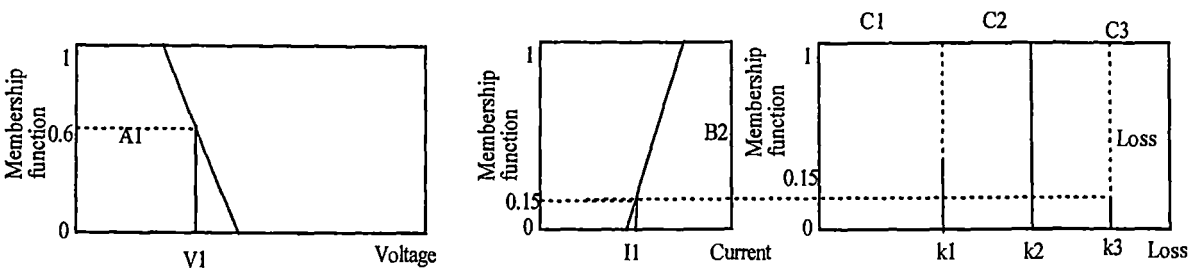

Figure 3.20. Rule 2 evaluation.

For rule 3:

$$\mu_{A\cap B}(z) = \max[\mu_A(x), \mu_B(x)] = \max[0.60, 0.40] = 0.60$$

The graphical expression of the rule evaluation process is shown in Fig. 3.11.

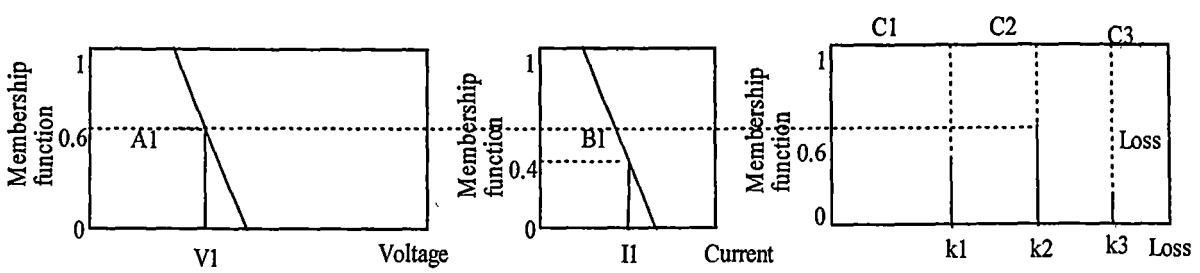

Figure 3.21. Rule 3 evaluation.

The third stage is known as the aggregation of the rule output which combines all the output number obtained from the rule evaluation. Fig. 3.22 shows the aggregation process.

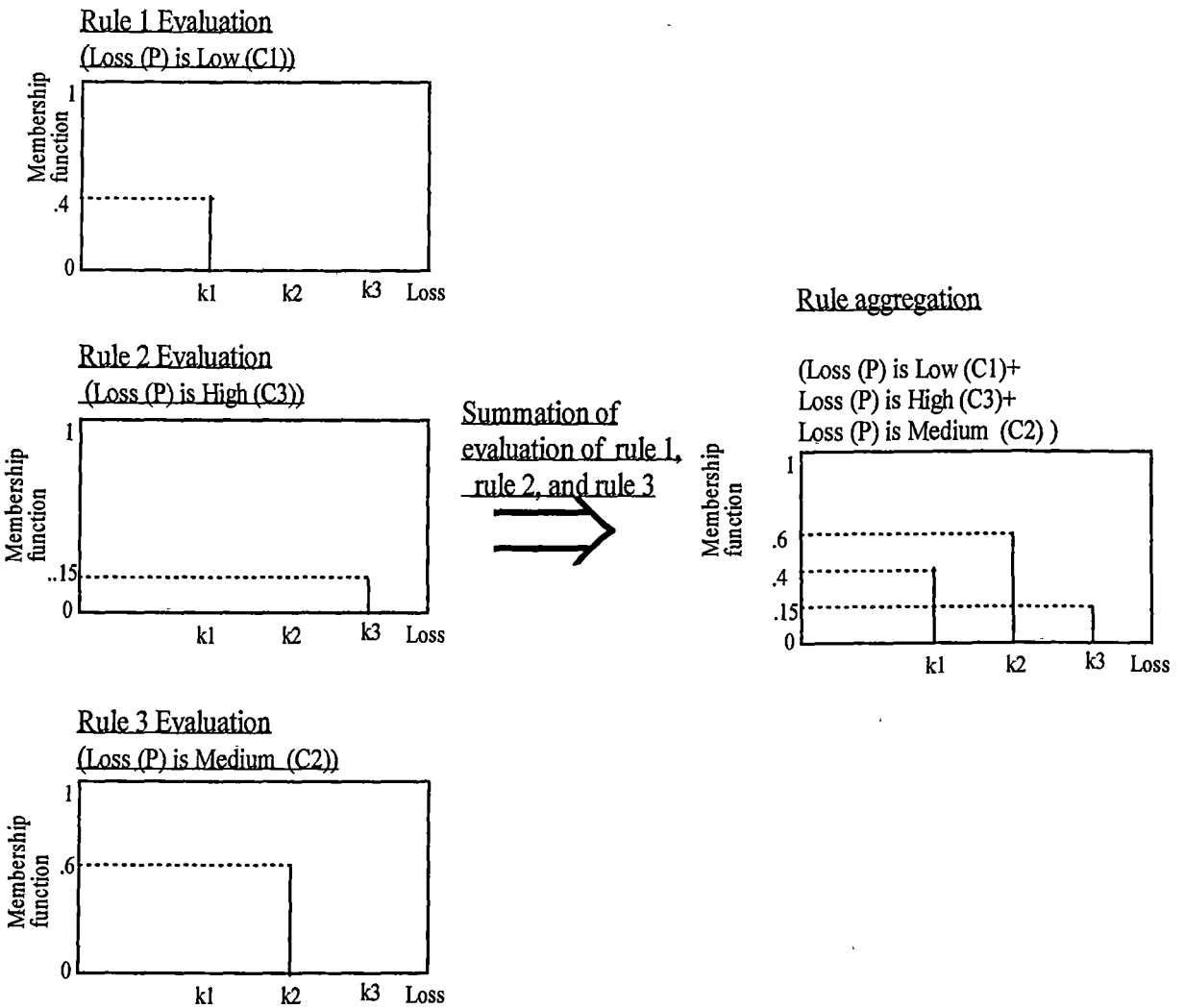

Figure 3.22. Rule aggregation process.

The fourth stage is know as the defuzzification process. In this stage, the weighted average (WA) of these singletons are calculated by using the following equation:

$$WA = \frac{\mu(k1)k1 + \mu(k2)k2 + \mu(k3)k3}{(\mu(k1) + \mu(k2) + \mu(k3))} \tag{3.20}$$

The value of the weighted average is calculated as follows:

$$WA = \frac{0.4x0.35 + 0.6x0.6 + 0.15x0.83}{(0.4 + 0.6 + 0.15)} = \frac{0.14 + 0.36 + 0.1245}{1.15} = 54.3$$

The result obtained from the defuzzification process demonstrates that, for a given crips input of voltage and current, the loss of transimission line is 54.3. The graphical representation is shown as follows;

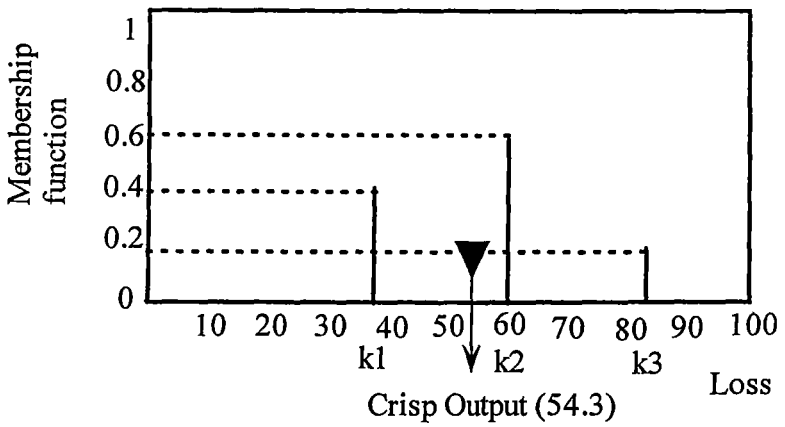

Figure 3.23. Defuzzification process.

The difference between these two types of fuzzy inference systems lies within the way they each determine outputs. The obvious advantage of Mamdani-style inference system is its ability to capture expert knowledge in fuzzy rule. However, it requires substantial computational time. Sugeno-style, on the other hand, is able to overcome this drawback by using a single spike in determining the membership function of the rule consequent part. A single spike is fuzzy singleton which is a fuzzy set with a membership function that is unity at a single particular point on the universe of discourse and zero in all other points. Moreover, the Sugeno-style inference system performs well in the field of optimization and adaptive techniques which is used widely in control, and the nonlinear dynamic system.

3.3.3 Membership function of fuzzy inference systems

The membership function of a fuzzy set is defined as the degree to which an element belongs to the entire set [4]. Mathematical representation of the membership function is shown in Eq. (3.21)

$$\mu_A(x): \quad X \rightarrow [0,1] \tag{3.21}$$

$\mu_A(x) = 1$, for x is fully in set A

$\mu_A(x) = 0$, for x is not in set A

$0 < \mu_A(x) < 1$, for x is partly in set A

Eq. (3.17) represents the membership of element x to set A. This is referred to as the degree of membership or membership value of element x in set A. The membership function itself can be an arbitrary curve whose shape we can define as a function that suits from the point of view of simplicity, convenience, speed, and efficiency. The popular membership function are discussed below [33]:

- Piecewise Linear functions
- Gaussian Distribution functions
- The Sigmoid Curve
- Quadratic and Polynomial Curves

A. Piecewise Linear functions

The piecewise linear functions are considered the simplest membership functions as they are formed using straight lines. The Triangular and Trapezoidal membership functions are the example of the piecewise linear function which is shown in Fig. 3.24. Their advantage is obtained through their simplicity.

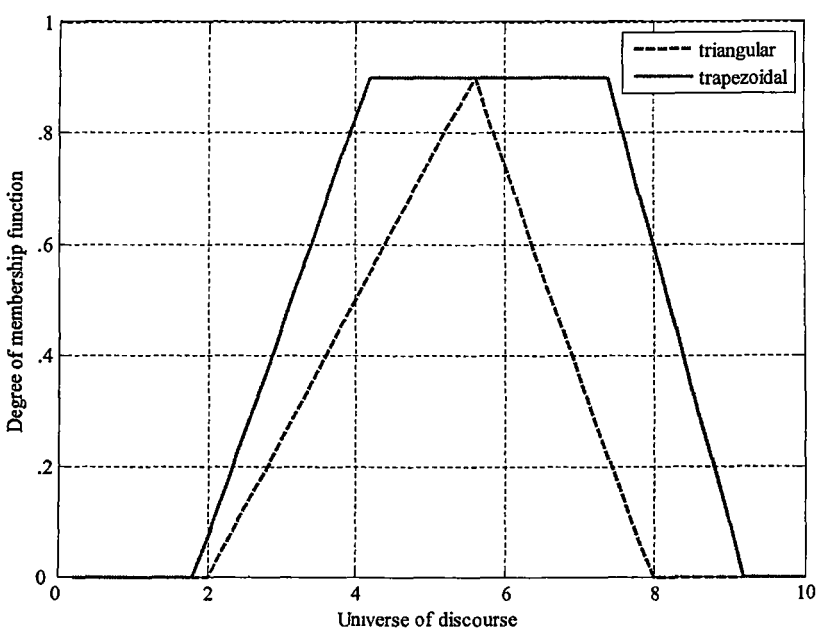

Figure 3.24. Triangular and Trapezoidal membership function.

B. Gaussian Distribution functions

The Gaussian distribution function includes two set of functions which are the simple Gaussian curve, the two-sided composite of two different Gaussian curves and the Generalised bell curve as shown in Fig. 3.25. These functions are popular methods for specifying fuzzy sets due to their smoothness and concise notation. However, the Generalised bell function is more popular than the Gaussian functions because of its ability to approach a non-fuzzy set if the free parameter is tuned. Although being unable to specify asymmetric membership functions, their advantage is obtained through their smoothness.

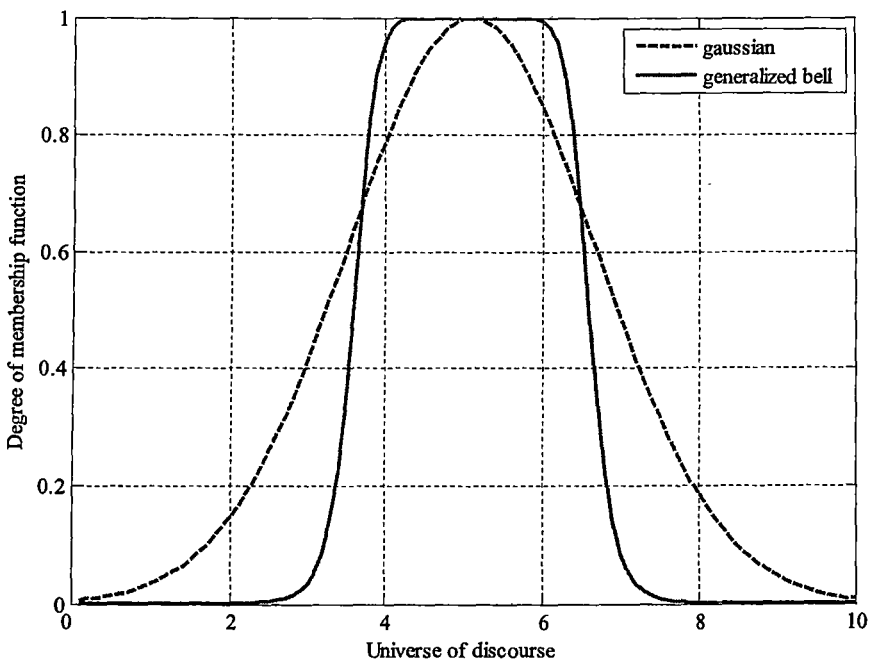

Figure 3.25. Simple Gaussian curve and generalized Bell membership function.

C. Sigmoid Curve:

Unlike the Gaussian and generalized bell functions, the Sigmoid curve, a sigmoidal membership function, has the ability to synthesis asymmetric and closed membership functions. In addition to the basic sigmoidal function, there is also a membership function that represents the difference between two sigmoidal functions

and also a membership function representing the product of two sigmoidal functions. These functions are shown in Fig. 3.26.

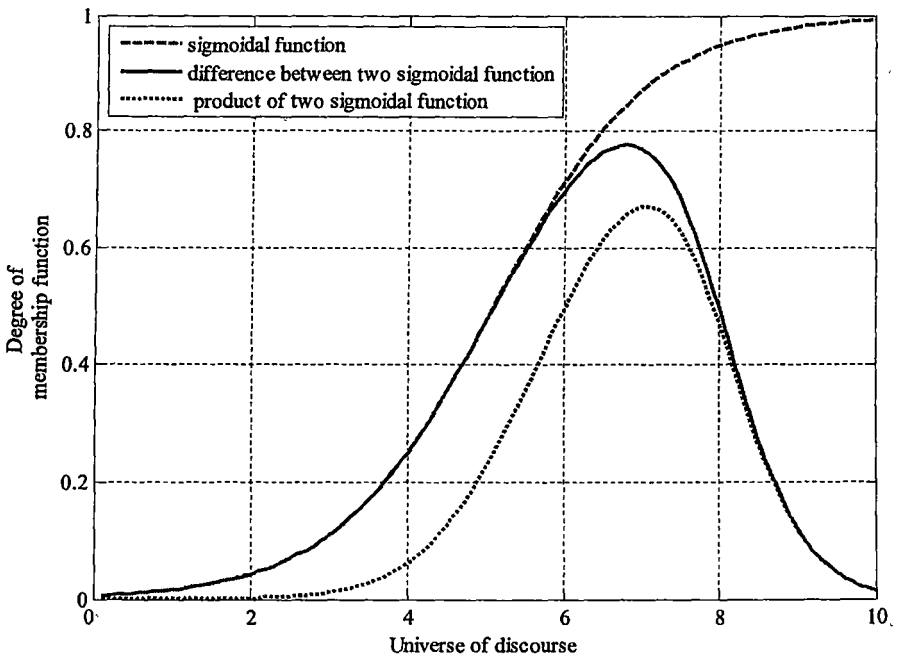

Figure 3.26. Simple Sigmoid membership function, difference between two sigmoidal functions and product of two sigmoid membership functions.

D. Quadratic and Polynomial curves:

Three membership functions based on polynomials are the Z, S and Pi curves. The membership function Z represents an asymmetrical polynomial curve which is open to the left. Function S is a mirror-image of the Z function which opens to the right. The Pi model however, is closed at both the left and right with a rise over the middle. The polynomial functions described here are shown in Fig. 3.27.

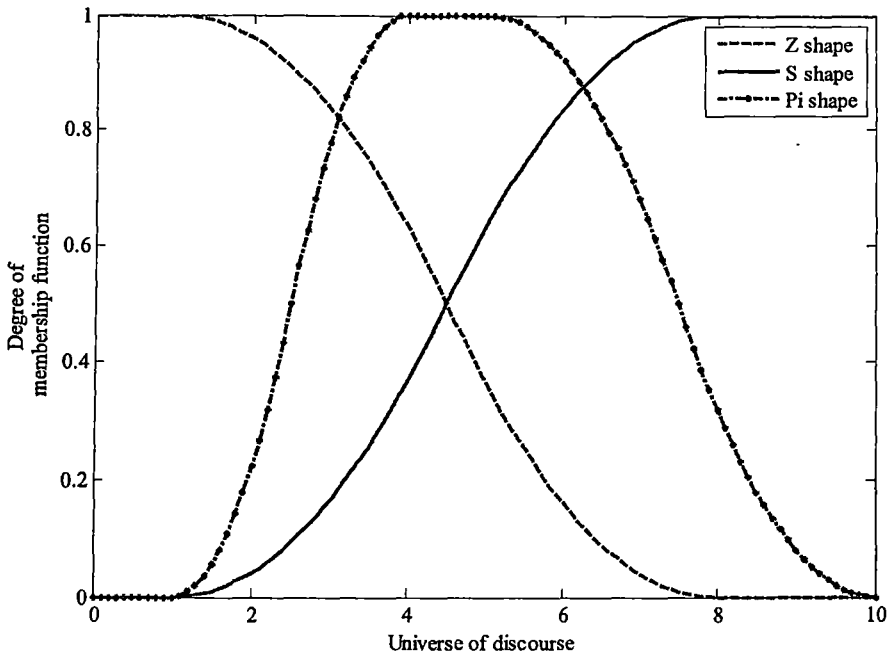

Figure 3.27. Quadratic and Polynomial curves (Z-shaped membership function, S-shaped membership function, pi-shaped membership function).

3.4 Adaptive Neuro-Fuzzy Inference Systems

ANFIS is a class of adaptive multi-layer feed-forward networks that is functionally equivalent to a fuzzy inference system. Such systems can be employed for situations where a collection of input/output data is presented to be modeled [32]. In such a case, the relationship between the input-output data sets may be non-linear and thus predetermining the model structure and shape of the membership functions could prove difficult and become quite a complex procedure. Rather than choosing the parameters associated with the models membership functions arbitrarily, the adaptive-neuro learning techniques incorporated by ANFIS are able to choose these parameters so as to reshape the membership functions according to the input/output data in order to extract the non-linear relationship that may exist between them.

The adaptive-neuro learning techniques work similar to that of adaptive neural networks as discussed previously, providing a method for the fuzzy modeling procedure to learn information about the data set it is trying to model [4]. This

concept of adaptive-neuro learning is quite simple and is incorporated to compute the membership function parameters that allow the associated fuzzy inference system to track the given input/output data.

ANFIS works by constructing a fuzzy inference system from a given input-output data set. The parameters associated with the membership functions of the constructed fuzzy inference system are adjusted or tuned throughout the training process using either a backpropagation algorithm, or a hybrid combination of both backpropagation and the least squares method. These methods allow the fuzzy inference system to learn from the input-output data set that it is trying to model.

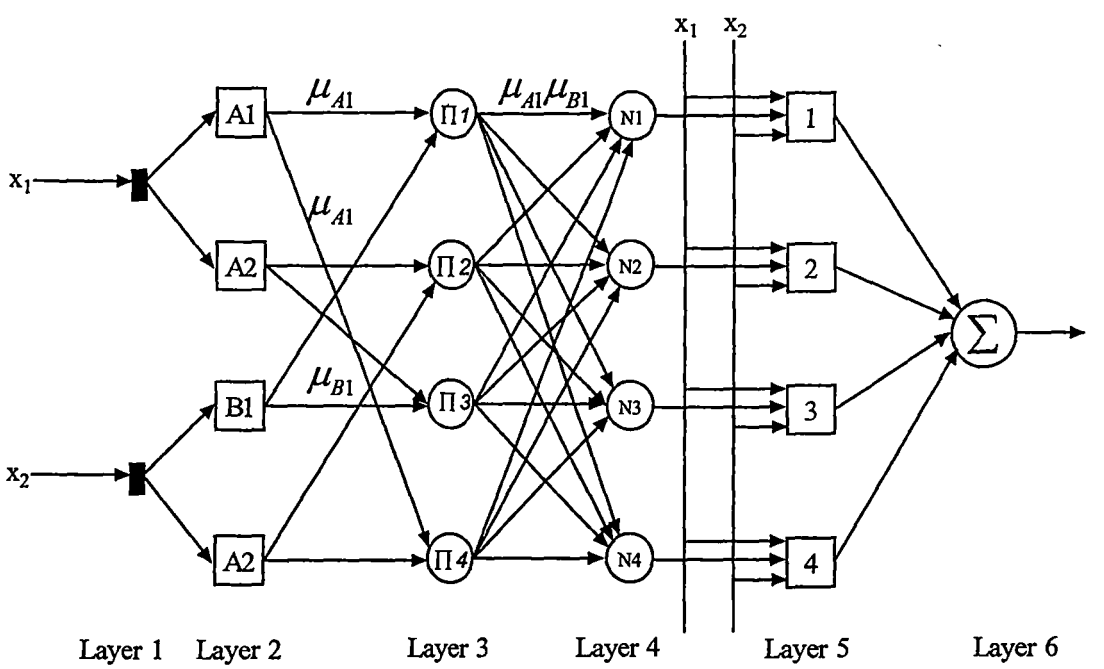

Figure 3.28. Typical ANFIS architecture [3].

Architecture of a typical ANFIS is shown in Fig. 3.28 [3]. The interconnected network consists of the following layers [32]:

Layer 1. This layer is known as the input layer. At this layer, the inputs x_1 and x_2 are applied and are passed without being processed to a number of neurons in Layer 2.

Layer 2. This layer is called the fuzzification layer. At this Layer, neurons perform fuzzification in the incoming inputs x_1 and x_2. The output of this layer is as follows:

$$y_{Ai} = \mu_{Ai}$$
$$y_{Bi} = \mu_{Bi} \tag{3.22}$$

Layer 3. This layer is known as the rule layer. At this layer each neuron evaluates a single Sugeno-type fuzzy rule. The rule neurons calculate the firing strength by determining the product of the incoming signals as shown below.

$$y_{\Pi i} = \prod_{j=1} x_{ji} \tag{3.23}$$

From Fig. 3.13, the output of the 1st neuron in layer 3 is given below:

$$y_{\Pi 1} = \mu_{A1}\mu_{B1} \tag{3.24}$$

where μ_{A1} represents the firing strength of Rule 1.

Layer 4. This layer is called the normalization layer. The neurons of this layer receive inputs from all neurons of Layer 3. Here the normalized firing strength is calculated as the ratio of the firing strength of a given rule to the sum of firing strengths of all rules as shown below.

$$y_{Ni} = \frac{\mu_i}{\sum_{j=1}^{n} \mu j} = \overline{\mu_i} \tag{3.25}$$

Here the output represents the contribution of a particular rule to the final result.

Layer 5. This layer is known as the defuzzification layer. Each neuron in this layer has the inputs of both the original input signals x_1 and x_2 and the output from Layer 4. At this layer each neuron calculates the weighted consequent value of a particular rule as shown below :

$$y_i = \overline{\mu_i}(k_{i0} + k_{i1}x_1 + k_{i2}x_2) \tag{3.26}$$

where $\overline{\mu_i}$ - is the input of defuzzification neuron i in Layer 5;

y_i - is the output of defuzzification neuron i in Layer 5;

k_{i0}, k_{i1}, and k_{i2} are a set of consequent parameters of rule i.

These consequent parameters are learnt by the ANFIS during the training process and used to tune the membership functions.

Layer 6. This layer is known as the summation neuron layer. This layer consists of one neuron that adds together the outputs from Layer 5. The total sum of these inputs is the ANFIS output, y ANFIS, shown below.

$$y_{ANFIS} = \sum_{i=1}^{n} y_i \tag{3.27}$$

In ANFIS, for each iteration of the training algorithm, there is a forward pass and a backward pass [4]. In a forward pass, the inputs are applied to the ANFIS. Neuron outputs are calculated layer-by-layer and rule consequent parameters defined. Once the forward pass has been completed and the error is determined the second part of the iteration is implemented. Here the back-propagation algorithm is applied. The error is propagated back through the network. The antecedent parameters are updated according to the chain rule [4].

Using membership parameters and a training set of Z input-output data pairs, we are able to construct Z linear equations in terms of the consequent parameters as shown in Eq. (3.24).

$$\begin{aligned}
y_d(1) &= \overline{\mu_1}(1)f_1(1)+\overline{\mu_2}(1)f_2(1)+\ldots+\overline{\mu_n}(1)f_n(1)\\
y_d(2) &= \overline{\mu_1}(2)f_1(2)+\overline{\mu_2}(2)f_2(2)+\ldots+\overline{\mu_n}(2)f_n(2)\\
&\vdots \qquad\qquad \vdots \qquad\qquad \vdots\\
&\vdots \qquad\qquad \vdots \qquad\qquad \vdots\\
y_d(Z) &= \overline{\mu_1}(Z)f_1(Z)+\overline{\mu_2}(Z)f_2(Z)+\ldots+\overline{\mu_n}(Z)f_n(Z)
\end{aligned} \tag{3.28}$$

where y_d is a $Z\times 1$ desired output vector.

as $f_1(i) = k_{10} + k_{11}x_1(i) + k_{12}x_2(i) + k_{13}x_3(i)\cdots + k_{1m}x_m(i)$, substituting the value of $f_1(i)$ into Eq. (3.28),

$$
\begin{aligned}
y_d(1) &= \overline{\mu_1}(1)(k_{10} + k_{11}x_1(1) + k_{12}x_2(1) + k_{13}x_3(1) \cdots + k_{1m}x_m(1)) \\
&\quad + \overline{\mu_2}(1)(k_{20} + k_{21}x_1(1) + k_{22}x_2(1) + k_{23}x_3(1) \cdots + k_{2m}x_m(1)) + \ldots \\
&\quad + \overline{\mu_n}(1)(k_{n0} + k_{n1}x_1(1) + k_{n2}x_2(1) + k_{n3}x_3(1) \cdots + k_{nm}x_m(1)) \\
y_d(2) &= \overline{\mu_1}(2)(k_{10} + k_{11}x_1(2) + k_{12}x_2(2) + k_{13}x_3(2) \cdots + k_{1m}x_m(2)) \\
&\quad + \overline{\mu_2}(2)(k_{20} + k_{21}x_1(2) + k_{22}x_2(2) + k_{23}x_3(2) \cdots + k_{2m}x_m(2)) + \ldots \\
&\quad + \overline{\mu_n}(2)(k_{n0} + k_{n1}x_1(2) + k_{n2}x_2(2) + k_{n3}x_3(2) \cdots + k_{nm}x_m(2)) \qquad (3.29) \\
&\vdots \qquad\qquad \vdots \qquad\qquad \vdots \\
&\vdots \qquad\qquad \vdots \qquad\qquad \vdots \\
y_d(Z) &= \overline{\mu_1}(Z)(k_{10} + k_{11}x_1(Z) + k_{12}x_2(Z) + k_{13}x_3(Z) \cdots + k_{1m}x_m(Z)) \\
&\quad + \overline{\mu_2}(Z)(k_{20} + k_{21}x_1(Z) + k_{22}x_2(Z) + k_{23}x_3(Z) \cdots + k_{2m}x_m(Z)) + \ldots \\
&\quad + \overline{\mu_n}(Z)(k_{n0} + k_{n1}x_1(Z) + k_{n2}x_2(Z) + k_{n3}x_3(Z) \cdots + k_{n}x_m(Z))
\end{aligned}
$$

where m is the number of input variables, n is the number of neurons in Layer 3, In matrix form, we can write:

$$y_d = AK \qquad (3.30)$$

where

$$y_d = \begin{bmatrix} y_d(1) \\ y_d(2) \\ \vdots \\ y_d(Z) \end{bmatrix}, \text{ and}$$

$$A = \begin{bmatrix}
\overline{\mu_1} & \overline{\mu_1}(1)x_1(1) & \cdots & \overline{\mu_1}(1)x_m(1) & \cdots & \overline{\mu_n}(1) & \overline{\mu_n}(1)x_1(1) & \cdots & \overline{\mu_n}(1)x_m(1) \\
\overline{\mu_1} & \overline{\mu_1}(2)x_1(2) & \cdots & \overline{\mu_1}(2)x_m(2) & \cdots & \overline{\mu_n}(2) & \overline{\mu_n}(2)x_1(2) & \cdots & \overline{\mu_n}(2)x_m(2) \\
\vdots & \vdots & \ddots & \vdots & \ddots & \vdots & \vdots & \ddots & \vdots \\
\overline{\mu_1} & \overline{\mu_1}(Z)x_1(Z) & \cdots & \overline{\mu_1}(Z)x_m(Z) & \cdots & \overline{\mu_n}(Z) & \overline{\mu_n}(Z)x_1(Z) & \cdots & \overline{\mu_n}(Z)x_m(Z)
\end{bmatrix}$$

$n \geq 0$

$m \geq 0$

where k is $n(1+m)\times 1$ vector of unknown consequent parameters as shown in Eq. (3.30).

$$k = [k_{nm}]^T = [k_{10} \;\; k_{11} \;\; k_{12} \;\; \cdots \;\; k_{1m} \;\; k_{20} \;\; k_{21} \;\; k_{22} \;\; \cdots \;\; k_{2m} \;\; \cdots \;\; k_{n0} \;\; k_{n1} \;\; k_{n2} \;\; \cdots \;\; k_{nm}]^T$$

The actual network output, y_{ANFIS}, is determined once the rule consequent parameters have been established. The actual network output is then compared with

the desired output, y, which defines the error vector between these two outputs as shown in Eq. (3.31)

$$e = y_d - y \tag{3.31}$$

Once the forward pass has been completed and the error determined the second part of the epoch is implemented, the backward pass. Here the back propagation algorithm is applied. The error determined from Equation above is propagated back through the network. The antecedent parameters are updated according to the chain rule [4]. This process continues depending on how many epochs are specified for training.

To determine how well the fuzzy inference system has learnt during the training process it is important to validate the model. Here model validation is defined as the process by which the input vectors from the input-output data sets, on which the fuzzy inference system was not trained, are presented to the trained fuzzy inference system model with the model outputs compared to the output values which are expected [33]. The data set here is known as a Test Data Set. Another type of data set used for model validation is referred to as a Checking Data Set. This data set is used for testing the generalization capability of the fuzzy inference system at each epoch in order to control the potential for the model over fitting the data. When both checking data and training data are presented to the fuzzy inference system the model is selected to have parameters associated with the minimum checking data model error.

Let us consider an arc furnace model using the ANFIS model. The input of the model is the voltage and the current of the arc furnace and the output is the real power as shown in Fig. 3.29.

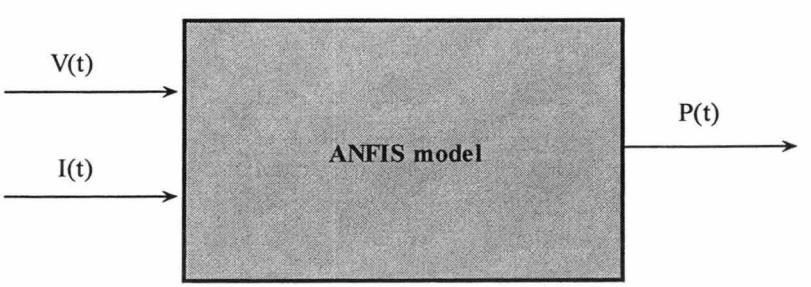

Figure 3.29. ANFIS model.

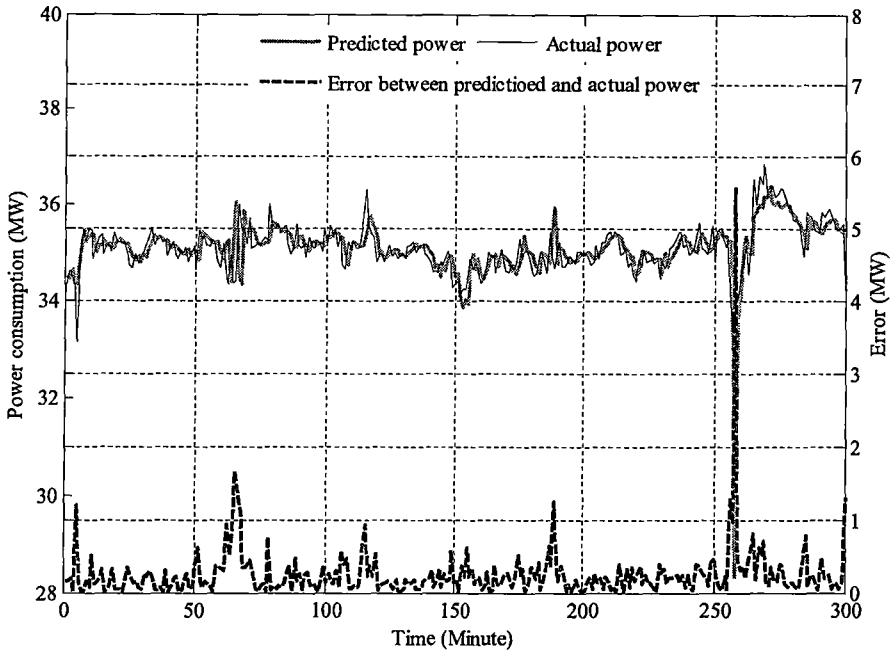

Figure 3.30. ANFIS output.

The power response of the arc furnace is obtained using ANFIS model based on the arc voltage and the arc current. In Fig. 3.30, the bold line represents the predicted power, the thin line represents the actual power consumption from the arc furnace, and the dotted bold line at the bottom of the graph represents the difference between the actual power and the predicted power. The accuracy of the model has improved dramatically and the MSE (mean square error) is about 0.35 MW.

3.4 Conclusion

This chapter provided an overview of computational intelligence as a major tool for modelling the arc furnace. Artificial neural networks, fuzzy inference systems and adaptive neuro fuzzy inference systems were investigated. Arc furnace models were developed using these different techniques. It was demonstrated that the arc power consumption changed randomly due to random change of the voltage and current. The MLP and ANFIS models were used to extract the non-linear and time-varying patterns of the arc power due to the variation of the arc voltage and current. The models were tested with actual power consumption data. It was

demonstrated that the accuracy of the MLP and ANFIS models was satisfactory. In the next chapter, these models will be used intensively for case studies and analysis. Short term-behaviour prediction models for the arc voltage and power response will be developed, and results will be presented and analysed.

Chapter 4: Model Implementation, Results, Case Study Analysis and Discussion

4.1 Introduction

The main objective of this chapter is to examine the implementation of different arc furnace models to obtain the arc furnace response and evaluate the performance of the presented models. In previous chapters, different modelling techniques including conventional and black-box modelling were discussed. In Chapter 1, arc furnaces were considered as a load and were modelled using load modelling techniques. In Chapter 2, arc furnaces were modelled using conventional mathematical methods. In Chapter 3, arc furnaces are modelled using artificial

intelligence techniques. In this chapter, the instantaneous response of the arc voltage and arc current are investigated using conventional methods. Using load modelling approaches and artificial intelligence techniques, random patterns of the arc voltage – power (real and reactive) relationships are investigated. In addition to that, techniques for predicting arc furnace parameters such as the arc voltage are developed using artificial intelligence techniques. Let us consider first a simple case, where the arc voltage and current response are achieved using conventional modelling approaches. In order to do that, a prototype metallurgical plant is developed, which is discussed in the following section.

4.2 A simple metallurgical plant

The key elements of a metallurgical plant are the voltage source *Vs(t)*, power cables (*Ls* and L_F); transforms (*T1* and *T2)*, power factor correction capacitors (*C)*, the arc furnace load as shown in Fig. 4.1.

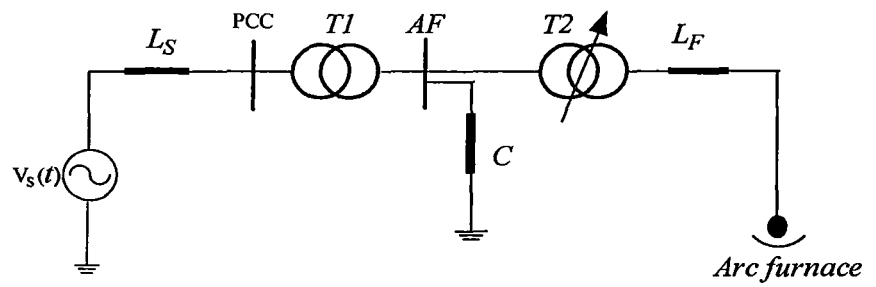

Figure 4.1. Prototype metallurgical plant.

For convenience of our analysis, the system is assumed to be a single phase balance load represented in Fig. 4.2.

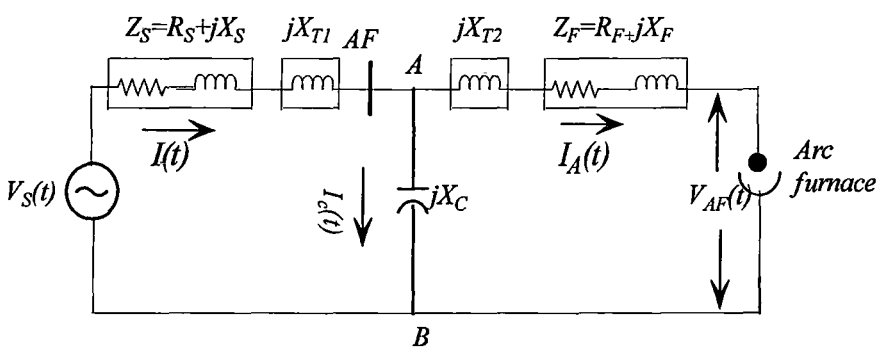

Figure 4.2. Single line diagram of a metallurgical plant.

In Fig. 4.2, the power cables (L_S and L_F) are modelled using the complex combination of the resistance (R) and reactance (X). The power factor correction capacitor is modelled using capacitive reactance (X_C). It is assumed that, $I_A(t)$ is the current passing through the arc furnace, $I_C(t)$ is the current passing through the power factor correction capacitor, $I(t)$ is the current from the supply system, and $V_{AF}(t)$ is the voltage of the arc furnace. Now the system can be described by the following equations:

Kirchhoff's Law applied to the plant shown in Fig. 4.2,

$$V_S(t) = R_S I(t) + (L_S + L_{T1})\frac{dI(t)}{dt} + R_{AF} I_A(t) + (L_{T2} + L_{AF})\frac{dI_A(t)}{dt} + V_{AF}(t) \quad (4.1)$$

The system shown in Fig. 4.2 can be simplified further using Thevenin theorem in points A and B. The expressions for the thevenin voltage and equivalent resistance are obtained as follows:

$$Z_{EQ} = \frac{jX_C(Z_S + jX_{T1})}{(jX_C + Z_S + jX_{T1})} = R_{EQ} + jX_{EQ} \quad (4.2)$$

$$V_{TH} = \frac{jX_C}{(jX_C + Z_S)} V_S(t) \quad (4.3)$$

Considering that $X_{AF} = X_F + X_{T2}$, $R_{AF} = R_F$, and $Z_{AF} = R_{AF} + jX_{AF}$, the system becomes as shown in Fig. 4.3.

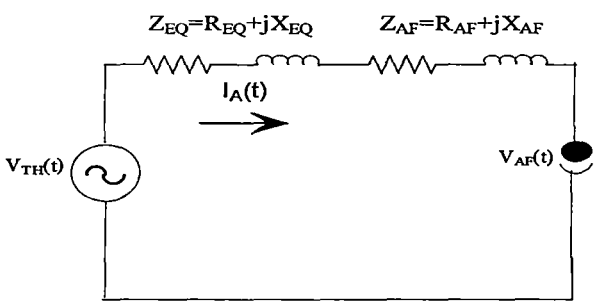

Figure 4.3. Equivalent Thévenin's circuit.

Applying Kirchhoff's Law to Fig. 4.3, we obtain:

$$V_{TH}(t) = (R_{EQ} + R_F) I_A(t) + (L_{EQ} + L_F)\frac{dI_A(t)}{dt} + V_{AF}(t) \quad (4.4)$$

A simulation study is conducted on the test system shown in Fig. 4.3 using MATLAB. A sinusoidal voltage is applied as an input. The network parameters are

assumed the same as in [34], that is the power rating of the arc furnace is 70 MVA, the tap setting for the arc furnace transformer is 33/.651 kV, and the system frequency is 60 Hz. The parameters of the equivalent circuit are given in Table 4.1 [34]:

Table 4.1: Equivalent Thévenin's circuit parameter

V_{TH} (V)	Z_{EQ} (mΩ)	Z_{AF} (mΩ)
566	0.0528+j0.468	0.3366+j3.22

The arc voltage and current responses for different models are discussed below.

Model 1. The arc furnace voltage and current response of Model 1 can be obtained by substituting the value of the arc voltage from Eq. (2.1) into Eq. (4.4) as shown below:

$$v = \begin{cases} iR_1; & 0 \le i \le i_{ig} \\ iR_2 + V_{ig}(1 - \dfrac{R_2}{R_1}); & i_{ig} < i \le i_{ex} \end{cases} \quad (2.1);$$

and $$V_{TH}(t) = \left(R_{EQ} + R_F\right) I_A(t) + \left(L_{EQ} + L_F\right) \frac{dI_A(t)}{dt} + V_{AF}(t) \quad (4.4)$$

Substituting the value of arc voltage (v) from (2.1) to arc voltage $(V_{AF}(t))$ in Eq. (4.4):

$$V_{TH}(t) = \begin{cases} \left(R_{EQ} + R_F\right) I_A(t) + \left(L_{EQ} + L_F\right) \dfrac{dI_A(t)}{dt} + I_A(t) R_1; & 0 \le I_A(t) \le i_{ig} \\ \left(R_{EQ} + R_F\right) I_A(t) + \left(L_{EQ} + L_F\right) \dfrac{dI_A(t)}{dt} + I_A(t) R_2 + V_{ig}(1 - \dfrac{R_2}{R_1}); & i_{ig} < I_A(t) \le i_{ex} \end{cases}$$

The response of the arc voltage and the arc current is presented in Fig. 4.4. The parameters of Model 1 are shown in the following [24]:

R_1= 50 m Ω;

R_2= -0.76 m Ω;

i_{ig}= i_{ex} = 7.02 k A.

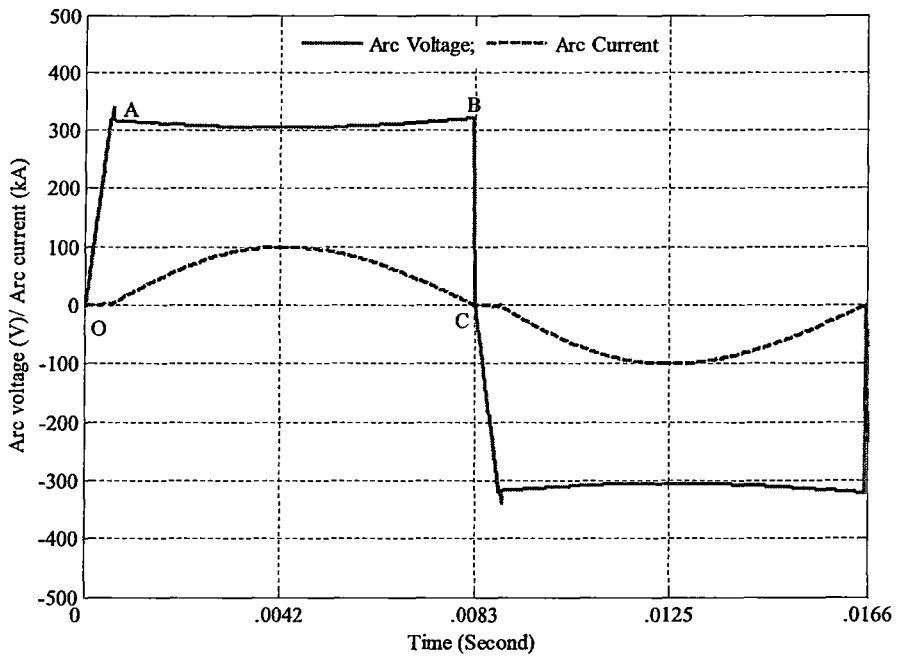

Figure 4.4. Response of arc voltage and arc current of Model 1.

In Fig. 4.4, line OA represents the arc voltage that increases linearly from zero to the arc ignition voltage (v_{ig}). This period is known as pre-ignition stage and was discussed in Section 2.2. Line AB represents the ignition stage when the arc is established. During ignition stage, the arc voltage decreases slowly as the value of the arc current increases and vise-versa because of the presence of the negative resistance (R_2) in the arc furnace. When the arc extinguishes, the arc voltage drops rapidly to zero as can be seen from the position of line BC.

Model 2. The arc furnace voltage and current response of Model 2 can be achieved by applying the value of arc voltage from Eq. (2.6) into Eq. (4.4) as shown below.

$$v=\begin{cases} iR_1; & \left(i\le i_1 \quad \& \quad \dfrac{di}{dt}>0\right) \quad or \quad \left(i\le i_4 \quad \& \quad \dfrac{di}{dt}<0\right) \\ R_2(i-i_1)+V_1; & i_1<i\le i_2 \quad \& \quad \dfrac{di}{dt}>0 \\ R_3(i-i_2)+V_2; & i_3<i\le i_2 \quad \& \quad \dfrac{di}{dt}<0 \\ R_4(i-i_3)+V_3; & i_4<i\le i_3 \quad \& \quad \dfrac{di}{dt}<0 \end{cases} \tag{2.6}$$

and $$V_{TH}(t)=\left(R_{EQ}+R_F\right)I_A(t)+\left(L_{EQ}+L_F\right)\frac{dI_A(t)}{dt}+V_{AF}(t) \tag{4.4}$$

Substituting the value of arc voltage (v) from (2.6) to arc voltage $(V_{AF}(t))$ in Eq. (4.4), we have:

$$V_{TH}(t)=\begin{cases} \left(R_{EQ}+R_F\right)I_A(t)+\left(L_{EQ}+L_F\right)\dfrac{dI_A(t)}{dt}+I_A(t)R_1; & \left(I_A(t)\le i_1 \;\&\; \dfrac{dI_A(t)}{dt}>0\right) or \left(I_A(t)\le i_4 \;\&\; \dfrac{dI_A(t)}{dt}<0\right) \\ \left(R_{EQ}+R_F\right)I_A(t)+\left(L_{EQ}+L_F\right)\dfrac{dI_A(t)}{dt}+R_2\left(I_A(t)-i_1\right)+V_1; & i_1<I_A(t)\le i_2 \quad \& \quad \dfrac{dI_A(t)}{dt}>0 \\ \left(R_{EQ}+R_F\right)I_A(t)+\left(L_{EQ}+L_F\right)\dfrac{dI_A(t)}{dt}+R_3\left(I_A(t)-i_2\right)+V_2; & i_3<I_A(t)\le i_2 \quad \& \quad \dfrac{dI_A(t)}{dt}<0 \\ \left(R_{EQ}+R_F\right)I_A(t)+\left(L_{EQ}+L_F\right)\dfrac{dI_A(t)}{dt}+R_4\left(I_A(t)-i_3\right)+V_3; & i_4<I_A(t)\le i_3 \quad \& \quad \dfrac{dI_A(t)}{dt}<0 \end{cases}$$

The response of the arc voltage and the arc current is presented in Fig. 4.5. The parameters of Model 2 are shown in the followings [22, 24]:

$R_1 = R_4 = 50\ m\Omega$;

$R_2 = -0.76\ m\Omega$;

$R_3 = 3.76\ m\Omega$;

$V_1 = 300$ V;

$V_2 = 304$ V;

$V_3 = 281$ V.

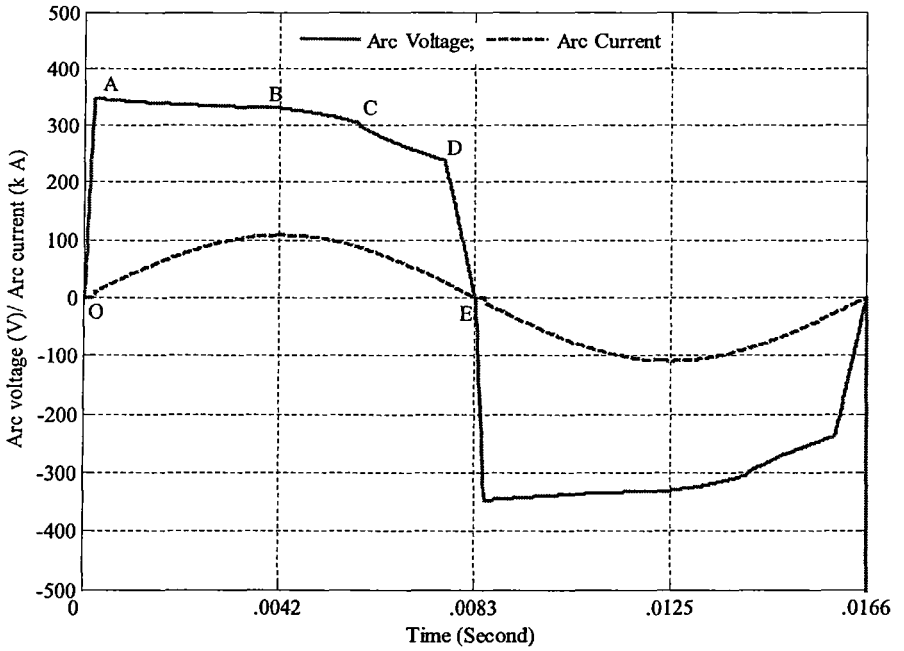

Figure 4.5. Response of arc voltage and arc current of Model 2.

In Fig. 4.5, line OA represents the arc voltage that increases linearly from zero to the arc ignition voltage (v_{ig}) as the arc current increases from zero to the arc ignition current (i_1). Lines AB, BC and CD represent the arc voltage in the ignition stage that corresponds to the resistances R_2, R_3 , and R_4, respectively. Line DE represents the arc voltage at the arc extinguishing period.

Model 3. The arc furnace voltage and current response of Model 3 can be obtained by applying the value of the arc voltage from Eq. (2.8) into Eq. (4.4) as shown below.

$$v=\begin{cases} iR_1, & 0\le i\le i_1 \quad \& \quad \dfrac{di}{dt}>0 \\ V_1+(V_{ig}-V_1)\exp\left(\dfrac{(i-i_1)}{i_T}\right), & i_1<i\le i_2 \& \dfrac{di}{dt}>0 \\ R_3(i-i_2)+V_2, & i_2<i\le i_3 \& \dfrac{di}{dt}<0 \\ iR_1, & 0\le i\le i_4 \quad \& \quad \dfrac{di}{dt}<0 \end{cases} \tag{2.8}$$

and $$V_{TH}(t)=\left(R_{EQ}+R_F\right)I_A(t)+\left(L_{EQ}+L_F\right)\frac{dI_A(t)}{dt}+V_{AF}(t) \tag{4.4}$$

Substituting the value of arc voltage (v) from (2.8) to arc voltage $(V_{AF}(t))$ in Eq. (4.4), we have:

$$V_{TH}(t)=\begin{cases} \left(R_{EQ}+R_F\right)I_A(t)+\left(L_{EQ}+L_F\right)\dfrac{dI_A(t)}{dt}+I_A(t)R_1, & 0\le I_A(t)\le i_1 \quad \& \quad \dfrac{dI_A(t)}{dt}>0 \\ \left(R_{EQ}+R_F\right)I_A(t)+\left(L_{EQ}+L_F\right)\dfrac{dI_A(t)}{dt}+{}_1+(V_{ig}-V_1)\exp\left(\dfrac{\left(I_A(t)-i_1\right)}{i_T}\right), & i_1<I_A(t)\le i_2 \quad \& \quad \dfrac{di}{dt}>0 \\ \left(R_{EQ}+R_F\right)I_A(t)+\left(L_{EQ}+L_F\right)\dfrac{dI_A(t)}{dt}+R_3\left(I_A(t)-i_2\right)+V_2, & i_2<I_A(t)\le i_3 \quad \& \quad \dfrac{dI_A(t)}{dt}<0 \\ \left(R_{EQ}+R_F\right)I_A(t)+\left(L_{EQ}+L_F\right)\dfrac{dI_A(t)}{dt}+iR_1, & 0\le I_A(t)\le i_4 \quad \& \quad \dfrac{dI_A(t)}{dt}<0 \end{cases}$$

The response of the arc voltage and the arc current is presented in Fig. 4.6. The parameters of Model 3 are shown in the followings [23, 24]:

R_1= 50 mΩ;

R_3= - 0.76 mΩ;

V_{ig}= 350.75 V;

V_1= 289.7 V;

V_3=305 V;

i_T= 30 kA.

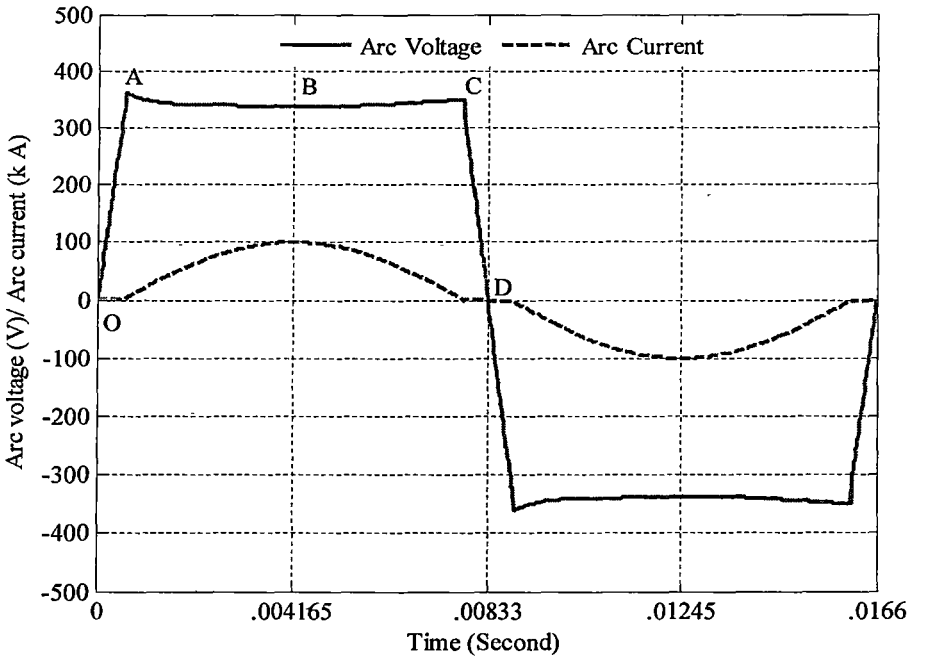

Figure 4.6. Response of arc voltage and arc current of Model 3.

In Fig. 4.6, line OA represents the arc voltage that increases linearly from zero to the arc ignition voltage (v_{ig}) as the arc current increases from zero to a certain value known as the arc ignition current (i_{ig}). The arc ignites when the arc current becomes greater that the arc ignition current. During the ignition period, the arc voltage is assumed to decrease exponentially with the time constant i_T as the arc current increases. This phase is represented by line AB. Line BC represents the arc voltage during ignition period when it increases as the arc current decreases due to the presence of the negative resistance. Line CD represents the arc voltage when the arc extinguishes.

Model 4. The arc furnace voltage and current response of Model 4 can be achieved by applying the value of the arc voltage from Eq. (2.10) into Eq. 4.4:

$$v = sign(i)\left(V_D + \frac{C}{D + |i|}\right) \tag{2.10}$$

and $$V_{TH}(t) = \left(R_{EQ} + R_F\right) I_A(t) + \left(L_{EQ} + L_F\right)\frac{dI_A(t)}{dt} + V_{AF}(t) \tag{4.4}$$

Substituting the value of arc voltage (v) from (2.10) to arc voltage $(V_{AF}(t))$ in Eq. (4.4), we have:

$$V_{TH}(t) = \left(R_{EQ} + R_F\right) I_A(t) + \left(L_{EQ} + L_F\right)\frac{dI_A(t)}{dt} + sign\left(I_A(t)\right)\left(V_D + \frac{C}{D + \left|I_A(t)\right|}\right)$$

The response of the arc voltage and the arc current is presented in Fig. 4.7. The parameters of Model 4 are assumed as following [23, 24]:

C= 1.68 MW;

D= 20.65 k A; and

V_D= 289.7 V.

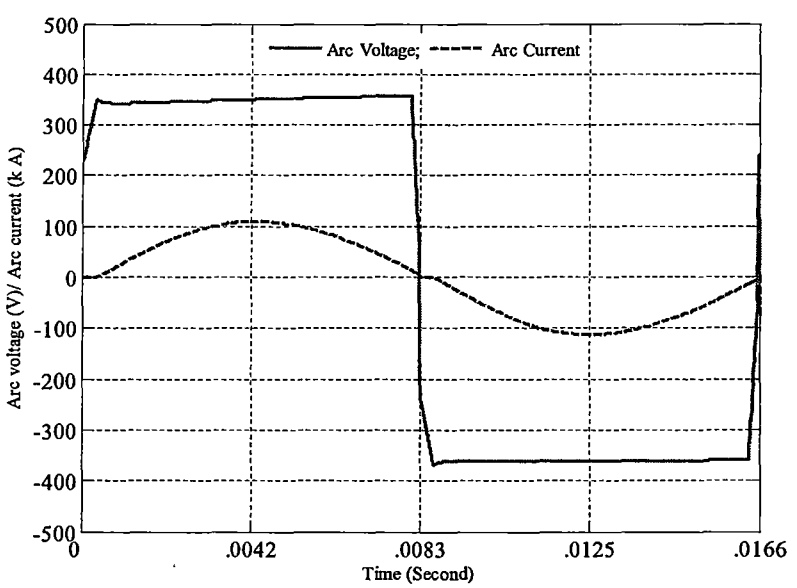

Figure 4.7. Response of arc voltage and arc current in Model 4.

From Fig. 4.7 the arc voltage develops sharply as the arc current passes the zero crossing value. Once the arc voltage is developed, it tends to be constant and has very little effect with the change of the arc current. The arc voltage extinguishes rapidly as the arc current reaches the zero crossing point.

Model 5. The arc furnace voltage and current response of Model 5 can be achieved by applying the value of arc voltage from Eq. (2.18) into Eq. (4.4) as shown below:

$$V(t) = R_A(t) I_A(t) \tag{2.18}$$

and $$V_{TH}(t) = \left(R_{EQ} + R_F\right) I_A(t) + \left(L_{EQ} + L_F\right) \frac{dI_A(t)}{dt} + V_{AF}(t) \tag{4.4}$$

Substituting the value of arc voltage $(V(t))$ from (2.6) to arc voltage $(V_{AF}(t))$ in Eq. (4.4), we have:

$$V_{TH}(t) = \left(R_{EQ} + R_F\right) I_A(t) + \left(L_{EQ} + L_F\right) \frac{dI_A(t)}{dt} + R_A(t) I_A(t)$$

where,
$$R_A = \begin{cases} R_{ig}; & 0 \le |I_A(t)| < I_{ig} \text{ and } \dfrac{d(|I_A(t)|)}{dt} > 0 \\ \dfrac{\left(V_D - (V_{ig} - V_D) e^{(|I_A(t)| - I_{IG})/\tau_1}\right)}{|I_A(t)|}; & |I_A(t)| \ge I_{IG} \text{ and } \dfrac{d(|I_A(t)|)}{dt} > 0 \\ \left(V_T - (V_{ig} - V_T) e^{(|I_A(t)|)/\tau_2}\right) \Big/ (|I_A(t)| + I_{ig}); & \dfrac{d(|I_A(t)|)}{dt} < 0 \end{cases}$$

The response of the arc voltage and the arc current is presented in Fig. 4.8. The parameters of Model 5 are shown in the following [24, 26]:

$V_{ig} = 300$ V;

$V_D = 289.7$ V;

$R_A = 50\ \text{m}\Omega$.

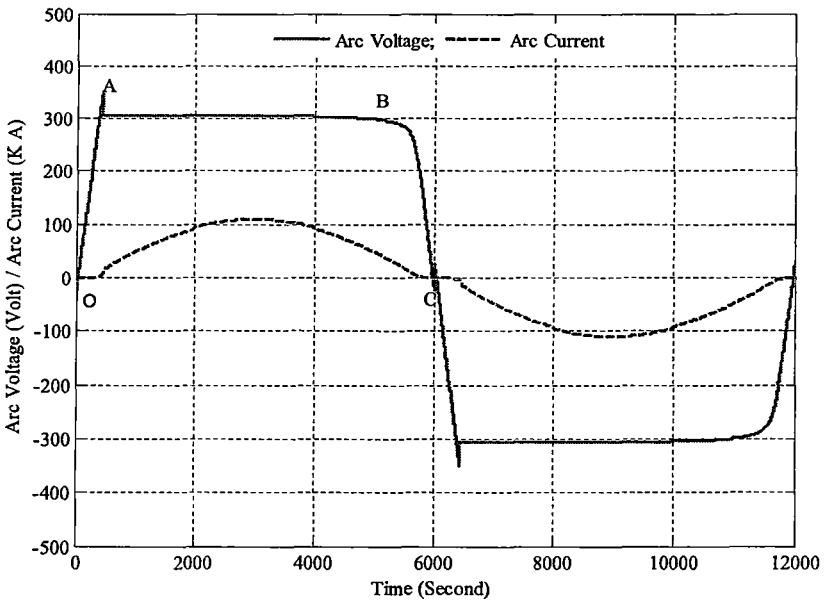

Figure 4.8. Response of arc voltage and arc current of Model 5.

In Fig. 4.8, line OA represents the arc voltage that increases linearly proportional to the arc current from zero to the arc ignition voltage (v_{ig}). This phase is known as pre-ignition stage. Line AB represents the ignition stage, when the arc voltage remains constant. Line BC represents the extinction stage when the arc voltage decreases sharply.

Model 6. The arc furnace voltage and current response of Model 6 can be achieved by substituting the arc voltage from Eq. (2.18) into Eq. (4.4) as shown below.

$$v_a = \frac{2V_0 \sin \omega t}{1 - \dfrac{\sin(2\omega t + \psi_a)}{\sqrt{1+(\tau_a)^2}}} \tag{2.19}$$

and $$V_{TH}(t) = \left(R_{EQ} + R_F\right) I_A(t) + \left(L_{EQ} + L_F\right) \frac{dI_A(t)}{dt} + V_{AF}(t) \tag{4.4}$$

Substituting the value of arc voltage (v_a) from (2.6) to arc voltage $(V_{AF}(t))$ in Eq. (4.4), we have:

$$V_{TH}(t) = \left(R_{EQ} + R_F\right) I_A(t) + \left(L_{EQ} + L_F\right) \frac{dI_A(t)}{dt} + \frac{2V_0 \sin \omega t}{1 - \frac{\sin(2\omega t + \psi_a)}{\sqrt{1+(\tau_a)^2}}}$$

where, and $V_0 = \frac{P_{ro}}{\sqrt{2}I}$, $\tan\psi_a = \frac{1}{2\omega\tau_a}$

The response of the arc voltage and the arc current is presented in Fig. 4.9. The parameters of Model 6 are shown in the following [26]:

$V_O = 300$ V and $P_{ro} = 1.8$ MW.

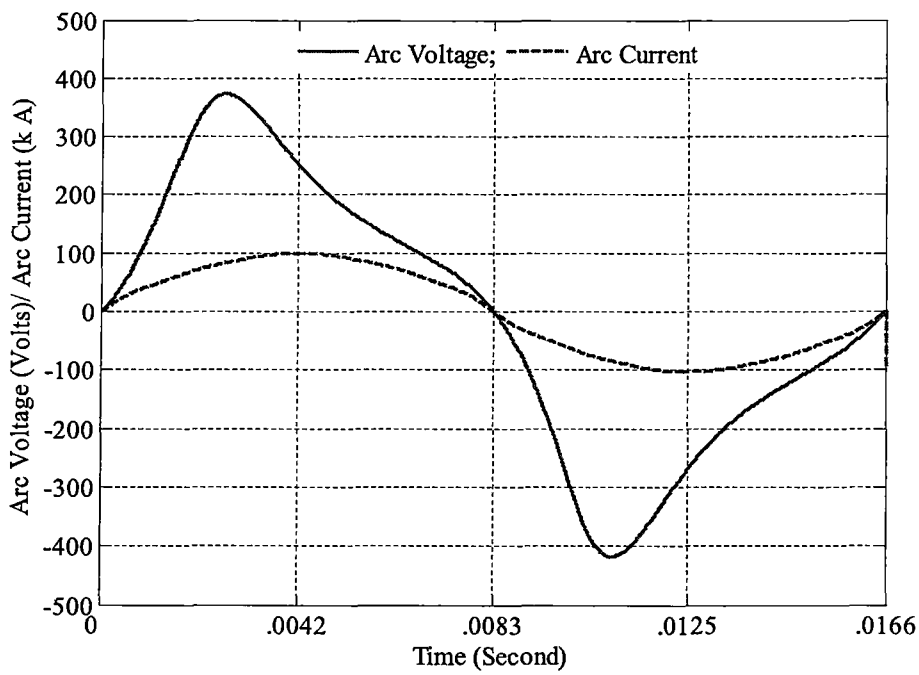

Figure 4.9. Response of arc voltage and arc current of Model 6.

As can be seen from Fig. 4.9, the arc voltage increases to a certain value and decreases slowly for each half cycle. The arc current demonstrates almost sinusoidal behaviour.

Model 7. The arc voltage and current response of Model 7 can be achieved by substituting the expression of the arc voltage from Eq. (2.20) into Eq. (4.4) as shown below.

$$v = V_D \; x \; sign(i) \tag{2.20}$$

and $$V_{TH}(t) = \left(R_{EQ} + R_F\right) I_A(t) + \left(L_{EQ} + L_F\right) \frac{dI_A(t)}{dt} + V_{AF}(t) \tag{4.4}$$

Substituting the value of arc voltage $(V(t))$ from (2.20) to arc voltage $(V_{AF}(t))$ in Eq. (4.4), we have:

$$V_{TH}(t) = \left(R_{EQ} + R_F\right) I_A(t) + \left(L_{EQ} + L_F\right) \frac{dI_A(t)}{dt} + sign\left(I_A(t)\right) V_D$$

The response of the arc voltage and the arc current is presented in Fig. 4.10. The parameters of Model 7 are assumed as following [26]:

$V_D = 350$ V.

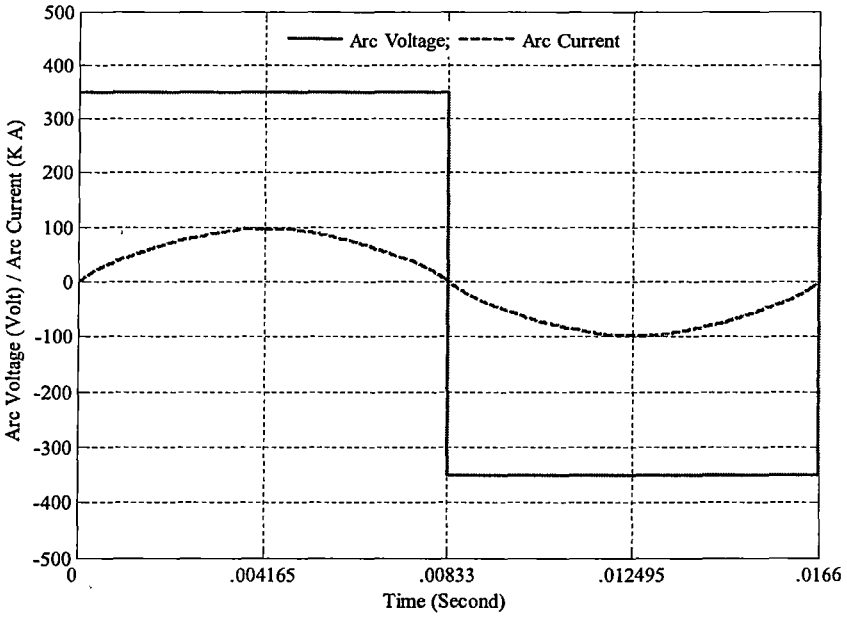

Figure 4.10. Response of arc voltage and arc current of Model 7.

It can be seen from Fig. 4.10, the arc voltage develops suddenly as the arc current passes its zero value. The arc current shows almost sinusoidal behaviour.

The general comparison about the arc voltage and arc current obtained from the different models are as follows:

- Models 1, 2, 3, 4, 5, and 6 demonstrate that it takes time to generate the arc because of the presence of higher resistance in pre-ignition stage.
- The arc current initially increases slowly until the arc current reaches some specific current as the presence of high resistance in pre-ignition stage.

The main advantage of the conventional models is their ability to capture the instantaneous wave-form of the arc voltage and arc current. As a result, these models work efficiently for a single cycle of operation. However, because of random nature

of process, it is not possible to predict the behaviour of the arc furnace, and thus conventional modelling is not quite suitable for the time series prediction of the arc furnace responses. A black box modelling approaches such as artificial neural networks and neuro-fuzzy systems are used in order to simulate random nature of the arc furnace responses. As black box models are based on empirical relationships between the input and the output variables, the input-output data are collected from a typical metallurgical plant situated in the northern Tasmania. A brief description of this plant is presented in the following section:

4.3 Description of a metallurgical plant

A single line diagram of a metallurgical plant consists of four arc furnaces and few auxiliary loads such as induction motors and lightings is shown in Fig. 4.11.

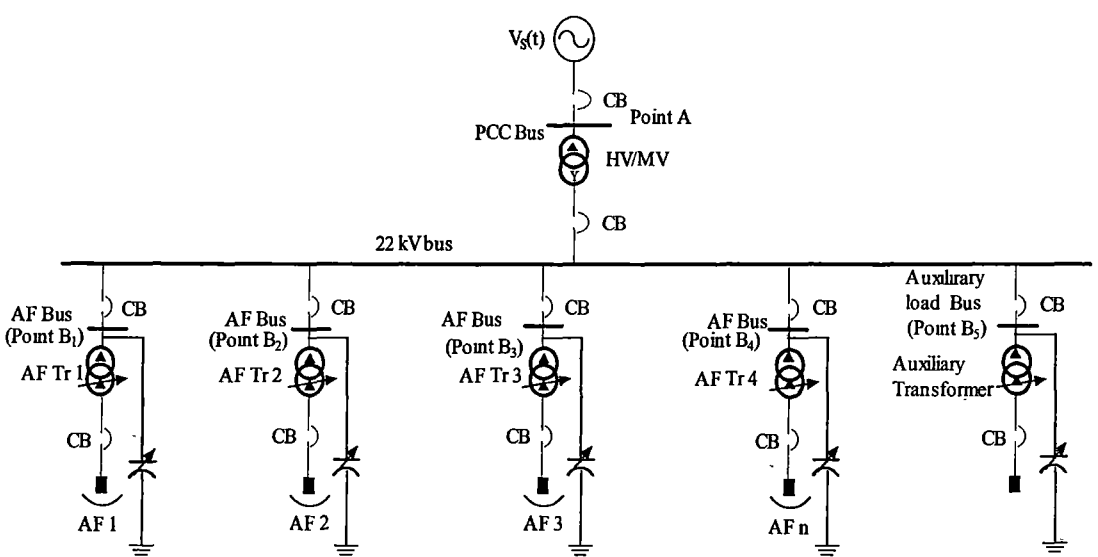

Figure 4.11. A metallurgical plant with four arc furnaces and auxiliary loads.

The plant is supplied by the 110 kV utility system. A HV/ MV transformer is connected to the utility system to convert voltage level from 110 kV to 22 kV. The 22 kV bus is connected with four arc furnaces via four arc furnace transformers. The

auxiliary loads are connected to the 22 kV bus via auxiliary load transformer. The arc furnace transformer is a tap changer, where the primary side voltage is 22 KV and the secondary side voltage varies from 120 V to 270 V. The rating of the auxiliary transformer is 22 kV/3.3 kV. The load pattern of this plant is similar to the load pattern of the arc furnace load as four arc furnaces consume about 85% of the total power of the plant. The important points of the plant are identified as the PCC bus (point A), arc furnace buses (point B_1, point B_2, point B_3, point B_4) and the auxiliary load bus (point B_5). The responses of the PCC bus (point A) represent the characteristics of the entire pant, the arc furnace buses (points B_1, B_2 , B_3, and B_4) represent the characteristics of individual arc furnace, and auxiliary load bus (point B_5) represents the combine characteristic of all auxiliary loads of the plant. In this section, load modelling techniques and artificial intelligence techniques are used to obtain power (both real and reactive) response because of the changes in bus voltage.

4.3.1 The load response of PCC bus (Point A)

The first step is to analyse the time series data of the bus voltage and power consumption and examining how the variations of the bus voltage effect the power consumption. The time series representation of the bus voltage and power consumption is shown in Fig. 4.12.

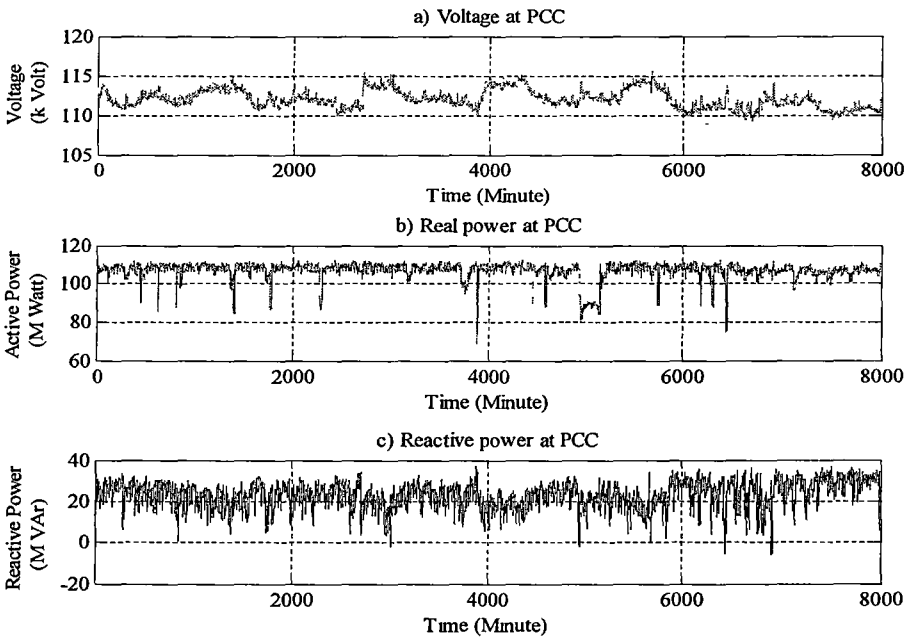

Figure 4.12. Time series data of a) voltage, b) real power consumption, and c) reactive power consumption at PCC (point A)

Fig. 4.12 presents the one minute interval time series data at PCC bus of the metallurgical plant for 8000 minutes. As the pattern of the power-voltage relationship of the PCC bus is similar to the arc furnace, arc furnace load characteristics are applied to model PCC bus response. From [7], arc furnaces can be treated as a static load, which is modelled using the exponential load model discussed in Section 1.3.5. In contrast, from [36] arc furnaces can also be treated as a random load.

In this chapter, the arc furnace behaviour will be examined by using both static load model and artificial intelligence techniques. The first step is to apply the values real and reactive power dependency parameters (np and nq) discussed in Section 1.3.5. Applying the values of np and nq as 2.3 and 1.6 in Eq. (1.9) and

(1.10), respectively, the values of the real and the reactive power consumption is calculated and presented in Fig. 4.13 and Fig. 4.14, respectively.

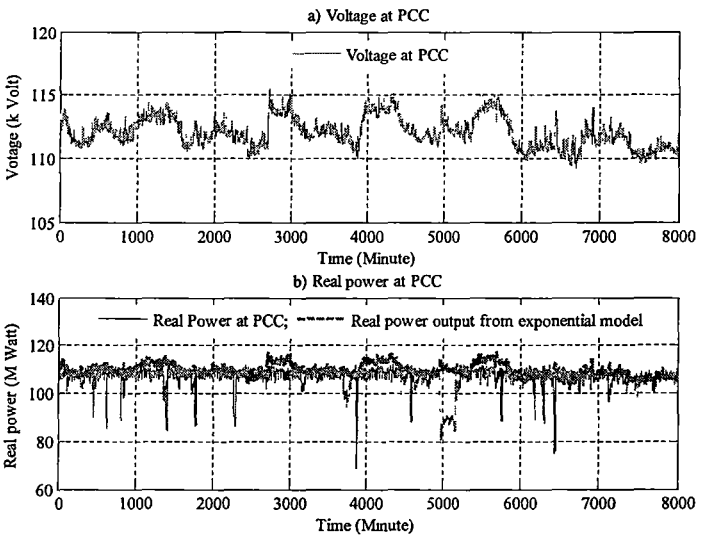

Figure 4.13. Time series data of a) voltage, b) real power consumption, at PCC (point A).

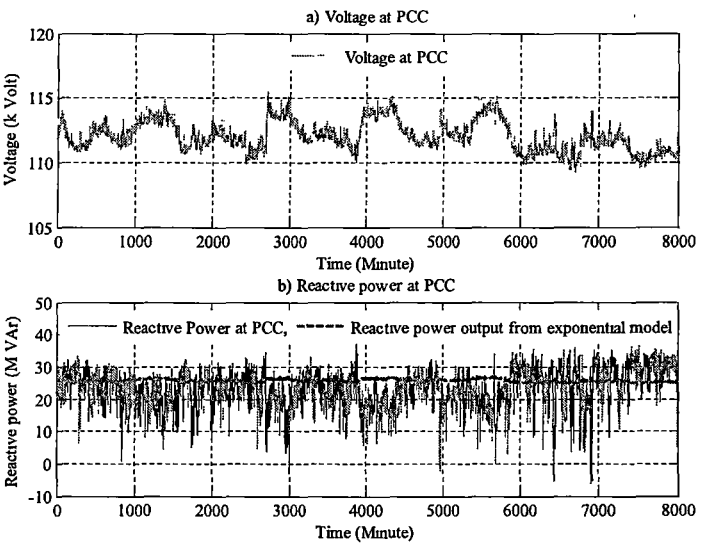

Figure 4.14. Time series data of a) voltage, b) reactive power consumption, at PCC (point A)

The performance of the load modelling techniques are evaluated using mean square error (MSE). The expression of the mean square error is:

$$MSE = \sqrt{\frac{1}{N}\sum_{i=1}^{N}\left(y_i^{actual} - y_i^{predicted}\right)^2} \tag{4.5}$$

The MSE of the static modelling approach for the real and the reactive power is 11.758 kW and 15.321 kVAr respectively. As can be seen from Fig. 4.12 and Fig. 4.13, the load modelling approaches cannot track the random changes of the power. It is obvious that this approach is unable to provide satisfactory results, and hence artificial intelligence techniques have to be applied to achieve the load response due to voltage variations. The first approach is to use a multi-layer perceptron (MLP) model discussed in Section 3.2.1. The voltage at PCC bus is used as the input and the bus power consumption is as the output of the MLP model. Out of 8000 data of 1 minute interval, data from time of 1 minute to time of 1000 minutes are used as training, and data from time of 1001 minutes to time of 2000 minutes are used to validate of the model. The real and reactive power consumption from time of 4000 minute to time of 4400 minute are shown in Fig. 4.14 and Fig. 4.15, respectively.

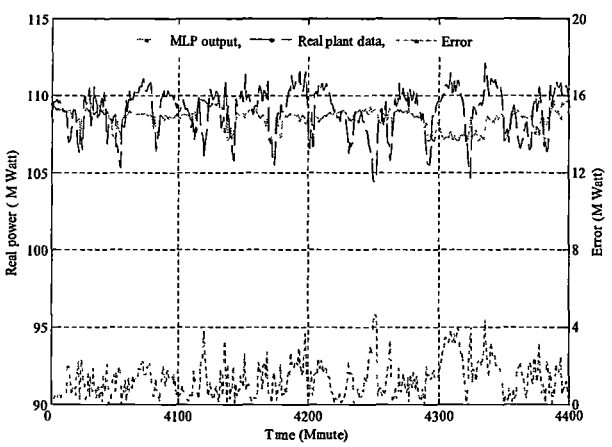

Figure 4.15. Real power consumption of PCC bus.

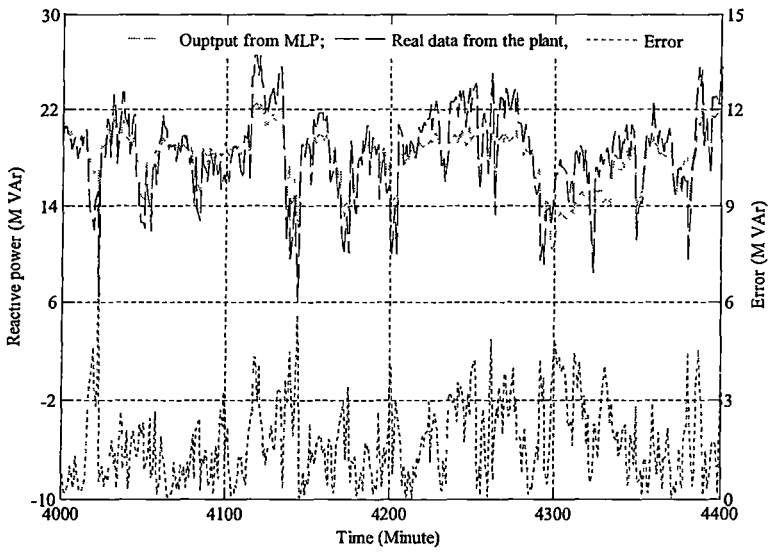

Figure 4.16. Reactive power consumption of PCC bus

The performance of the MLP model is measured by evaluating the MSEs which is 2.43 MW and 2.76 MVAr for the real and reactive power, respectively. Moreover, from Fig. 4.15 and Fig. 4.16, the MLP model is able to track the random changes of the power consumption at PCC bus. Thus the MLP model offers significant improvement comparing with the load modelling approach in recognising the voltage–power pattern of the arc furnace.

In the next stage, in order to improve performance of the model even further, Adaptive Neuro Fuzzy Inference System (ANFIS), which was discussed in Section 3.4 is implemented to obtain the power (both real and reactive) response to voltage variations. In the ANFIS model, the bus voltage is considered as the input vector and the power (real and reactive) is considered as the output vector. In this model, out of 8000 data from time of 1 minute to time of 8000 minutes, data from time of 1 minutes to time of 1000 minutes are used for training and data from time of 1001 minutes to time of 2000 minutes are used for testing. The real and reactive power

consumption from time of 4000 minute to time of 4400 minute are shown in Fig. 4.17 and Fig. 4.18, respectively.

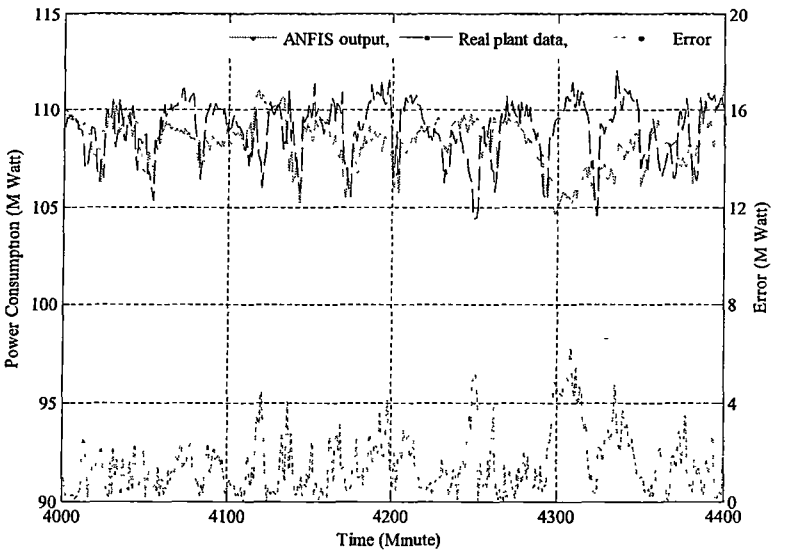

Figure 4.17. Real power consumption of PCC bus (ANFIS model).

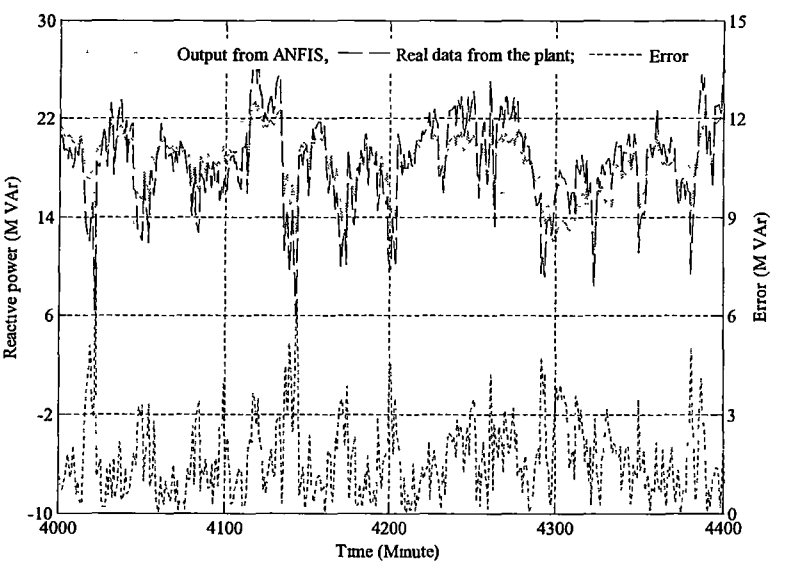

Figure 4.18. Reactive power consumption of PCC bus (ANFIS model).

In order to evaluate the performance of the ANFIS model, the MSEs for the real and the reactive power are calculated which are 2.17 MW and 2.93 MVAr, respectively. Thus, the ANFIS model offers slight improvement in recognising the voltage–power pattern of the arc furnace comparing with the MLP model. Moreover, like the MLP model, the ANFIS model is also able to track random changes of power as a result of voltage variation. The next step in this research is to evaluate the performance of the MLP and ANFIS models when the voltage disturbances occur. After analysing the entire time series voltage data shown in Fig. 4.12, a voltage disturbance is identified at time of 2703 minutes. Fig. 4.19 represents the time series data from time of 2500 minute to time of 3000 minutes of voltage and power consumption at PCC.

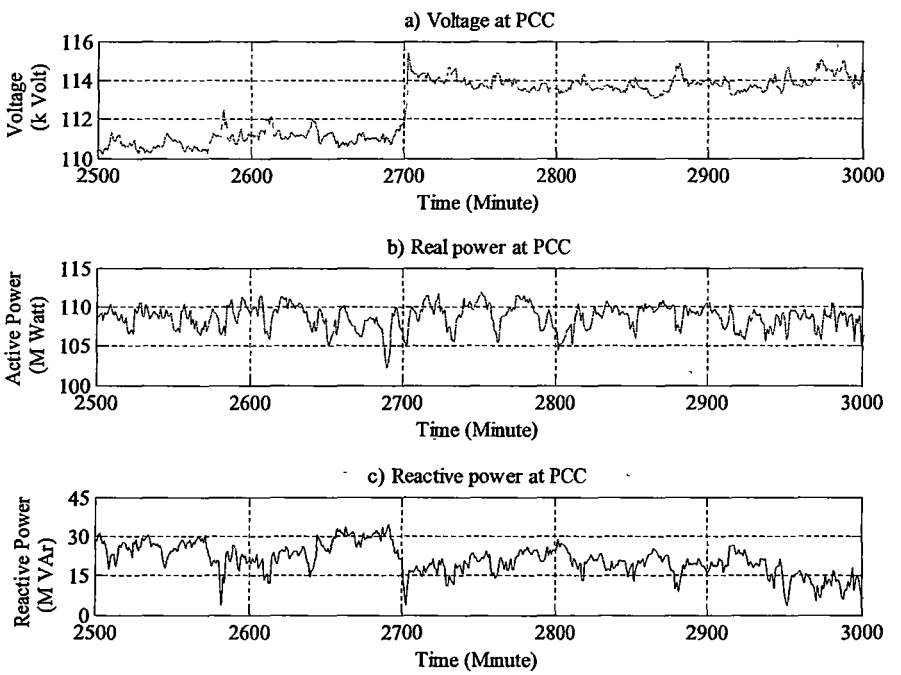

Figure 4.19. Time series data from time of 2500 minutes to time of 3000 minutes of a) voltage, b) real power consumption, and c) reactive power consumption at PCC.

The output responses of the MLP model for the real power and the reactive power are shown in Fig. 4.20 and Fig. 4.21, respectfully. The MSEs for the real and the reactive power are calculated for the data points from time of 2500 minutes to time of 3000 minutes are 3.37 MW and 3.19 MVAr respectively.

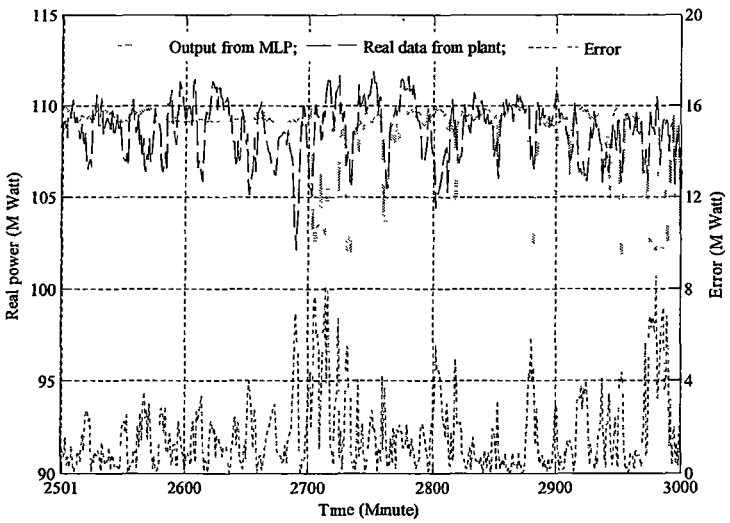

Figure 4.20. Real power consumption of PCC bus (MLP model).

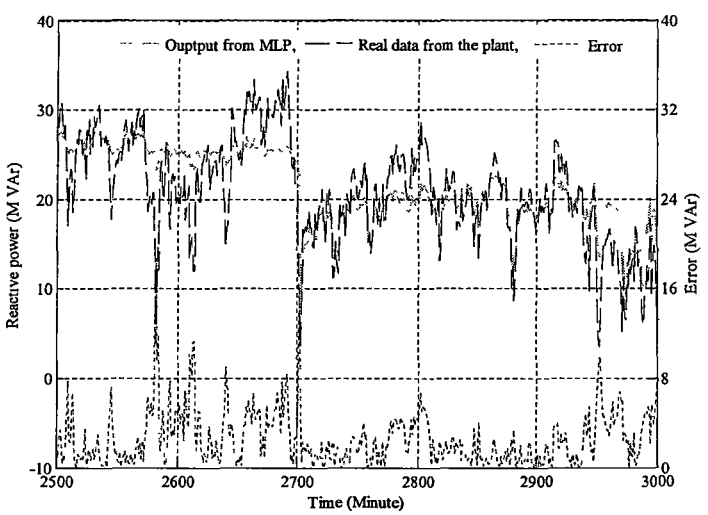

Figure 4.21. Reactive power consumption of PCC bus (MLP model).

A similar investigation is undertaken using the ANFIS model. Figs. 4.22 and 4.22 show the output of the ANFIS model for real and reactive power responses, respectively.

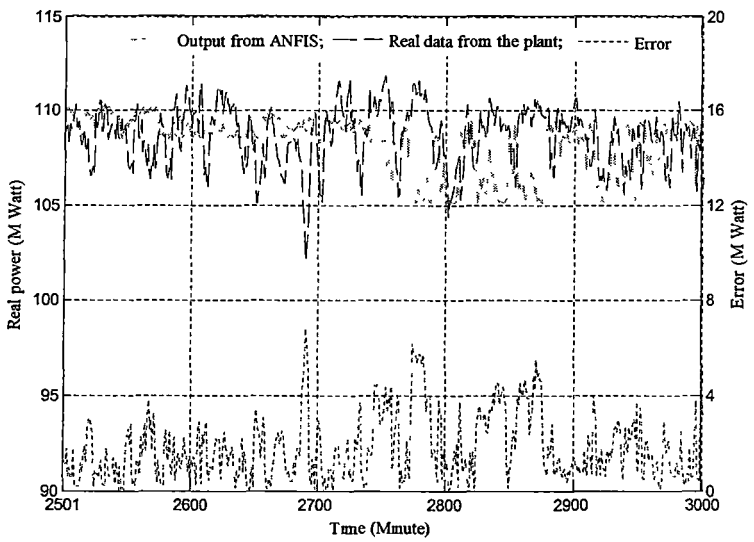

Figure 4.22. Real power consumption of PCC bus (ANFIS model).

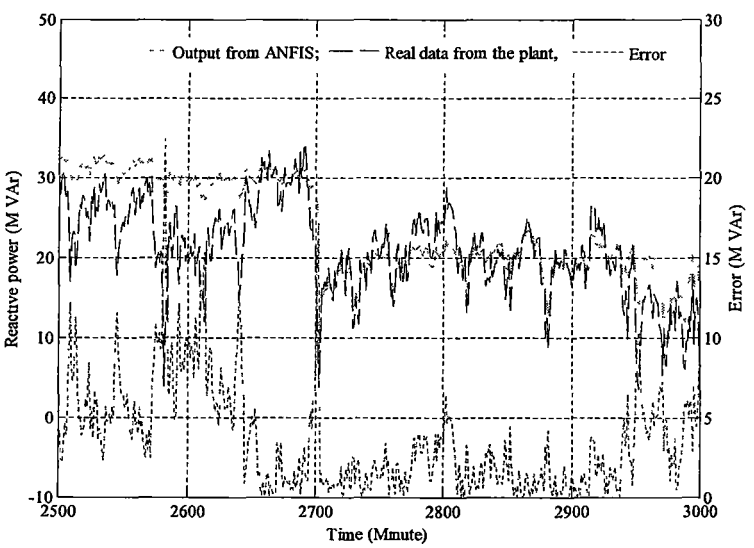

Figure 4.23. Reactive power consumption of PCC bus (ANFIS model).

MSEs for the real and the reactive power response of the ANFIS model are calculated as 2.43 MW for real power and 3.32 MVAr for reactive power.

4.3.2 Load response of arc furnace 1 (Point B1)

The MLP and ANFIS models can be applied in similar manner to obtain the load response of the arc furnaces shown in Fig. 4.11. The first step is to investigate the time series patterns of the voltage and power consumption shown in Fig. 4.24 of arc furnace 1 (point B1).

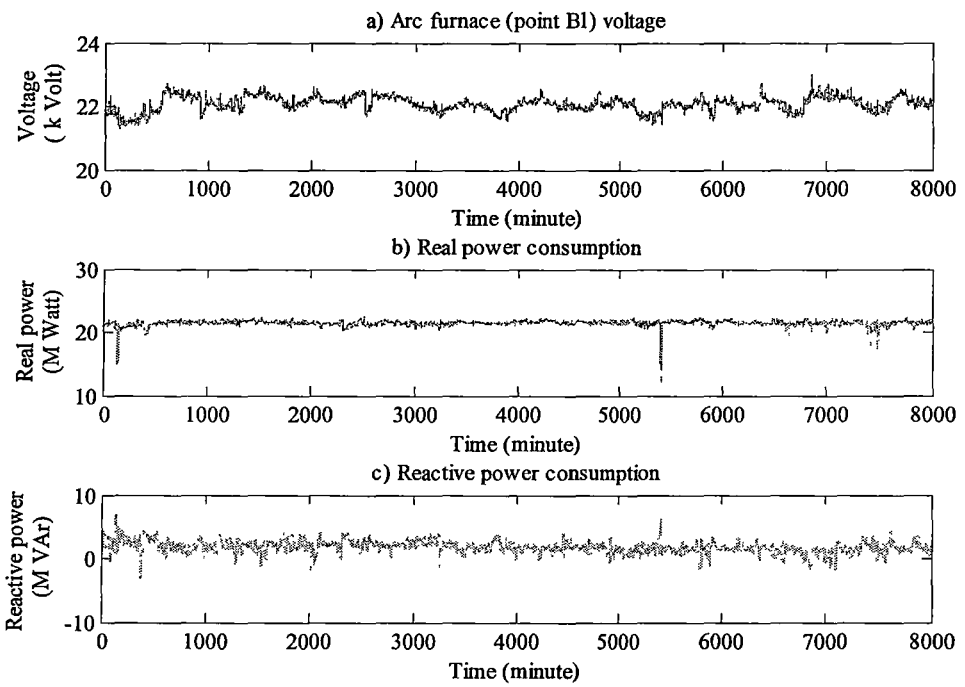

Figure 4.24. Time series data of a) voltage, b) real power consumption, and c) reactive power consumption at arc furnace 1 (point B_1).

The MLP and ANFIS models are applied to evaluate the power response of arc furnace 1 due to the voltage variations. In order to do this, a test case is

considered which starts at time of 7000 minutes and finishes at time of 8000 minutes; this is where the arc voltage fluctuates most. The output of the MLP and ANFIS models are shown in Figs. 4.25 – 4.28.

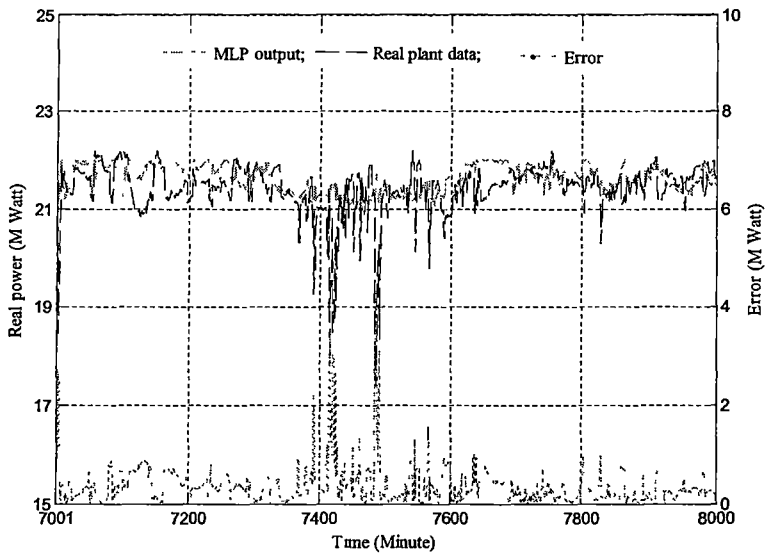

Figure 4.25. Real power consumption of arc furnace 1 (MLP model).

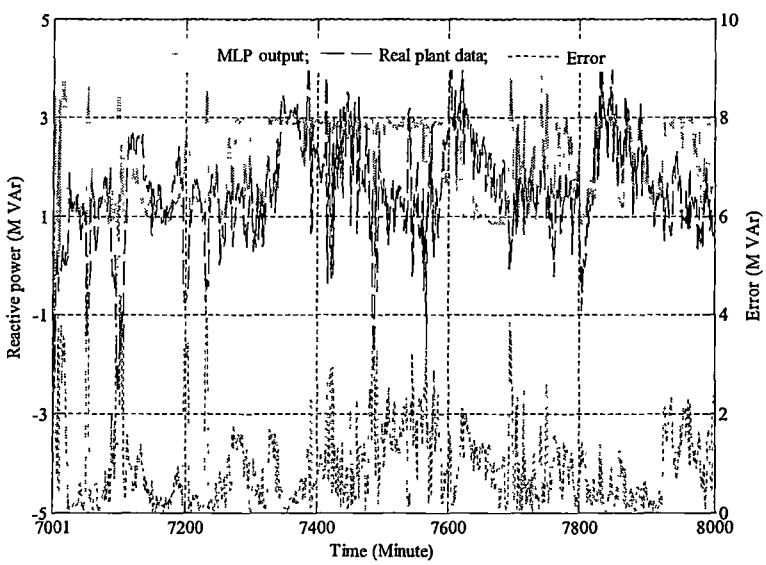

Figure 4.26. Reactive power consumption of arc furnace 1 (MLP model).

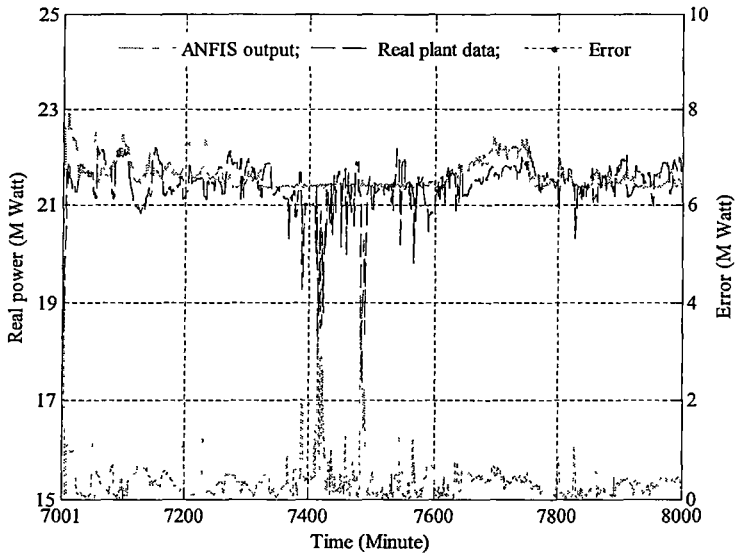

Figure 4.27. Real power consumption of arc furnace 1 (ANFIS model).

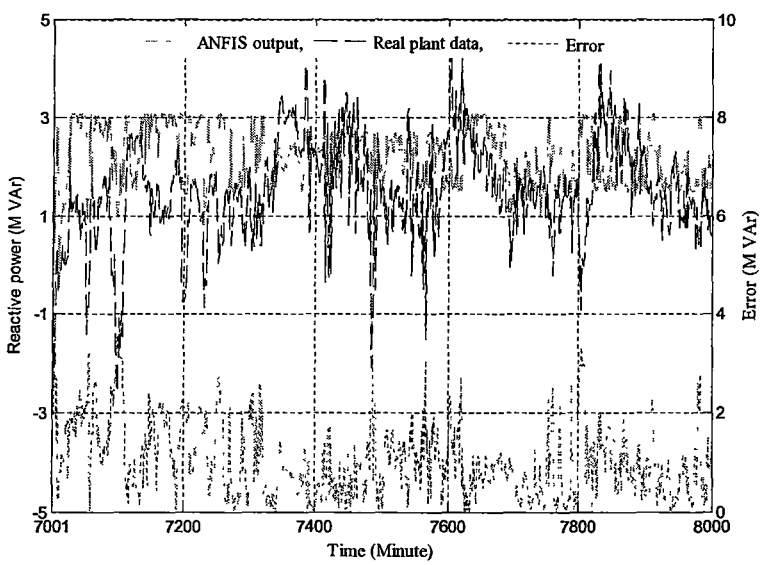

Figure 4.28. Reactive power consumption of arc furnace 1 (ANFIS model).

The MSEs for the real and reactive power of arc furnace 1 between time of 7001 minutes and time of 8000 minutes are 0.61 MW and 1.65 MVAr respectively

for MLP model. The ANFIS model is able to provide better result by reducing the MSEs for the real and reactive power are calculated as 0.39 M Watt and 1.02 M VAr respectively.

4.3.3 Load response of arc furnace 3 (Point B3)

Similarly, The MLP and ANFIS models are applied to obtain the load responses of the arc furnaces 3 shown in Fig. 4.11. The first step is to investigate the time series pattern of the voltage and power consumption of arc furnace 3 (point B_3) which is shown in Fig. 4.29.

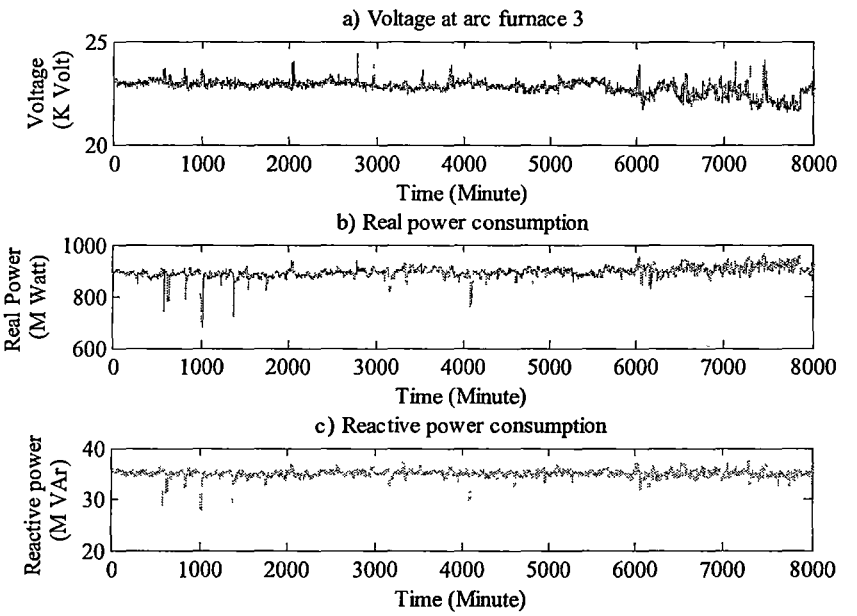

Figure 4.29. Time series data of a) voltage, b) real power consumption, and c) reactive power consumption at arc furnace 3 (point B_3).

The response of arc furnace 3 power consumption is obtained using the MLP and ANFIS models. The performance of these model is obtained by considering a test case which starts at time of 6001 minutes and finishes at time of 7000 minutes;

this is where the arc voltage fluctuates most. The output of the MLP and ANFIS models are shown in Figs. 4.30 –4.33.

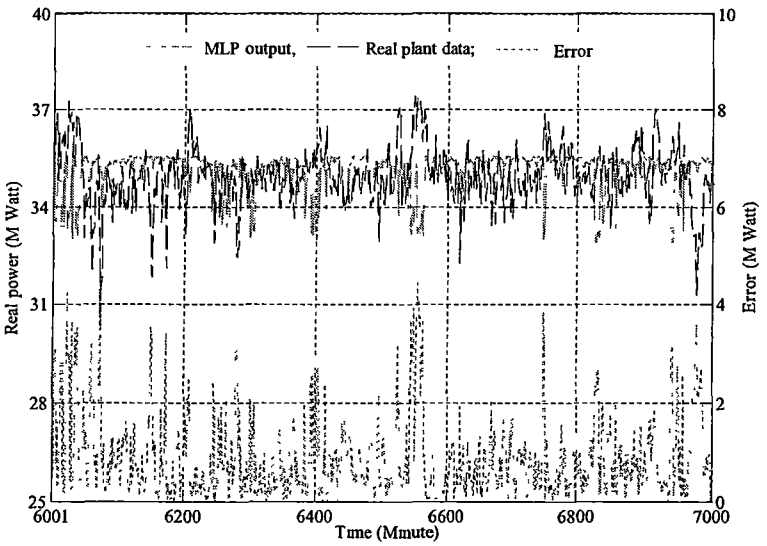

Figure 4.30. Real power consumption of Arc furnace 3 (MLP model).

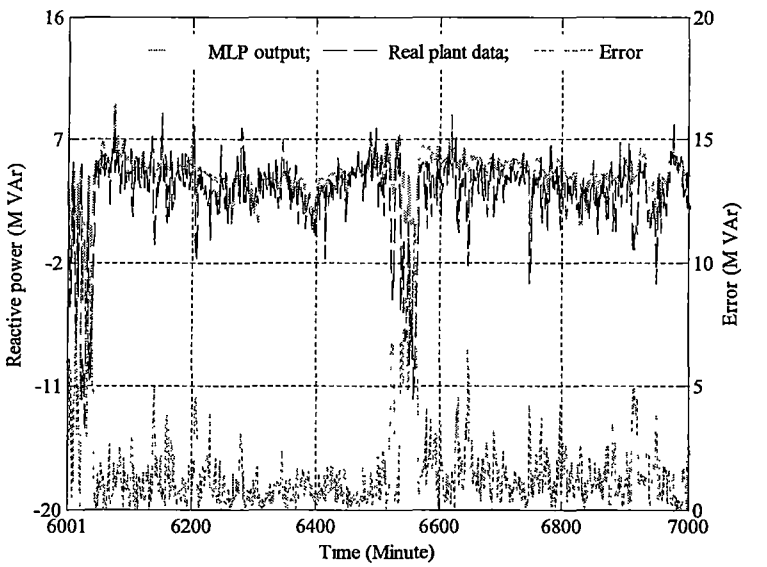

Figure 4.31. Reactive power consumption of Arc furnace 3 (MLP model).

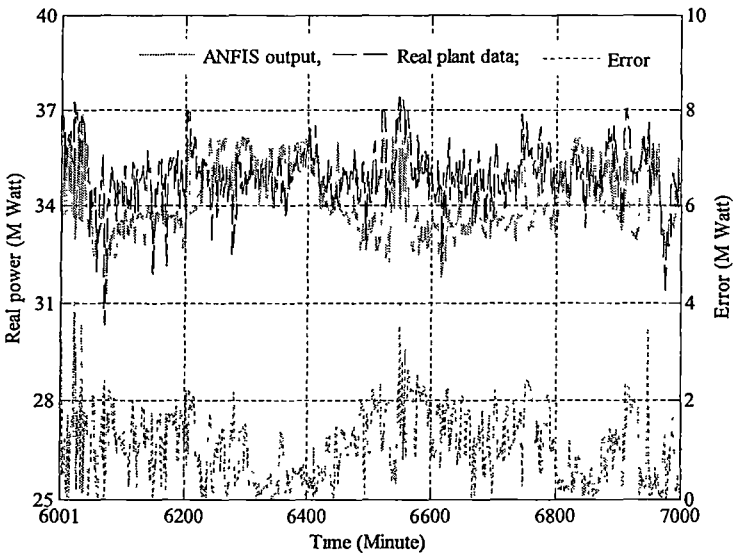

Figure 4.32. Real power consumption of Arc furnace 3 (ANFIS model).

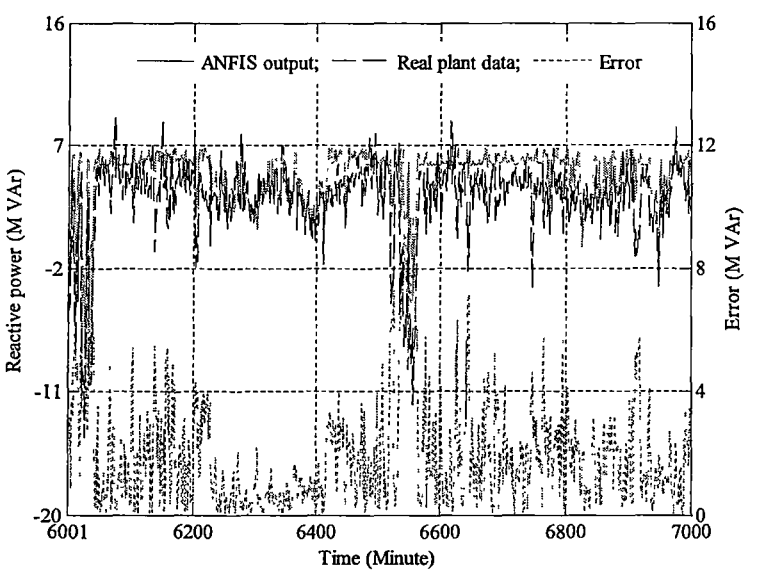

Figure 4.33. Reactive power consumption of arc furnace 3 (ANFIS model).

The MSEs for the real and the reactive power between time of 6001 minutes and time of 8000 minutes are 0.78 MW and 1.36 MVAr respectively for MLP model. In case of the ANFIS model, the MSEs are almost similar to MLP model which are 0.89 MW and 1.52 MVAr respectively.

4.4 Prediction of the arc furnace response

In this research, the ANFIS model is also used to predict the voltage of different point of the plant shown in Fig. 4.11 based on the historical data. The goal of the time-series prediction is to use past values of bus voltage up until present time to predict the future value of arc voltage. Let us consider an ANFIS model that can predict the value of arc voltage of m unit time ahead using the n numbers of historic data. The input-output relationship of the ANFIS model is shown in the following:

$$[x_{AF}(t+m)] = f([x_{AF}(t-nm) \quad \ldots \quad x_{AF}(t-2m) \; x_{AF}(t-1m) \; x_{AF}(t)])$$

where, $[x_{AF}(t+m)]$ is the output vector of ANFIS model; and $[x_{AF}(t-mn) \quad \ldots \quad x_{AF}(t-2n) \; x_{AF}(t-1n) \; x_{AF}(t)]$ are n numbers of historical data used as the input vector. The model is validated by conducting some case studies presented as follows:

4.4.1 Prediction of the PCC bus voltage

The prediction of the PCC bus voltage is achieved using the ANFIS model. Out of 8000 data of 1 minute interval, data at time of 1 minute to time of 1000 minute are used as training, and data from time of 1001 minutes to time of 2000 minutes are used as the validation of the model. A case study is provided to evaluate the performance the ANFIS model that starts at time of 3500 minutes and finishes at time of 4500 minutes. The prediction of the future voltage of 1, 3, and 5 minutes ahead of time which are shown in Figs. 4.34 – 4.36.

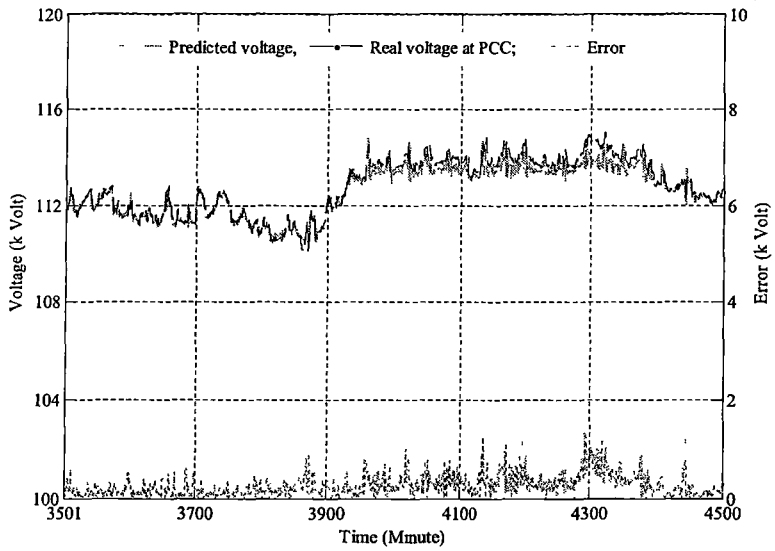

Figure 4.34.. PCC bus voltage prediction (1 minute future value).

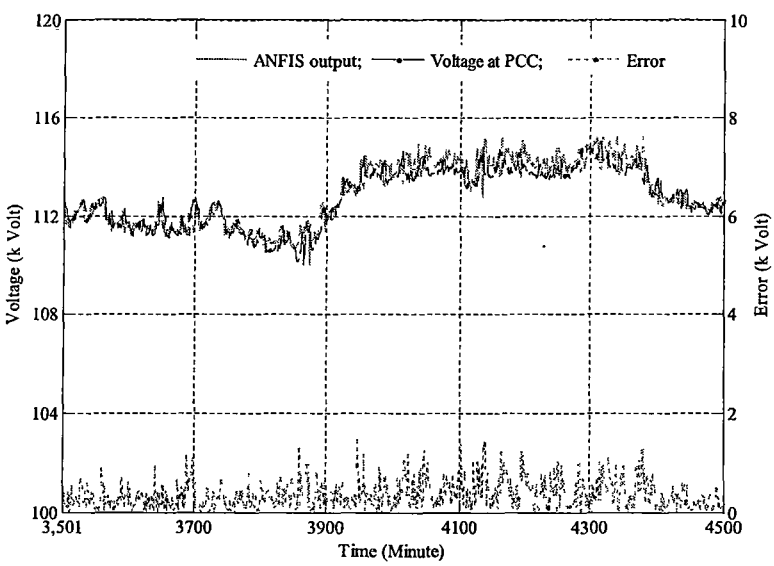

Figure 4.35. PCC bus voltage prediction (3 minute future value).

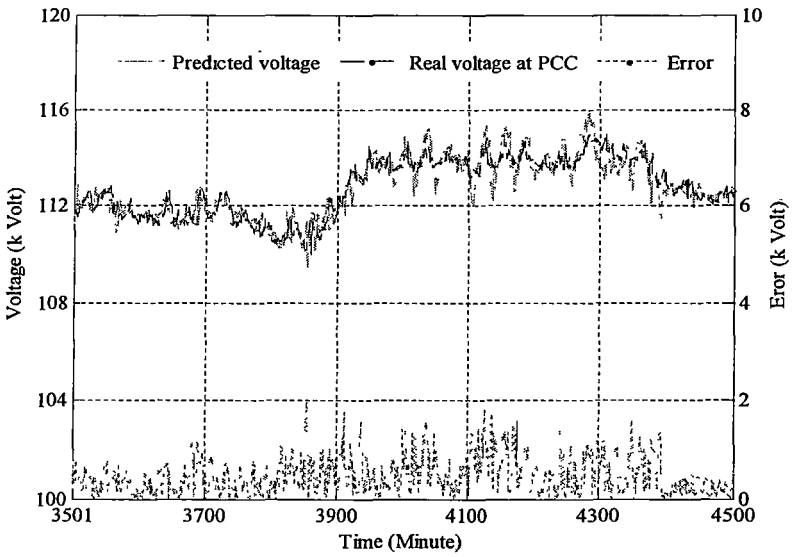

Figure 4.36. PCC bus voltage prediction (5 minute future value).

The MSEs (mean square error) for voltage predictions are calculated for the data points at time of 3501 minutes to time at 4500 minutes are 0.09 kV, 0.17 kV, and 0.48 kV for the 1, 3 and 5 minute ahead of future voltage prediction of the PCC bus, respectively.

4.4.2 Prediction of the bus voltage of arc furnace 1

Similarly, the ANFIS model is implemented to predict the voltage response of the arc furnace 1. Similar approach is undertaken for the training and validation of data as in the case of the prediction of the PCC bus voltage. A case study is provided to evaluate the performance of the ANFIS model which starts at time of 3500 minutes and finishes at time of 4500 minutes. The prediction of the future voltage of 1, 3, and 5 minutes ahead of time which are shown in Figs. 4.37 – 4.39.

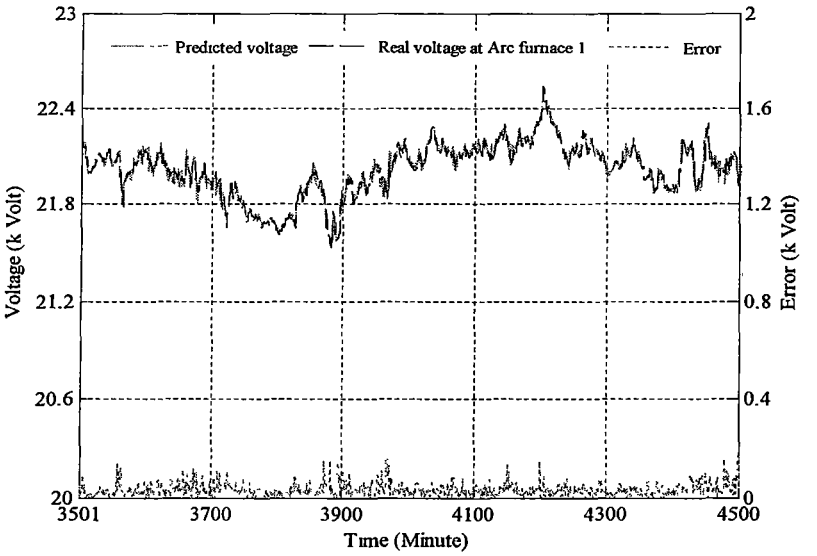

Figure 4.37. Arc furnace 1 bus voltage prediction (1 minute ahead).

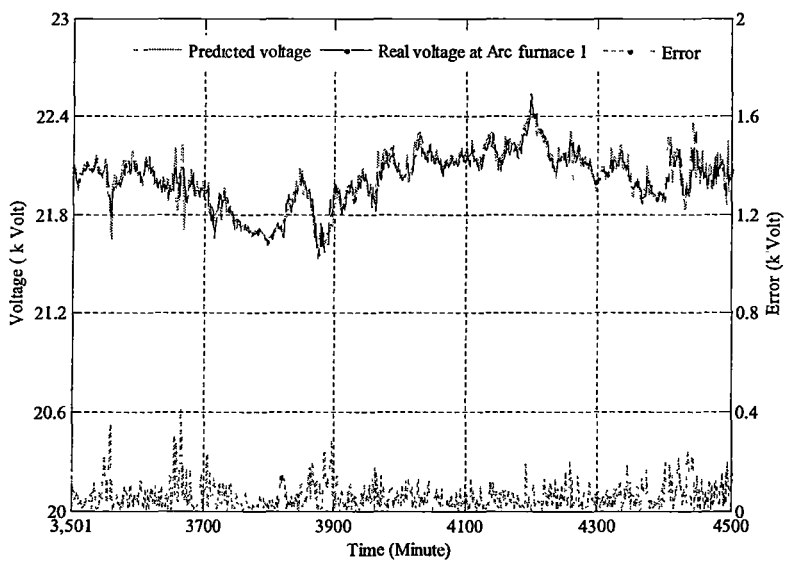

Figure 4.38. Arc furnace 1 bus voltage prediction (3 minute ahead).

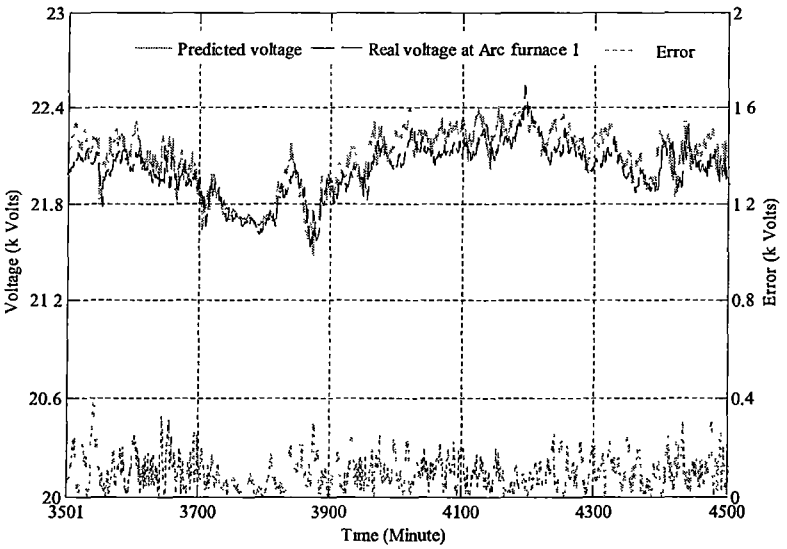

Figure 4.39. Arc furnace 1 bus voltage prediction (5 minute ahead).

The MSEs for voltage predictions are calculated for the data points at time of 3501 minutes to time at 4500 minutes are 0.034 kV, 0.069 kV, and 0.11 kV for the prediction of voltage for 1, 3, and 5 minute of future time ahead values, respectively.

4.4.3 Prediction of the bus voltage of Arc furnace 3

Similarly, the ANFIS model is implemented to predict the voltage response of the arc furnace 3. Similar approach is undertaken for the training and validation of data as in the case of the prediction of the PCC bus voltage. A case study is provided to evaluate the performance of the ANFIS model which starts at time of 3500 minutes and finishes at time of 4500 minutes. The prediction of the future voltage of 1, 3, and 5 minutes ahead of time which are shown in Figs. 4.40 – 4.42.

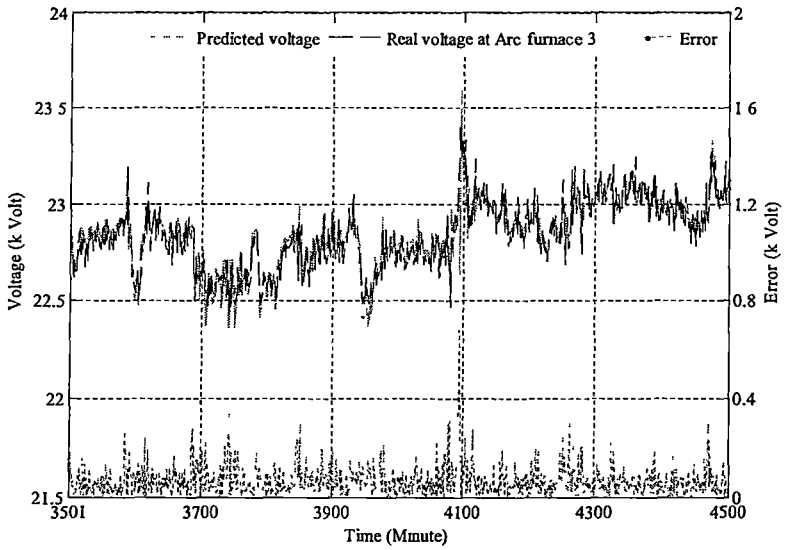

Figure 4.40. Arc furnace 3 bus voltage prediction (1 minute ahead).

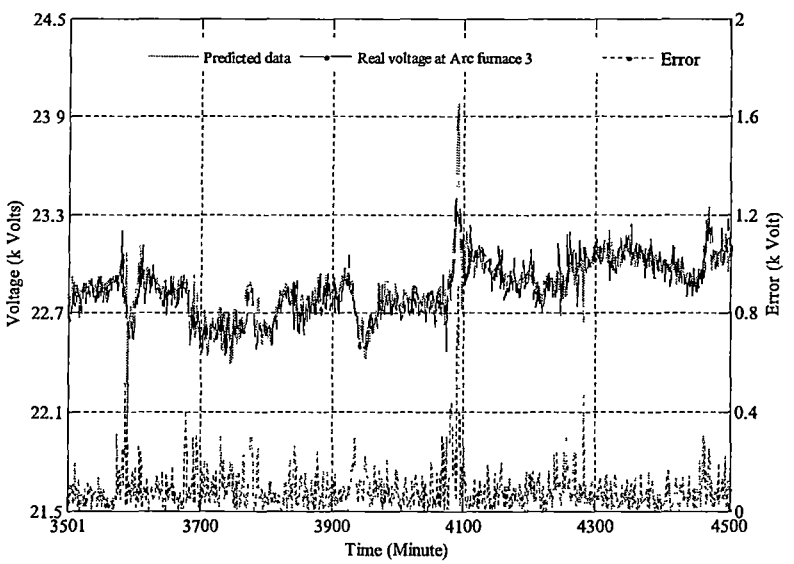

Figure 4.41. Arc furnace 3 bus voltage prediction (3 minute ahead).

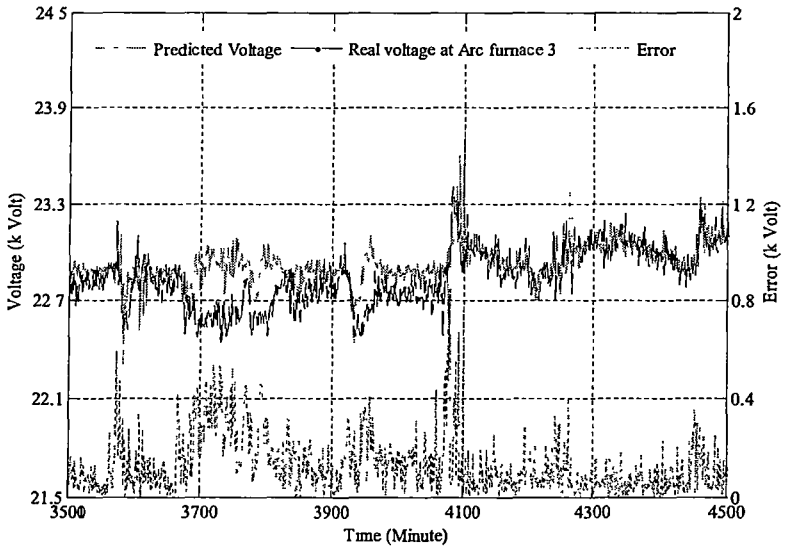

Figure 4.42. Arc furnace 3 bus voltage prediction (5 minute ahead).

The MSEs for voltage predictions are evaluated for the data points at time of 3501 minutes to time at 4500 minutes are 0.043 kV, 0.051 kV, and 0.32 kV for the prediction of voltage for 1, 3, and 5 minute of future time ahead values, respectively.

4.5 Conclusion

In this chapter, different arc furnace models were used in case studies based on data collected at the metallurgical plant in Tasmania. Conventional models were used to demonstrate and analyse the instantaneous wave form of the arc current and the arc voltage. It was demonstrated that these models were useful in analysing the arc furnace responses of one cycle. However, they fail to provide satisfactory results in handling the random and time-varying nature of arc furnace. Load modelling techniques and artificial intelligence techniques are applied to obtain the random pattern of the arc furnace power-voltage relationship. It was demonstrated that load modelling techniques are unable to capture the random nature of the voltage-power

relationship of the arc furnace. On the other hand, artificial intelligence techniques such as the MLP model and the ANFIS model were successful to obtain the random and time-varying pattern of the arc furnace responses. The performances of these models were evaluated by measuring the mean square error (MSE) of the MLP and the ANFIS model for different case studies. It was demonstrated that the MSEs for the MLP and ANFIS model are significantly low comparing with the load modelling techniques in the case of recognising the voltage-power patterns of the arc furnace. Moreover, ANFIS models are used to predict the voltage in different points of the plant. It was shown in this chapter that, the ANFIS model is very efficient in prediction as mean squire errors of those models are significantly low.

Conclusion and Future Work

The representation of random and time-varying loads such as industrial arc furnaces, rolling mills and so on remains an area of great uncertainty for industrial plant operators and planners. Accurate modelling of such loads plays an important role in efficient operation and control of industrial plants. The main focus of this thesis was the development of an accurate representation of random and time-varying behaviour of arc furnaces.

In this thesis, different modelling techniques such as conventional and black box approaches have been discussed and their application to represent the arc furnace behaviour has been investigated. Using conventional modelling approaches discussed in Chapter 2, the arc voltage and current wave forms were obtained based on the voltage-current characteristic of arc furnaces. These models were proved to be efficient for a single cycle of operation. However, they cannot provide satisfactory results for long term responses as these models are unable to handle random and time-varying patterns of the arc furnace.

Load modelling techniques were outlined to represent the arc furnace behaviour. In this thesis, firstly, the arc furnace was considered as a 'load' and load modelling techniques were applied to model the arc furnace behaviour. Several case studies were performed to obtain load response of arc furnace due to the change in bus voltage. However, it was demonstrated that, load modelling approaches failed to capture random and time-varying patterns of power consumption (both real and reactive) of the arc furnace as a result of random variation in bus voltage.

Finally, artificial intelligence approaches such as artificial neural network and fuzzy inference system were used in the proposed arc furnace model. Multi-layer perceptron (MLP) and adaptive neuro-fuzzy inference system (ANFIS) were used to obtain random and time-varying pattern of the power (both real and reactive) consumption of the arc furnace. The outputs of the models were compared with the industrial data which demonstrated that the models were able to provide satisfactory results. Moreover, using ANFIS model, the bus voltage of different points of the

plant was predicted with the accuracy of more than 99%. This prediction model was proved to be efficient as the prediction error is significantly low.

The proposed models can be used in various process industries that involve arc furnaces applications. Firstly, using these models, a new energy management system based on artificial intelligence techniques can be to develop. As a result, industrial plants would be able to improve their energy consumption and maximise the production.

Secondly, an intelligent control system based on artificial intelligence techniques to control the movement of arc electrode can be developed using the models proposed in this thesis. As the arc electrode length plays an important role in metal and slag production, an intelligent arc electrode controller can assure the proper positioning of the arc electrode that would optimise the production of metal and slag.

Finally, the proposed model can be used for the protection of the plant from external disturbances such as large voltage deviations. Using the proposed voltage prediction model, it would be possible to detect major voltage disturbances ahead of time that may have an adverse effect on the plant and its machinery.

Reference

1. 'world steel organization', website: http://www.worldsteel.org/index.php?action=storypages&id=196
2. http://en.wikipedia.org/wiki/Electric_arc_furnace
3. M. Negnevitsky, "Artificial Intelligence: a guide to intelligent systems", 2nd Edition, Addison-Wesley, Harlow, England, 2005
4. A. R. Sadeghian, J. D. Lavers, "Application of radial basis function networks to model electric arc furnaces", International Joint Conference on Neural Network (IJCNN '99), Volume 6, 10-16 July 1999, Page(s): 3996-4001, vol.6, Digital Object Identifier 10.1109/IJCNN.1999.830798
5. Kundur, P., "Power System Stability and Control", ISBN 0-07-035958-X, New York, McGraw-Hill, 1994, Chapter 7.
6. Navarro, I. R., "Dynamic Load Models for Power Systems", Dept. of Industrial Electrical Engineering and Automation, Lund University, Sweden
7. Navarro, I. R., Samuelsson, O., Lindahl, S., "Influence of normalization in dynamic load model", IEEE transaction in power system, vol. 18, no. 2, page 972-973, May 2003
8. Echavarria, R., Claudia, A., and Cotorogea, M., "Analysis, design and implementation of a fast on-load tap changing regulator", IEEE transaction on power electronics, vol. 22, no. 2, march 2007
9. IEEE Task Force Report: "Load Representation For Dynamic Performance Analysis", IEEE Transactions on Power Systems, Vol. 8, No. 2, May 1993, pp. 472-482.
10. Khodabakhchian, B., and Vuong, G. T. "Modeling a mixed residential-commercial load for simulation involving large disturbances", IEEE transaction on power system, vol. 12, no. 2, pp. 791-796, May 1997.
11. Price, W. W., Wirgau, K. A., Murdoch, A.., Mitsche, J. V., Vaahedi, E., and El-Dady, M. A., "Load modeling for power flow and transient stability computer studies", IEEE transaction on power system, vol. 3, no. 1, pp. 180-187, Feb. 1988

12. Choi, B.-K., Chiang, H.-D., Li, Y., Li, H., Chen, Y. T., Huang, D. H., and Lauby, M. G. "Measurement-based dynamic load models: deviation, comparison, and validation", IEEE transaction on power system, vol. 21, no. 3, august 2006

13. C. –J. Lin, Y. –T. Chen, H. –D. Chiang, and J. –C. Wang, "Dynamic Load models in power systems using the measurement approach", IEEE transaction of power system. Vol. 8, no. 1, pp. 309-315, February 1993

14. D. Karlsson, and D. J. Hill, "Modeling and identification of nonlinear dynamic loads in power system", IEEE transaction of power system. Vol. 9, no. 1, pp. 157-166, February 1994

15. D. J. Hill, "Nonlinear dynamic load models with recovery for voltage stability study", IEEE transaction of power system. Vol. 8, no. 1, pp. 166-176, February 1993

16. W. Xu, and Y. Mansour, "Voltage stability analysis using generic dynamic load models", IEEE transaction of power system. Vol. 9, no. 1, pp. 479-493, February 1994

17. Baghzouz, Y., and Quist, C., "Composite load model deviation from recorded field data" Proceeding in IEEE Eng. Society winter meeting, page 713-718 Jan. – Feb. 31-4, 1999

18.. Lin, C. J., Chen, Y. T., Jiang, H. D., Wang, J. C., "Dynamic load models in power systems using the measurement approach", IEEE transaction in power system, vol. 8, no. 1, pp. 309-315, Feb. 1993.

19. Hiskens, I. A., "Nonlinear dynamic model evaluation from disturbance measurement", IEEE transaction in power system, vol. 16, no. 4, pp. 702-710, Nov. 2001.

20. Dugan, R. C., "Simulation of arc furnace power system", IEEE transaction on industrial application, vol. IA – 16, no. 6, November 1980, pp 813-818.

21. Varadan, S., Makram, E. B., and Girgis, A. A., "A new time domain voltage source model for an arc furnace using EMPT", IEEE transaction on power delivery, Vol. 11, No. 3, July 1996.

22. Alonso, M. A. P., and Donsion, M. P., "An improved time domain arc furnace model for harmonic analysis", IEEE transaction on power delivery, vol. 19, no. 1, January 2004.

23. Plata, E. A. C, and Tacca, H. E. "Arc furnace modelling in ATP-EMPT"

proceedings of the international conference on power system transients (IPST'05), June 19-23, 2005, Montreal, Canada.

24. Zheng, T.; Makram, E.B.; Girgis, A.A.; Effect of different arc furnace models on voltage distortion, , 1998. Proceedings on the 8th International Conference on Harmonics And Quality of Power, Volume 2, 14-16 Oct. 1998, Page(s):1079 - 1085

25. G. C. Montanari. M. Loggini A, Cavallini. "Arc furnace model for the study of flicker compensation in electrical networks", IEEE Transaction on Power Delivery, Vol. 9. No. 4, October 1994. pp. 2026-33

26. Tongxin Z.; Makram, E.B.; An adaptive arc furnace model ; IEEE Transactions on Power Delivery, Vol. 15, No. 3, July 2000, Page(s): 931 – 939

27. Emanuel, A. E.; Orr, J. A.; "An improved method of simulation of the arc voltage-current characteristics" Proceeding 9th international conference on harmonics and quality of power, pp. 148-150, October 1-4, 2000, Orlarndo, Florida.

28. Schau H.; and Stade D., "Mathematical Modeling of Three- Phase Arc Fumace", Proceedings of IEEE ICHPS VI, Bologna, Sep. 21-23, 1994, pp. 422-28

30. http://en.wikipedia.org/wiki/Artificial_intelligence

31. http://en.wikipedia.org/wiki/Intelligence

32. J. -S. R. Jang, C. –T. Sun and E. Mizutani, "Neuro-Fuzzy and Soft Computing" A Computational Approach to Learning and Machine Intelligent. Prentice Hall. Englewood Cliffs, NJ, 1993

33. The MathWorks Inc. 'Fuzzy Logic User's Guide: Version 2', 2002.

34. A. M. O. Haruni, Kashem M. Muttaqi, M. Negnevitsky, "Artificial Intelligent Approach to Arc Furnace Response Prediction", The Eighth International Conference on Intelligent Technologies (InTech 2007), Sydney, Australia, Dec. 12-14, 2007